THE EFFECT OF VEGETATION ON THE SPECTRAL RESPONSE OF MINERALS/ROCKS, AND PERFORMANCE OF A FORCED INVARIANCE VEGETATION SUPPRESSION ALGORITHM ON MULTI-SPECTRAL IMAGERY, SW TANZANIA.

GEBRESELASSIE GEBREMICHEAL GEBREMEDHIN
Feb 2018

SUPERVISORS:
Dr. Robert Hewson
Prof.dr. F.D. van der Meer (Freek)

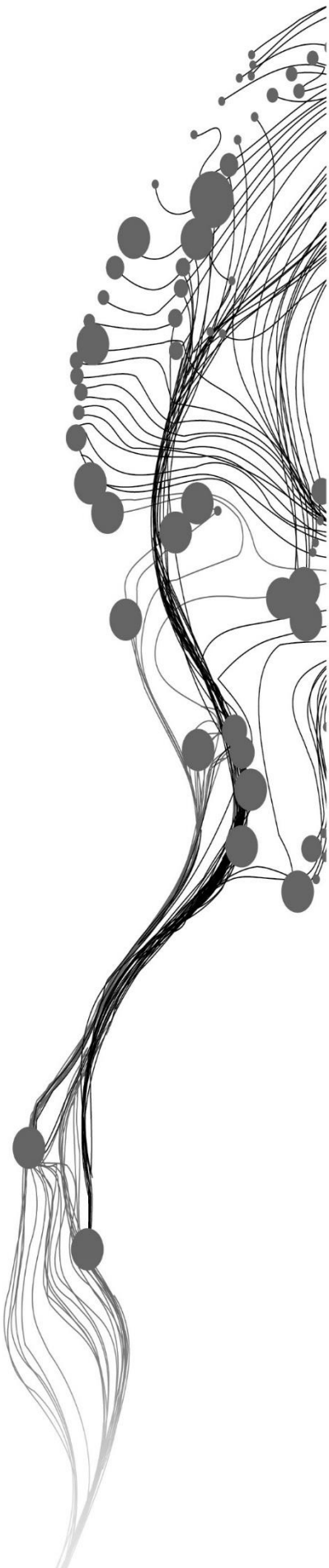

THE EFFECT OF VEGETATION ON THE SPECTRAL RESPONSE OF MINERALS/ROCKS, AND PERFORMANCE OF A FORCED INVARIANCE VEGETATION SUPPRESSION ALGORITHM ON MULTI-SPECTRAL IMAGERY, SW TANZANIA.

GEBRESELASSIE GEBREMICHEAL GEBREMEDHIN
Enschede, The Netherlands, February 2019

Thesis submitted to the Faculty of Geo-Information Science and Earth Observation of the University of Twente in partial fulfilment of the requirements for the degree of Master of Science in Geo-information Science and Earth Observation.
Specialization: Applied Earth Sciences in Geological Remote Sensing

SUPERVISORS:
Dr. Robert Hewson
Prof.dr. F.D. van der Meer (Freek)

THESIS ASSESSMENT BOARD:
Prof. Dr. M. (Mark) van der Meijde (Chair)
Dr. Martin Schodlok (External examiner; BGR, Germany)

ABSTRACT

Vegetation affects the spectral information that would be acquired from minerals/rocks imaged by remote sensing sensors. This research assessed the potential influence of green vegetation cover on the spectral responses of minerals and/or rocks imaged by Landsat and ASTER in the sub-tropical to tropical environment of Mbeya, South West Tanzania. Also, the work evaluated the role of the Crippen and Blom's algorithm in suppressing vegetation and enhancing spectral responses of mineral/rocks imaged by both Landsat and ASTER sensors. A bare-vegetation simulation model was used. The model linearly mixes certain amount of vegetation and bare ground to assess the influence of vegetation on the spectral response of bare ground (i.e. mineral, rock and/or their weathered products). NDVI ranges and false colour composite were used to extract the endmembers from the Landsat and ASTER imagery for the input of the simulation model. A detailed evaluation of the effect of vegetation on the spectral response of a bare ground was done using the results of nine simulation models within the VNIR-SWIR wavelength ranges of the Landsat and ASTER sensors. To evaluate the role of the Crippen's and Blom's algorithm in spectral enhancement and vegetation suppression, results were compared before and after applying the algorithm on ratio images, ROI based spectral signatures, RGB combinations of ratio images and NDVI images. The results of the simulation model show that a green vegetation cover of 20% or above causes strong mixing effects on the VNIR -SWIR spectra of both the Landsat and ASTER images. The evaluation of the Crippen and Blom's algorithm show more or less similar before and after results for both the Landsat and ASTER images. The algorithm qualitatively increased the clarity/contrast of the features in images of both sensors. However, the algorithm does not have a significant role to enhance the spectrally interpretable content of mineralogical/lithological information from both sensors. It seems useful for qualitative discrimination of geological boundaries, but not useful for mineral group identification via diagnostic spectral absorption features. Also, for the case of the lithological boundary discriminations, it shows more better qualitative enhancement results given that principal component analysis (PCA) is applied on top of the qualitative Crippen & Bloom RGB products.

Keywords: Vegetation, Spectral response, minerals/rocks, Multispectral image, Crippen and Blom's algorithm.

ACKNOWLEDGEMENTS

First, I thank the Almighty 'God' for everything!

My gratitude begins with a special thanks to my supervisors Dr. Rob Hewson and Prof.dr. F.D. van der Meer (Freek) for their outstanding and enthusiastic supervision starting from the proposal development up to the end of the thesis work, otherwise this thesis research would not be possible.

My hot gratefulness continues to Mr. Bart Krol, the course coordinator, for his invaluable advices, his wonderful guidance and all managing activities in the Programme.

I am also grateful of the NUFFIC full scholarship for all the financial support including the tuition fee, transport, insurance and living expenses, otherwise I would not be able to attend the course.

Next, I would like to appreciate the ITC Faculty for the admission and the whole ITC community including all the staffs in ITC and my colleges for the wonderful time that we had together.

I am grateful to Dr. Elisante Mshiu of the Dept of Geology, University of Dar Es Salaam, Dar Es Salaam, Tanzania, for supplying the Geological map of the study area.

I would like also to thank suppliers of the datasets used in this study, the ASTER (NASA, USGS and Japanese METI) and the Landsat (NASA and USGS) imagery.

Finally, I would like to give wonderful thanks to my family, all my relatives and friends who stood on my side to successfully complete my studies.

TABLE OF CONTENTS

Contents

LIST OF FIGURES

LIST OF TABLES

1. INTRODUCTION

1.1. Background

One of the main tasks in the use of remote sensing for earth surface interpretation is to decode mineral and rock information from images (Gupta, 2017). For example, geologic interpretation of multispectral images, can be used for mineral exploration and lithologic mapping (Gupta, 2017; Hunt, 1977). Advanced Spaceborne Thermal Emission and Reflection Radiometer (ASTER) and Landsat images are among the remote sensing satellite images that can be used for interpreting of mineral and rock information (Carranza & Hale, 2002; Cŕosta, De Souza Filho, Azevedo, & Brodie, 2003; Gad & Kusky, 2006; Gupta, 2017; R. D. Hewson, Cudahy, & Huntington, 2001; R. D. Hewson, Cudahy, Mizuhiko, Ueda, & Mauger, 2005; R. Hewson, Robson, Carlton, & Gilmore, 2017; Rob Hewson, Carlton, Gilmore, Jones, & Robson, 2018; Novak & Soulakellis, 2000; Pournamdari, Hashim, & Pour, 2014; Sultan, Arvidson, & Sturchio, 1986; van der Meer et al., 2012).

However, the potential spectral information that could be acquired by the remote sensing techniques can be affected by the vegetation unless the study area is a well exposed barren terrain. This is because of the remote sensing techniques are well established for arid and semiarid terrains where there is no vegetation (Ager & Milton, 1987; Grebby, 2011). However, a great proportion of our earth is covered by vegetation (Murphy & Wadge, 1994). So, within vegetated terrains the spectra of the geology could be the mixed average of the spectra of the vegetation and the spectra of the geology, thus, leading to a misinterpreted result.

Previous works have shown that the presence of vegetation could affect the geologic image interpretation either by obscuring the spectra of underlying minerals and rocks (Carranza & Hale, 2002; Crippen & Blom, 2001; Fraser & Green, 1987; Grebby, 2011; Grebby, Cunningham, Tansey, & Naden, 2014; Murphy, 1995; Murphy & Wadge, 1994; Yu, Porwal, Holden, & Dentith, 2011) or by completely dominating the overall spectrum (Siegal & Goetz, 1977). (Grebby et al., 2014) used airborne multispectral data within the VNIR range and concluded that 30-40 %, 50-65% and 75% green grass vegetation can obscure low, medium and high albedo rocks respectively; 20-40% of dry grass obscures most of the rocks and 30% -50%, 50-70 % of lichen can obscure and completely mask rocks respectively. (Siegal & Goetz, 1977), used MSS data, and concluded that a 10% green grass cover can mask the spectral characteristics of andesite and limestone. In addition, (Murphy & Wadge, 1994) has concluded that amalgamated granite and slate soils are largely confused at a vegetation cover greater than 50-60 % from airborne and ground imaging spectrometer data.

According to (Clark, 1999), vegetation spectra can be characterized into two general forms: the green and wet (photosynthetic), and the dry non-photosynthetic (Figure 1 below).

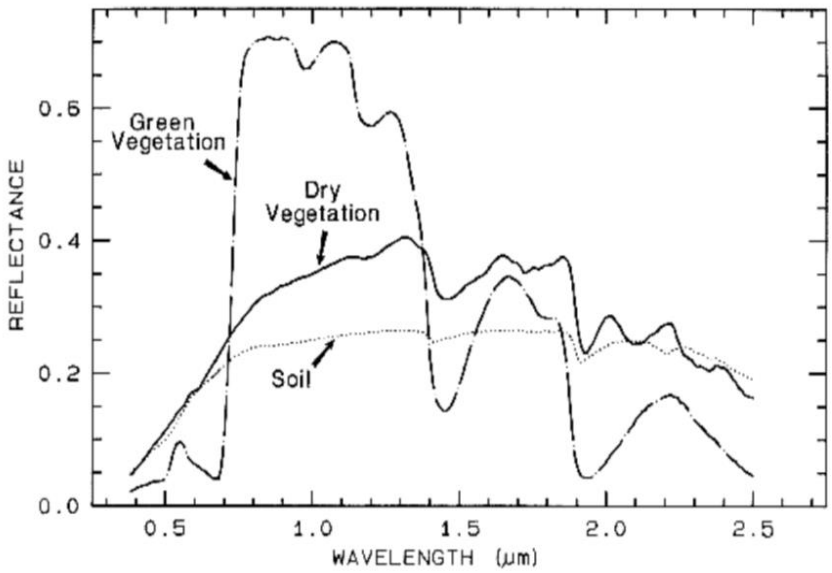

Figure 1: Reflectance spectra of photosynthetic (green) vegetation, non- photosynthetic (dry) vegetation, and a soil (Clark, 1999).

The near-infrared spectra of green vegetation are dominated by liquid water vibrational absorptions, where the water bands are shifted to slightly shorter wavelengths than in liquid water, due to hydrogen bonding (Clark, 1999). The dry, non-photosynthetic vegetation spectrum show absorptions due to cellulose, lignin, and nitrogen and some of these absorptions can be confused with mineral absorptions, unless a careful spectral analysis is done (Clark, 1999). Thus, different types of vegetation in different conditions might affect the spectral response of the minerals and/or rocks differently. However, in this research only the amount of green vegetation is taken in to consideration because of data and time constraints.

A little attention has been given to explicitly show how the reflectance of minerals and/or rocks within a given wavelength range vary because of a certain amount of vegetation and how much vegetation cover causes a sever effect. Also, there have not been detailed demonstrations showing the effect of vegetation on the spectra of the minerals and rocks imaged by ASTER. In addition, very few studies have used Landsat TM 5 for similar investigations (Crippen & Blom, 2001; Yu et al., 2011), indicating that much is yet to be known. Despite the general acceptance, that vegetation can have an influence on the spectral responses of minerals and rocks, there are limited published demonstrations that show the relationship between the spectral responses of the vegetation and non-vegetated (i.e. minerals, rocks) including the VNIR-SWIR bands of the ASTER and Landsat datasets. An understanding of the nature and extent of influence of vegetation on the spectral responses of the mineral/rock imaged by Landsat and ASTER is vital for deciding the type of data sets suitable for the mapping of minerals and rocks across vegetated terrains.

Apart from evaluating and understanding the effect of vegetation on the spectral signatures or minerals and rocks, it is also important to understand how to overcome the influence of vegetation and enhance the geological/mineralogical interpretation. Accordingly, previous studies have developed and /or used spectral mixing-unmixing, integrating ancillary data, linear regression model, unsupervised classification, forced invariance and other techniques to overcome the influence of vegetation on the spectral discrimination of the underlying geological information (Bierwirth, 1990; Chabrillat, Ceuleneer, Pinet, Mustard, & Johnson, 2000; Crippen & Blom, 2001; Dong & Leblon, 2004; Fraser & Green, 1987; Haest & Caccetta, 2013; Morison, Cloutis, & Mann, 2014; Mshiu, 2011; Rodger & Cudahy, 2009; Rogge, Rivard, Grant, & Pardy, 2010; Zhang, Rivard, & Sánchez-Azofeifa, 2005).

According to (Crippen & Blom, 2001), all the previous techniques to overcome the influence of vegetation are related to spectral unmixing which requires a detailed knowledge of the spectral signature of materials known or assumed to be present in a scene. In contrary, (Crippen & Blom, 2001)'s Landsat TM 5 based technique (forced invariance technique, which subdues vegetation and enhance spectral response of lithology), require neither a detail knowledge of the spectral signatures of materials nor any complex mixing models.

According to (Crippen & Blom, 2001) the 'forced invariance' algorithm calculates images that are invariant with respect to vegetation index. The features represented by the vegetation index will not appear in the resultant images, since they will contribute no variance (Crippen & Blom, 2001). Thus, data for each spectral band are altered in an empirically derived way to produce a superior band that largely excludes contrasts related to variations in the abundance of vegetation (Crippen & Blom, 2001). According to the authors, the algorithm works well mostly for imagery of areas with open canopy forest and little understory so that strong lithologic spectra can remain after the vegetation spectra is suppressed. (Crippen & Blom, 2001) suggested that the forced invariance algorithm can also work well on other multispectral imageries. (Yu et al., 2011), who implemented the (Crippen & Blom, 2001)'s algorithm with some improvements using Landsat TM+7, also suggested the applicability of the algorithm for other multispectral imagery including ASTER. Despite the cited works on the use of the Forced invariant algorithm, there is no quantitative demonstrations on the performance of this algorithm in different scenarios of vegetation cover. Given the suggestions from previous studies, it is interesting to evaluate the role of the algorithm on ASTER imagery using Landsat as a control.

1.2. General objective

The main objective of this research is to evaluate the effect of vegetation cover on the spectral responses of minerals/rocks, and the performance of forced invariance algorithm to supress vegetation and enhance spectral response of mineral/rock in Landsat and ASTER imageries.

1.3. Specific objectives

1. To assess the potential influence of green vegetation cover that might have on spectral responses of minerals and/or rocks imaged by Landsat and ASTER.
2. To evaluate the role of the Crippen's and Blom's algorithm in suppressing vegetation and enhancing spectral responses of mineral/rocks on both the Landsat and ASTER images.

1.4. Research questions

1. How does a green vegetation affect the spectral responses (reflectance) of minerals and/or rocks imaged by Landsat and ASTER?
2. What amount of green vegetation cover can have a significant effect on the spectral responses (reflectance) of minerals and/or rocks imaged by Landsat and ASTER?
3. How comparable is the Crippen's and Blom's algorithm applied to ASTER VNIR-SWIR bands with the previously utilized Landsat to suppress the spectral expression of vegetation and enhance the spectral responses of minerals and rocks?
4. How good is the Crippen and Blom's algorithm to quantitatively enhance spectral responses of the minerals/rocks as applied to both sensors?

1.5. Hypothesis

1. Vegetation can reduce the diagnostic potential of the spectral responses (reflectance) of minerals and/or rocks imaged by both the VNIR-SWIR ranges of Landsat and ASTER imageries.

2. Any amount of vegetation cover can result in a false information on the interpretation of the spectral responses of minerals and/or rocks imaged by the VNIR-SWIR ranges of Landsat and ASTER.
3. The Crippen's and Blom's vegetation suppressing Landsat based algorithm can be better utilized in optical ASTER imagery to enhance mineralogical and/or lithological information under vegetated terrains compared to previously utilized Landsat.

1.6. Thesis structure

The thesis is organized with six chapters. **Chapter 1; the introduction** which describes the general introductory to the thesis including the background information, the statement of the problem, the objectives, research questions and the hypothesis of the thesis as well as the thesis structure of the thesis. **Chapter 2;** describes the geographic location, climate, topography, vegetation, tectonic and geologic setting of the study area as well as the datasets used in this study. **Chapter 3;** describes all the methodology used in the thesis including the procedures of the methodology. **Chapter 4;** Contains all the output results of chapter 3. **Chapter 5;** Includes the discussion of the results presented under chapter 4. **Chapter 6;** presents the conclusions and recommendations drawn based on this thesis work.

2. STUDY AREA AND DATA SETS

2.1. Location

The study site (covering approximately 1025 Km^2) is in the Rungwe Volcanic Province (RVP), SW Tanzania. The study site is approximately bounded by Latitude 8° 64' S and 8° 85' S and Longitude 32.97° E -33.36° E. The RVP covering about 3000 km^2 containing the Ngozi, Rungwe and Kiejo volcanoes (Fontijn, Williamson, Mbede, & Ernst, 2012; Macheyeki, 2016.) is found in the Rungwe district of Mbeya region, southwest Tanzania (Figure 2) bounded by approximately 8° 30' S and 9° 30' S and Longitude 33° E and 34° E. RVP is in the southern highland province of Tanzania, northwest of Lake Nyasa approximately 1000 km from the business city of Dar es Salaam (Mshiu, 2011). Rungwe district borders Kyela district in the South, Ileje district in the West, Makete district in the East and Mbeya district in the North (Tilumanywa, 2013)

2.2. Tectonic setting and Geology

Rungwe Volcanic Province (RVP) is a district found in the Mbeya region of South Western Tanzania across the East African Rift System (EARS) (Fontijn et al., 2012). It is located within the triple junction of EARS over the NW trending Rukwa rift, NW trending Nyasa rift and NE trending Usangu rift (Figures 2 & 3) (Delvaux et al., 2010; Fontijn et al., 2012). The RVP is known for its Neogene to recent volcanic eruptions, overlying the Cretaceous red sandstone and Karoo sediments and the Precambrian basement (Mshiu, 2011). The Ngozi, Rungwe and Kiejo volcanoes in RVP are trachy-dacite while the Kiejo volcano is basaltic to basaltic trachy-andesite (Macheyeki, 2016). RVP is also the area where the Geothermal system in Mbeya region with characteristic Ngozi-Songwe hydrothermal system, at the junction between the eastern and western branches of the EARS, is found (Delvaux et al., 2010).

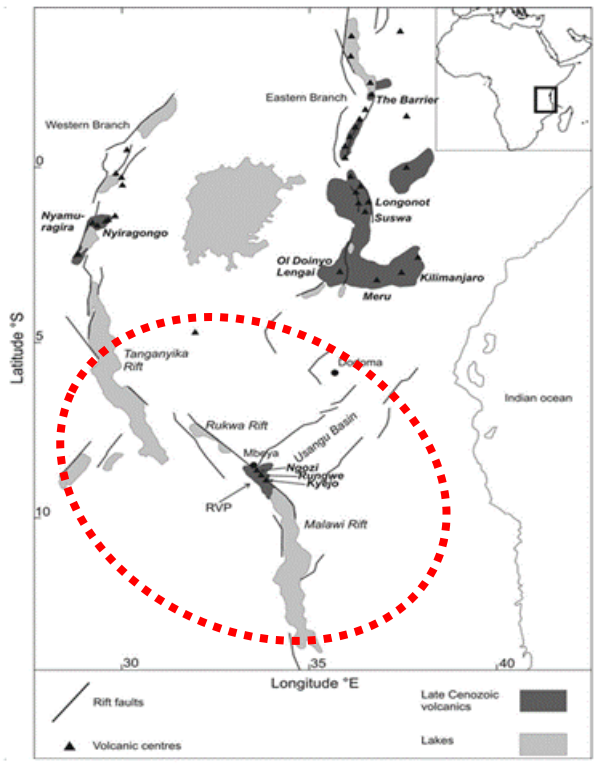

Figure 2: Location map of RVP within EARS showing surrounding rift basins: Malawi Rift, Tanganyika/Rukwa Rifts and Usangu Basin after (Fontijn et al., 2012). The red circle is referring to the RVP.

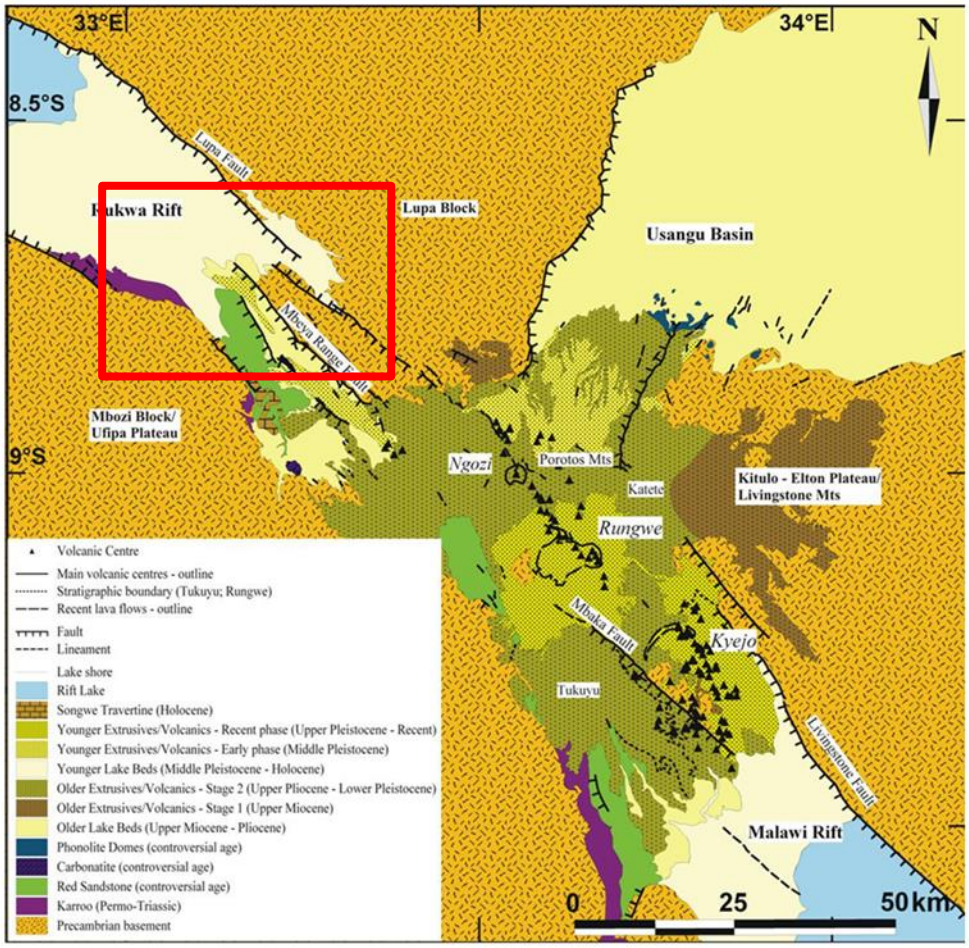

Figure 3: Geological map of Rungwe volcanic province (Fontijn et al., 2012); the red box is the study site.

2.3. Climate

The study area is part of the tropical climate with characteristic seasonal variations of dry (October to may) and rainy seasons (June to September) (Government, 2016). The rainfall varies from 650mm per Unum in the low lands to 2600mm in the highlands (Government, 2016). The temperature varies from about 16°C in the highlands to 30°C in the lowland areas (Government, 2016)

2.4. Topography

The study area is mountainous with Mt Rungwe forming the second highest peak in southern Tanzania at an altitude of 2, 981m and forms the northern extent of the Southern Rift in the Great Rift Valley (URT, 2017). The topographical features of Mt Rungwe include the mountain peaks and the dormant volcanic crater at the top of the mountain, Mt Rungwe, a dormant volcano, (URT, 2017). SRTM shaded relief DEM showing the general topography of the Rungwe volcanic province (RVP) is given below (Figure 4).

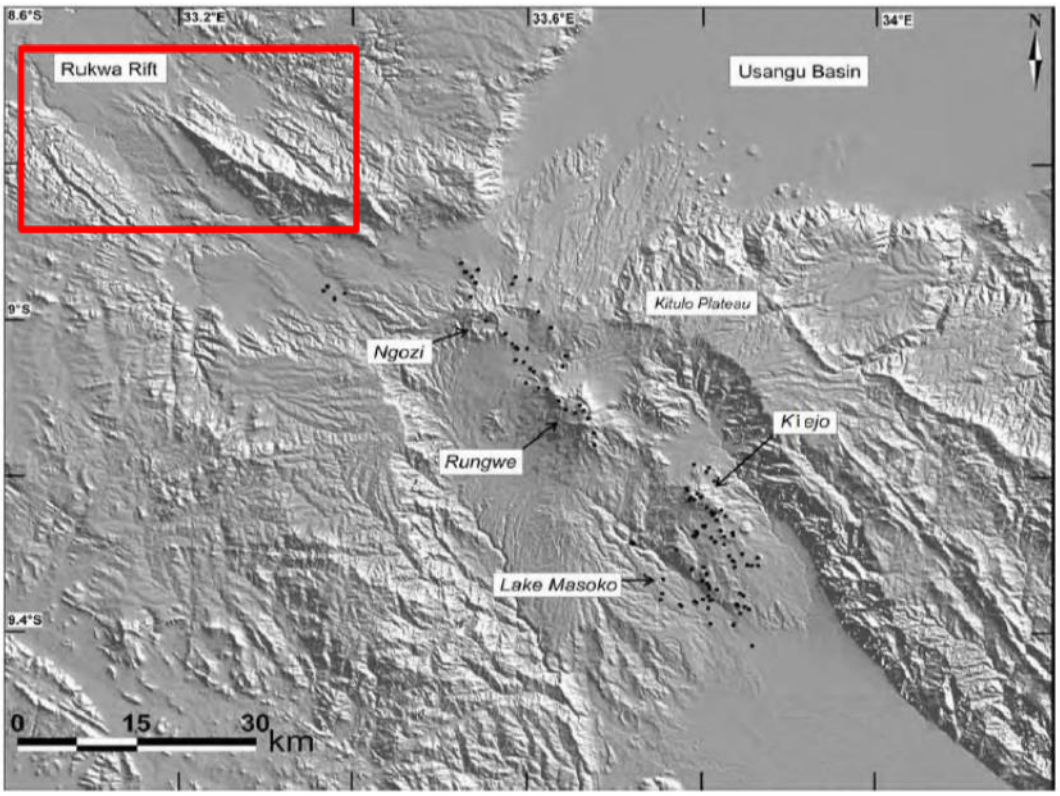

Figure 4: SRTM shaded relief DEM at 90m resolution of the Rungwe volcanic province region and main recent volcanic centres (the red box is the study site and the black dots represent eruptive centers) (after Macheyeki, 2016).

2.5. Soil

The soils in the study area are weathered products of the rocks found in the study area (Msanya, Otsuka, Araki, & Fujitake, 2007; Tilumanywa, 2013). Rock type where the soils are weathered from include: phonolitic-trachyte lavas and tuffs, olivine-basalts, pumice and ash (Msanya et al., 2007; Tilumanywa, 2013). The soils are characteristic of different colours and layers including black to brownish-gray top soil, dark greyish and dark brown as well as dark-yellowish-brown with sandy and clay loams on the steep slopes of Mt Rungwe with thin and quite rocky soils of the high grasslands and alternating layers of pumice-gravel-soil subsoils (Msanya et al., 2007; Tilumanywa, 2013).

2.6. Vegetation

The study contains a diversified natural vegetation (Figure 5) due to variation in climate, soils and topography (Range, 2016; Tilumanywa, 2013). Among the most dominant vegetation types include evergreen and semi evergreen species. These include indigenous trees, planted trees, grassland, bushland, miombo woodlands, bushed grassland, bush-shrubland, shrub grassland (Range, 2016; Tilumanywa, 2013). The largest open grassland consists of Eucalyptus spp "mikaratusi", Cynodon spp and Digitaris spp and is found in the relatively flat areas of the Rungwe volcanic mountain (Range, 2016). The vegetation in the study area has been one of the challenges for geologic mapping using remote sensing techniques (i.e. Landsat TM) by causing an overlapping problem in the spectra of minerals/lithologies (Mshiu, 2011)

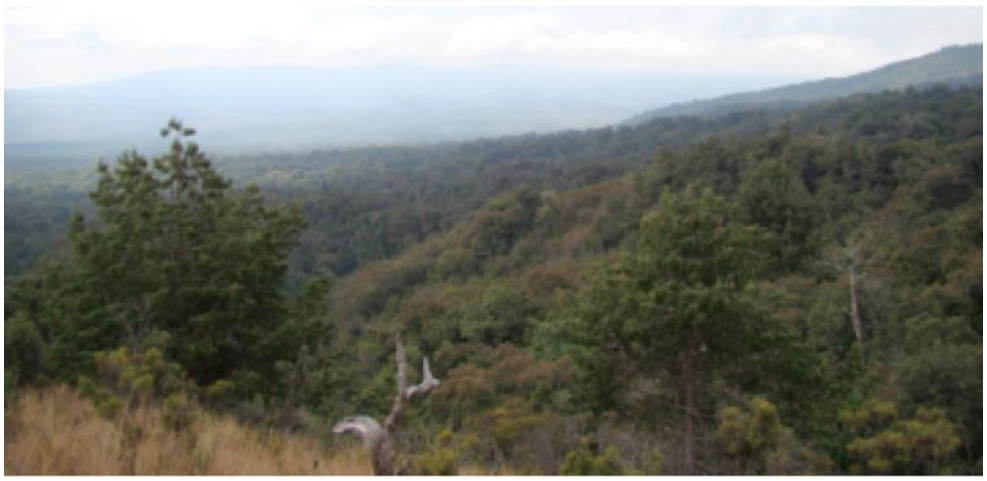

Figure 5: Picture showing thick vegetated areas around mount Rungwe in Rungwe Volcanic Province (Mshiu, 2011).

2.7. Data sets

The research has utilized ASTER VNIR surface reflectance and crosstalk corrected SWIR surface reflectance and Landsat surface reflectance imageries. The dates of acquisition and sources are presented in table 1 below.

Table 1: Data sets used in this research.

Sensor type	Data type	Source of data	Date of acquisition
Landsat TM 5 scene 1	Surface reflectance	https://earthexplorer.usgs.gov/	09-Jun-2005
Landsat TM 5 scene 2	Surface reflectance	https://earthexplorer.usgs.gov/	16-Jun-2005
ASTER	Surface reflectance	https://earthdata.nasa.gov/	11-Aug-2005

Due to limitations of full scene coverage, two Landsat images were mosaicked into one scene (figure 6A) for subsequent use. Then a subset between the resulting Landsat (figure 6A) and ASTER (figure 6B) images was done to obtain the intersecting area between both images within the study area.

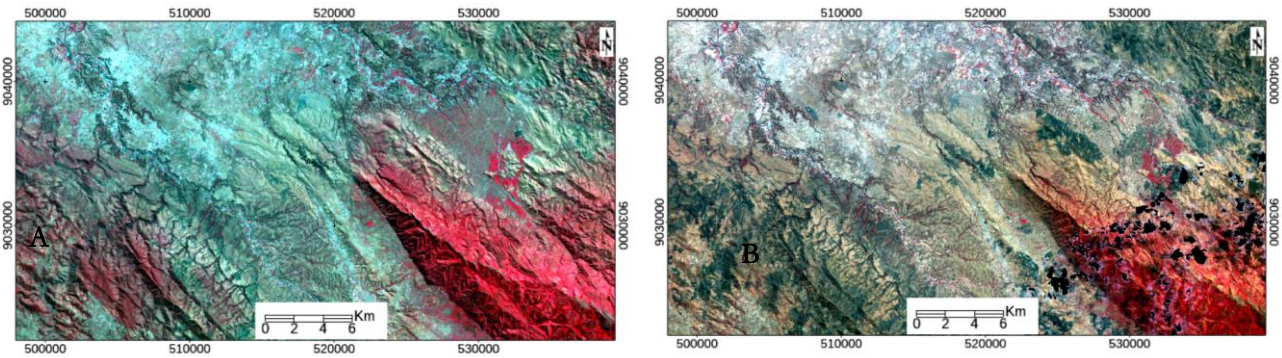

A: Landsat (RGB, 432) **B:** ASTER (RGB, 321)

Figure 6: Landsat (A) and ASTER (B) images acquired from RVP, SW Tanzania, over the same spatial position. The red shades in the false colour composite of both satellite images represent vegetation, while the grey colour represent non-vegetated areas. The dark pixels within and around the vegetated area in the ASTER image represent data of zero value (masked out pixels), which previously were occupied by clouds.

ASTER and Landsat are multispectral satellite sensors with fourteen and seven spectral bands respectively. The fourteen ASTER spectral bands cover 0.52 to 11.65 μm wavelength range while the seven Landsat spectral bands cover 0.45 to 12.5 μm wavelength range of the electromagnetic spectrum, only the six bands excluding band 6, are used in this research, however. ASTER contains three bands in the VNIR region (15m resolution), six bands in the SWIR region (30m resolution), and five bands in the TIR region (90m resolution) while Landsat contains four bands in the VNIR region (30m resolution), two bands in the SWIR region (30m resolution) and one band in the TIR region (120m resolution). The spectral characteristics of both the Landsat and ASTER are summarized in table 2.

Table 2: Spectral characteristics of the ASTER and Landsat Sensors (after Dagodzo, 2014)

ASTER				Landsat			
Subsystem	Band No	Spectral range (μm)	Spatial resolution (m)	Subsystem	Band No	Spectral range (μm)	Spatial resolution (m)
					1	0.45-0.52	30
VNIR	1	0.52-0.60	15	VNIR	2	0.52-0.60	
	2	0.63-0.69			3	0.63-0.69	
	3	0.78-0.86			4	0.76-0.90	
SWIR	4	1.60-1.70	30	SWIR	5	1.55-1.75	30
	5	2.145-2.185			7	2.08-2.35	
	6	2.185-2.225					
	7	2.235-2.285					
	8	2.295-2.365					
	9	2.360-2.430					
TIR	10	8.125-8.475	90	TIR	6	10.40-12.50	120
	11	8.475-8.825					
	12	8.925-9.275					
	13	10.25-10.95					
	14	10.95-11.65					

3. METHODOLOGY

3.1. Data preparation

Data preparation was done in four steps; mosaicking, layer stacking, spatial subsetting and cloud masking. These steps are described below.

3.1.1. Mosaicking

The Landsat scenes acquired on 09-Jun-2005 and 16-Jun-2005 are mosaicked to get a full coverage of the required area using ENVI software. Data acquired in multiple dates for the same purpose could cause inconsistences (i.e. variability of the vegetation conditions). However, due to lack of full coverage scene of the required study area, two scenes acquired within one-week difference are used and the one-week difference is accepted tolerably as insignificant difference.

3.1.2. Layer stacking

The Landsat image was downloaded with panchromatic bands. For subsequent processing, the bands were stacked using a free software, Multispec MFC application (A Freeware Multispectral Image Data Analysis System); a more detail about it can be found in (Biehl & Landgrebe, 2002). In addition, the 15m resolution bands of the VNIR and the 30m resolution bands of the SWIR ASTER images were stacked to get the combined VNIR-SWIR band range of 30m resolution using ENVI software.

3.1.3. Spatial subsetting

Images of both Landsat and ASTER were spatially subsetted into a required size (where both the Landsat and ASTER images intersect) of the study area using ENVI software and GIS. In addition, the geological map of the study area with the same spatial position to the Landsat and ASTER scenes is prepared to be used as a reference to the type of lithologies in the study area.

3.1.4. Cloud masking

Manually generated ROI based cloud and cloud shadow masking is done on the ASTER image to eliminate extreme values in the subsequent processing. Cloudy pixels were carefully digitized using the ENVI working windows.

3.2. Simulation model: Evaluation of the effect of vegetation on the spectral response of a bare ground

The effect of vegetation on spectral response of bare ground was evaluated as described in the steps below.

3.2.1. Simulation of vegetated and non-vegetated spectra via spectral mixing process

Spectra based simulation model is done to evaluate the potential influence of vegetation on the spectral responses of minerals and/or rocks imaged by both the Landsat and ASTER multispectral sensors. The simulation model is done via pixel based spectral mixing analysis for both the Landsat and ASTER images.

3.2.2. The concept and procedure of the simulation model

A pixel based spectral mixing analysis is performed to evaluate the influence of vegetation that might have on the spectral responses of minerals and/or rocks. Two pixels representing pure vegetation and pure non-vegetated bare area were selected for the subsequent processing. These end members were selected based on the standard NDVI ranges adopted from [(Bhandari, Kumar, & Singh, 2012; Chouhan & Rao, 2004)] and false colour composite images (Section 3.2.3, figure 7). A pure bear with approximate NDVI values of 0.1 (for both the Landsat and ASTER) and pure vegetation with NDVI value of 0.8 (of the Landsat) and 0.7 (of the ASTER) were selected from images of both datasets for the subsequent processing in the spectral mixing simulation model, a

thermotical model that involves mixing certain amount of vegetation with a certain amount of bare area to evaluate the influence of vegetation on the spectral response of the bare. The term bare in this research is referring to a mineral/rock and/or their weathered products such as soil where there is no vegetation cover while the term vegetation represents green vegetation. The simulation model is aimed to show the spectral variations in the spectral response of bare area due to a certain mixed reflectance value of vegetation of a certain percent cover. The assumption of this model is: suppose we have 100% cover bare area where the reflectance value at a given wavelength and band B is R. So, what will happen to R at a given band B if we linearly mix a certain amount of reflectance values of a certain percent coverage of vegetation to a certain reflectance value of a certain percent coverage of bare area with in the same band B such that the sum of percent coverage is 100?

The process of the simulation model is: first a representative pure bare and pure vegetation are determined. Then, to assess the possible variations of the spectral response of the bare area that might be caused due to the presence of a certain amount of vegetation cover, variable amount of vegetation cover is linearly mixed with certain amount of bare coverage where the result is summed to 100%. The 100% cover of the bare area assumes 0% cover of vegetation and vice versa. The analysis is done for each band of the scenes (six bands of the Landsat and nine bands of the ASTER). To calculate the reflectance values of the pixels for each band in each band of any percent coverage between 0 and 100, first the percent cover of the pure pixels is assumed to be 100. Then the reflectance values of the pixels of a certain amount of the vegetated and bare cover are calculated by multiplying the observed reflectance of the 100% coverage of the bare and vegetated areas by the required presumed percent coverage of the bare and the vegetated areas (equation-1a, 1b). For example, if the observed reflectance value of the 100% bare area at band 1 is 0.05; to get the reflectance value of the presumed 90% coverage of the bare area at band 1; the observed reflectance at band 1 (0.05) is multiplied by 0.9 which results 0.045. Finally, to get a certain value of a mixed spectra of a certain value of bare area and certain value of vegetation at a given band and wavelength, the presumed values of corresponding calculated reflectance values are summed up such that the summation is 100% (equation-2). For example, if the calculated reflectance value of 90% of bare coverage is 0.045, and the calculated reflectance value of 10% vegetation cover is 0.002, the reflectance of the mixed classes of 90% of bare and 10% of vegetation is the sum of 0.045 and 0.002 which is 0.047. List of tables showing the detail of the calculations and results are given in the appendices (appendix I).

$$\mathrm{RpBi} = \mathrm{aB}/100 * \mathrm{RoBi} \quad (1a)$$

$$\mathrm{RpVi} = \mathrm{bV}/100 * \mathrm{RoVi} \quad (1b)$$

$$\mathrm{Rmi} = \mathrm{RpVi} + \mathrm{RpBi} \quad (2)$$

Where **RpBi** represents the presumed reflectance of a bare at i^{th} band B; **aB**, any value between 0 and 100 of the bare; **RoBi**, the observed reflectance of the bare at i^{th} band B; **RpVi** represents the presumed reflectance of a vegetation at i^{th} band B; **bV**, any value between 0 and 100 of the vegetation; **RoVi**, the observed reflectance of the vegetation at i^{th} band B and **Rmi**, a calculated mixed reflectance value of both the bare and the vegetation at the i^{th} band B.
A spectrum resulting from the above equations can be simplified in to the following equation (equation 3).

$$\text{Mixed spectra} = \text{x\% bare spectrum} + (100 - \text{x})\ \%\ \text{vegetation spectrum} \quad (3)$$

3.2.3. Selection of endmembers for the input of the simulation model

Two spectral signatures were selected from pure pixels in the image representing pure vegetation and pure bare area for subsequent processing. The selection of the endmembers is done using Normalized Difference Vegetation Index (NDVI) method, according to (Bhandari et al., 2012; Chen, Srinivasan, Fedosejevs, & Kiniry, 2003) and natural colour combinations. The NDVI is one of the common and widely used index to highlight a vegetated area in remotely sensed satellite images which is the result of the difference of near infrared band (NIR) and the red band of the visible (VIS) divided to their sum (equesion-4) (Bhandari et al., 2012; Chen et al., 2003).

The NDVI is defined as;

$$NDVI = \frac{NIR-VIS}{NIR+VIS} \qquad 4$$

The NDVI values range from -1.0 to +1.0 where the high reflectance of the near-infrared band and low reflectance of the red band on vegetation produce a positive NDVI while the low reflectance of the near-infrared band and high reflectance of the red band on cloud, snow, and water produce a negative NDVI (Bhandari et al., 2012). The various levels of NDVI values can be used to distinguish various land cover types. For example, very low value of NDVI (0.1 and below) correspond to barren areas of rock, sand, or snow, moderate values represent shrub and grassland (0.2 to 0.3), while high value indicates temperate and tropical rainforests (0.6 to 0.8), bare soil is represented with NDVI values close to 0 and water bodies are represented with negative values (Bhandari et al., 2012; Chouhan, Rajlaxmi; Neeraj, 2004).

In addition to the NDVI method, additional information from visual inspection of false colour RGB combinations of the satellite images were used to differentiate between bare areas and vegetated areas. The colour combination of the datasets is based on the RGB combinations of the wavelengths or wavelength regions within: 1.6μm (red band), 0.8μm (green band), and 0.6μm (blue band) where the reddish/pink shades, green shades, and cyan/blue shades are associated with bare area, vegetation and clouds/water (if any) respectively. Accordingly, bands 5, 4, 2 and bands 4, 3, 1 are used to make RGB colour composite of the Landsat and ASTER images respectively as shown in figure 7 below. The selected pixels are saved as ROIS' and Vector files so that they are used in the subsequent processing. Then, the spectral signatures of the selected pixels are generated from the statistical data of the ROIS' and the mean spectral signature of the ROI's were used as the spectra of the endmembers (Figure 7 below).

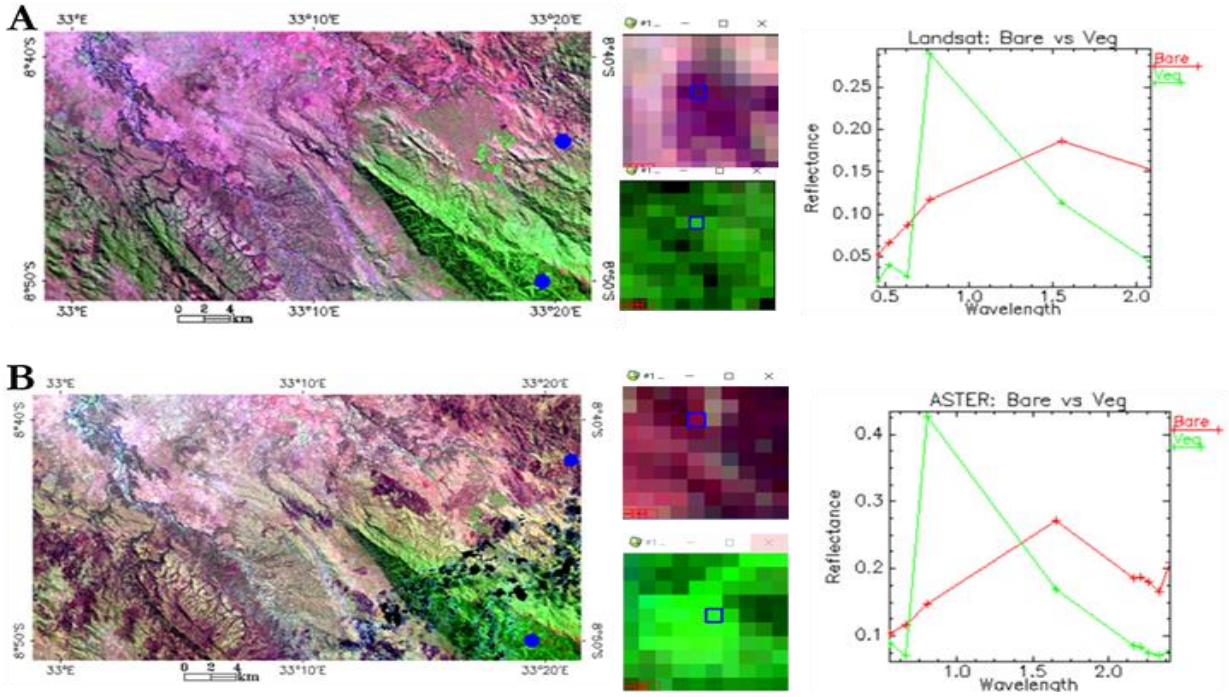

Figure 7: Endmembers of selected pixels from Landsat (A) and ASTER (B). The representative spectra are from a mean of a pixel (see zoomed images), their spatial position is shown in the full-size images.

As can be seen from the geological map (Figure 8 below) of the same spatial position of the Landsat and ASTER images, the vegetation endmember of both images is taken from the same spatial position (blue, Landsat and green, ASTER pixels overlapping in the geological map). However, the endmembers of the bare area are taken from different spatial positions of the Landsat and ASTER images because of the variations in the NDVI values of the images affecting the selection of the endmember based on the required NDVI threshold value.

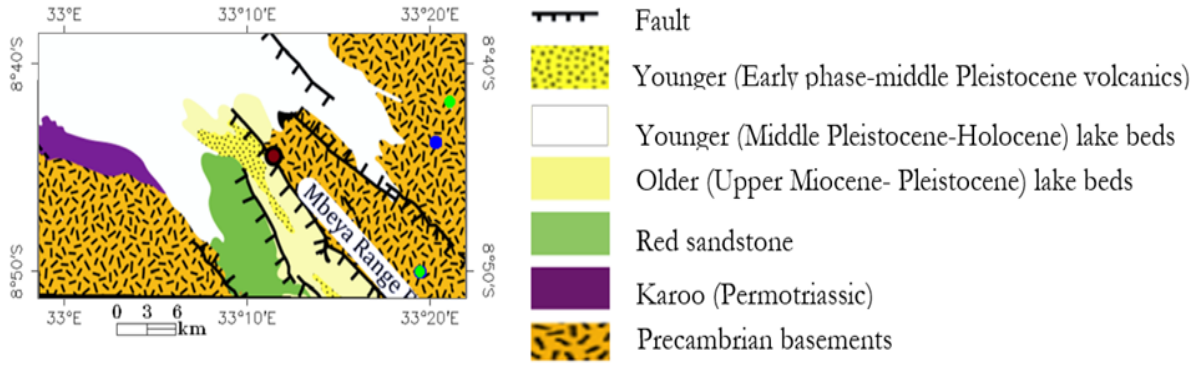

Figure 8: Geological map of the study area subsetted from the geological map of Rungwe volcanic province (RVP), after Fontijn (2012). The green and blue dots on the map are to show the spatial position (with respect to the geology of the area) of the endmembers selected from the Landsat and the ASTER images respectively.

3.2.4. Generation of the statistical data of the endmembers for the input of the simulation model

In this stage, the statistical data of the ROIs' of the selected pixels are generated and saved into a format that can be opened in Microsoft excel sheet. The statistics of the observed/original/ spectral signatures contains the reflectance values of the selected endmembers of each band in the corresponding wavelengths that are used as a basis for the simulation model. All the statistical information and the calculated numerical results can be found in the appendices (appendix I).

3.2.5. Simulation model: Bare and vegetation mixing procedure

In the mixing process one can choose any percent coverage between 0 and 100 of the representative bare and vegetated areas where the sum of the mixed values is 100%. In this research, nine mixing percent pairs of the bare and vegetation were used for the subsequent analysis of the endmembers of both the Landsat and ASTER imageries. These are: 95% bare, 5% vegetation; 90% bare, 10% vegetation; 80% bare, 20% vegetation; 60% bare, 40% vegetation; 50% bare, 50% vegetation; 40% bare, 60% vegetation; 20% bare, 80% vegetation; 10% bare, 90% vegetation; and 5% bare, 95% vegetation. A table showing these percent covers and their corresponding reflectance values at each band and wavelength is given in the appendices (appendix I).

3.2.6. Simulation model: Bare and vegetation simulation interpretation of results

The results of the simulation model (mixed spectra) of each data sets used (the Landsat and ASTER) were plotted together with the bare spectra, compared and interpreted using spectral ratio (the ratio of mixed spectra and bare spectra of each mixed model) and slope of the line of fit or trend lines (comparing trend lines generated from the mixed and the bare spectra in terms of the differences in their slope value). The purpose of these interpretations was to evaluate the influence of vegetation on the spectra of the bare.

3.2.6.1. Spectral ratios

The ratio of the mixed spectra (Bare plus vegetation) and the bare spectra are used to interpret the effect of vegetation on the spectral response of the bare across VNIR-SWIR bands of the Landsat and ASTER scenes. The assumption is that if the ratio of the mixed spectra to the pure bare is nearly or equal to one, the effect of

vegetation is less or unimaginable. Thus, the maximum possible bare information that can be acquired. However, when the ratio of the mixed spectra to the bare spectra is low or very low and/or high or very high (far from one), it implies that the effect of vegetation is high or sever so that the potential information that could be acquired from the bare is impossible. That means the spectra of the bare ground will be either obscured or overestimated (acquire higher values that are not from the bare ground, but from the vegetation).

3.2.6.2. Slope of linear equation

Trend lines were generated for both the observed and the mixed spectra and compared in terms of their slope values. The assumption is that the more the similarity of the slopes of the linear equations of the trend lines of the observed (expected) spectra and the mixed spectra, the more the similarity between the observed and the mixed spectra, and thus vegetation has no or very little effect on the spectral responses of the bare ground. That means the mixed spectra is overlapping or nearly overlapping to the expected spectra (bare), and thus, the less in the differences of their slope values.

The steps described above are summarized in figure 9 below.

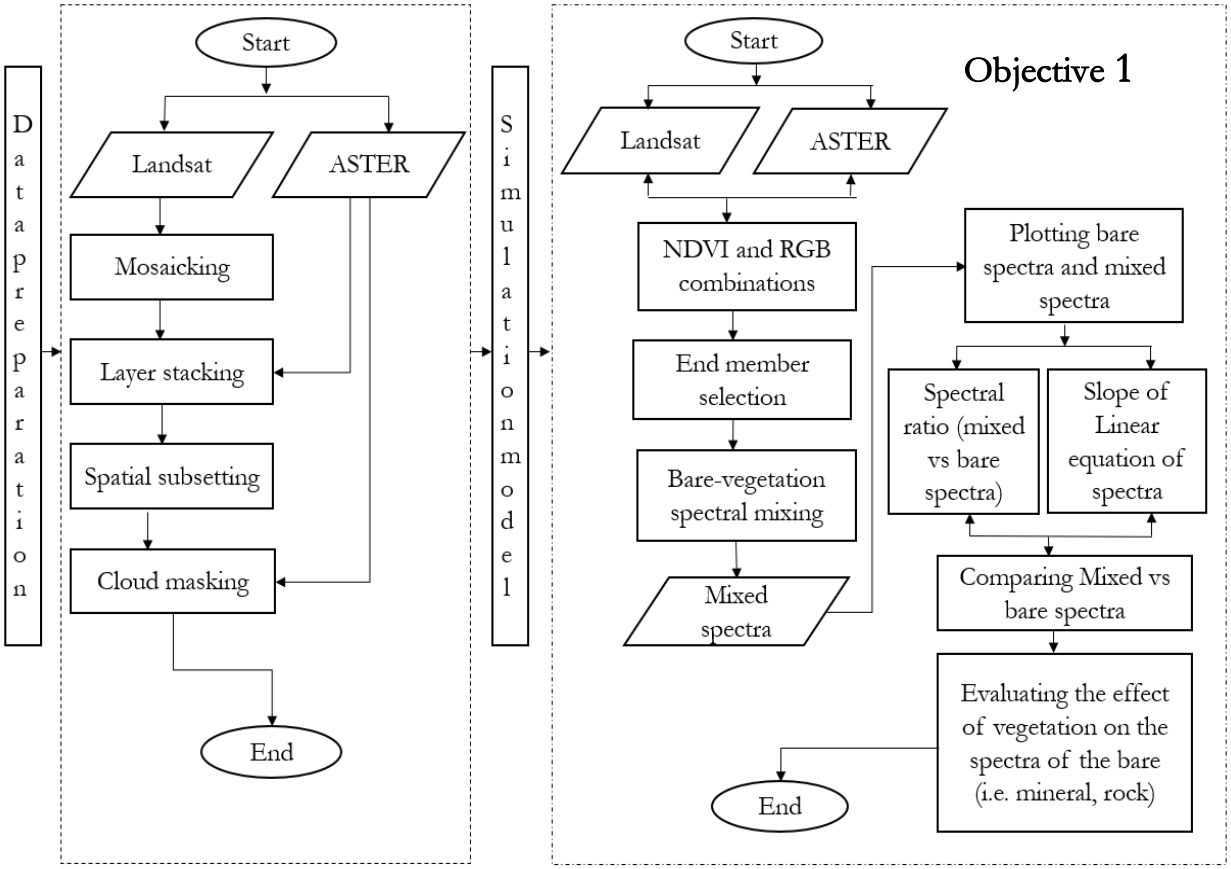

Figure 9: Flow chart showing the summary of the procedures of the evaluation of the effect of vegetation on the spectral response of bare ground (mineral/rock) (the right side) and the data preparation part (the left side).

3.3. Evaluation of the role of the vegetation suppressing Crippen's and Blom's algorithm

To assess the potential use of the Crippen and Blom's algorithm in the removal of the effect of vegetation followed by enhancement of minerals and rocks, first the algorithm is automatically applied to the Landsat and

ASTER images. Then, the processed (after applying the algorithm) images of both sensors are compared to their corresponding original images using different types of techniques including ratio images, NDVI images, ROI based spectral signatures and RGB combinations of ratio images.

3.3.1. The Crippen's and Blom's algorithm

The Crippen's and Blom's algorithm, "forced invariance", is an algorithm which subdues the spectral response of vegetation and enhance the spectral response of minerals/rocks forcing the image under process to be invariant with a vegetation amount (Crippen & Blom, 2001). The algorithm calculates images that are invariant relative to vegetation index so that features represented by that spectral index will not appear in the resultant images (Crippen & Blom, 2001). In the algorithm, data for each spectral band are altered empirically to produce a refined band (Crippen & Blom, 2001). The algorithm was previously utilized in Landsat 5 TM radiance data by (Crippen & Blom, 2001). Adopting the Crippen's and Blom's procedure, but based on the datasets used in this research (surface reflectance of Landsat, ASTER), the possible procedures of the algorithm could be;

- Preparing the data sets for the subsequent processing (i.e. mosaicking if we have more than one scene of the same sensor, layer stacking if our original data is downloaded as a set of panchromatic images or if we need to combine different wavelength regions of the same type of image sensor and spatial subsetting if needed and cloud masking if any).
- Calculation of vegetation index (NDVI)
- Rescaling the NDVI values to the reflectance values of the bands in the image
- Plotting reflectance values versus vegetation index values.
- Fitting a smooth best-fit curve to the plot by finding the average reflectance value at each scaled and quantized vegetation index value (or group of values) and smoothing the results over several quantized vegetation index values.
- Multiplicatively flatten the curve and drag all the pixels along with it. Selecting a target average reflectance value and multiplying all pixels at each vegetation index level by an amount that shifts the curve to that target. In other words, for each vegetation index level, multiply all pixels at that vegetation level by the target reflectance divided by the curve reflectance. Saturate any pixels that exceed the upper quantization limit.

  The above procedures can be summarized in the flow chart below (Figure 10)

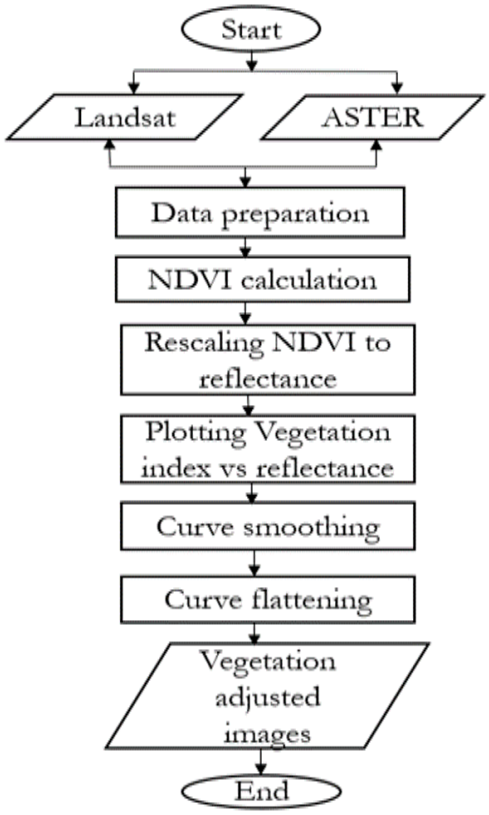

Figure 10: Generalized working procedures of the Crippen and Blom's algorithm

However, due to time constraints, this research does not cover the mathematical and computer codes (programming) of the algorithm to show the step by step functionality of the algorithm that are involved in the process. The algorithm is simply applied from the ENVI software automatically which only takes input images (pre-processed) and needs the visible and near infrared bands as input parameters.

Thus, this research rather assesses the role of the ENVI driven vegetation suppressing algorithm that might have on the Landsat and ASTER images in terms of suppressing vegetation and enhancing spectral responses of minerals/rocks. The aim is to assess the algorithm's utility using data analysis of the before and after results on both Landsat and ASTER, on an area with some geological control and diagnostic geological features, under variable vegetation covers. The original images of the Landsat and ASTER are compared to the corresponding processed images (after applying the algorithm) using the following techniques: (1). Ratio images (2) NDVI images (3), ROI based spectral signatures characterization (4) and RGB combinations of ratio images.

3.3.2. Ratio images

Ratio images of both LANDSAT and ASTER images were analysed to assess the role of the Crippen's and Blom's algorithm as applied to those datasets. The importance of this information processing is for evaluating the geologically interpretable signatures using band ratios whether they are enhanced with the Crippens and Blom's algorithm. Even though Landsat TM lacks ASTER's SWIR bands, both their ratio results can show spatially coherent geological meaningful anomalies (i.e. clay ratio B5/B7 and (B5+B7)/B6)) as well as examples of ferrous irons. Selected ratio images of both datasets were interpreted for checking possible mineralogical/lithological enhancements as the result of applying the Crippen's and Blom's algorithm. The selection of the mineral indices for this purpose is based on the similarity of the wavelength or wavelength ranges that the mineral indices have

a common feature as imaged by both the Landsat and ASTER images. This is because of the requirement that the comparison of the sensors for the role of the applied algorithm should be based on the common wavelength ranges that they cover.

The following examples of mineral indices were used to assess the Crippen and Blom's algorithm for both the ASTER (based on previously known indices) and the Landsat (empirically based on bands of similar wavelength regions).

I. AlOH group content (phengite, muscovite, paragonite, lepidolite, illite, brammalite, montmorillonite, beidellite, kaolinite, dickite) (B5+B7)/B6 (Cudahy, 2012)
[Landsat equivalent, (B5/B7)]
II. Ferrous iron index: (B5/B3) + (B1/B2) (Rowan, Mars, & Simpson, 2005)
[Landsat equivalent, (B7/B4) + (B2/B3)]

To evaluate the potential role of the Crippen's and Blom's vegetation suppressing algorithm that might have on the abundances inferred by the selected mineral indices, first ratio images of those mineral indices were generated using ENVI. Then, region of interests with respect to the different lithologies in the geological map are generated from the scenes of both datasets. Then, the abundances of the minerals based on the above indices as occurring in each lithology were compared between the abundances before and after applying the algorithm.

3.3.3. NDVI images

NDVI images of both LANDSAT and ASTER images were generated from the original and the processed images. Then those images were used to check the possible variations of NDVI values and NDVI trends before and after applying the Crippen and Blom's algorithm to assess the role of the algorithm that might have on the amount of the vegetation cover along a given profile. Scatter plotting of horizontal profiles across the NDVI images were generated from the same geographic position of each scenes both before and after applying the algorithm. Then the NDVI values of those profiles were compared using scatter plots to see the differences in the NDVI values of the before and after applying the algorithm.

3.3.4. ROI based spectral signatures

Vector defined regions of interests (ROI) were used to collect spectral signatures from the ASTER image both before and after applying the Crippen and Blom's algorithm. Due to limitation in the number of bands in the SWIR of the Landsat, only the ASTER scene is used for this purpose. First three ROIs' from areas of relatively low, medium, and high vegetation cover, were selected from the same lithology. Then the mean spectra of the ROI's were plotted and interpreted and compared in terms of wavelength absorption position and relative band depth (RBD) to check for any possible spectral feature differences due to the applied algorithm. In addition, in order to have a complete observation throughout the scene, another fourteen ROI's were generated from all parts of the images covering the different types of lithologies in the study area.

3.3.5. RGB combinations of ratio images

(Simon et al., 2016) showed RGB combinations of the ratio images of the Landsat scene including 4/3, 5/2, 3/1and 4/2, 5/3, 4/3 for lithological discriminations. In this research, the above ratio images were adopted to produce RGB composite images from the Landsat scene both before and after applying the Crippen and Blom's algorithm. This was done to examine the role of the algorithm in exposing previously vegetation obscured lithologies or lithologic boundaries. The RGB combinations of the ratio images before applying the Crippen and Blom's algorithm were compared to the corresponding results after applying the Crippen'a and Blom's algorithm in reference to the existing geological map of the study area.

3.3.6. RGB combinations of ratio images and principal component analysis (PCA)

Previous researches (Çorumluoğlu, Çorumluoğlu AVural, & Asri, 2013; Pournamdari et al., 2014), have shown that PCA and ratio images can be used for visual rock identification from images. In this research RGB combinations of ratio images of the same type obtained before and after applying the Crippen and Blom's algorithm were used for a better qualitative rock discrimination, given that the RGB combination of the ratio products are subject to PCA. Thus, each of the 3 ratio band products were used as input to PCA processing and then displayed as RGB images of the produced PC1, PC2 and PC3.

The summary of all the above methods is given in the following flowchart (Figure 11).

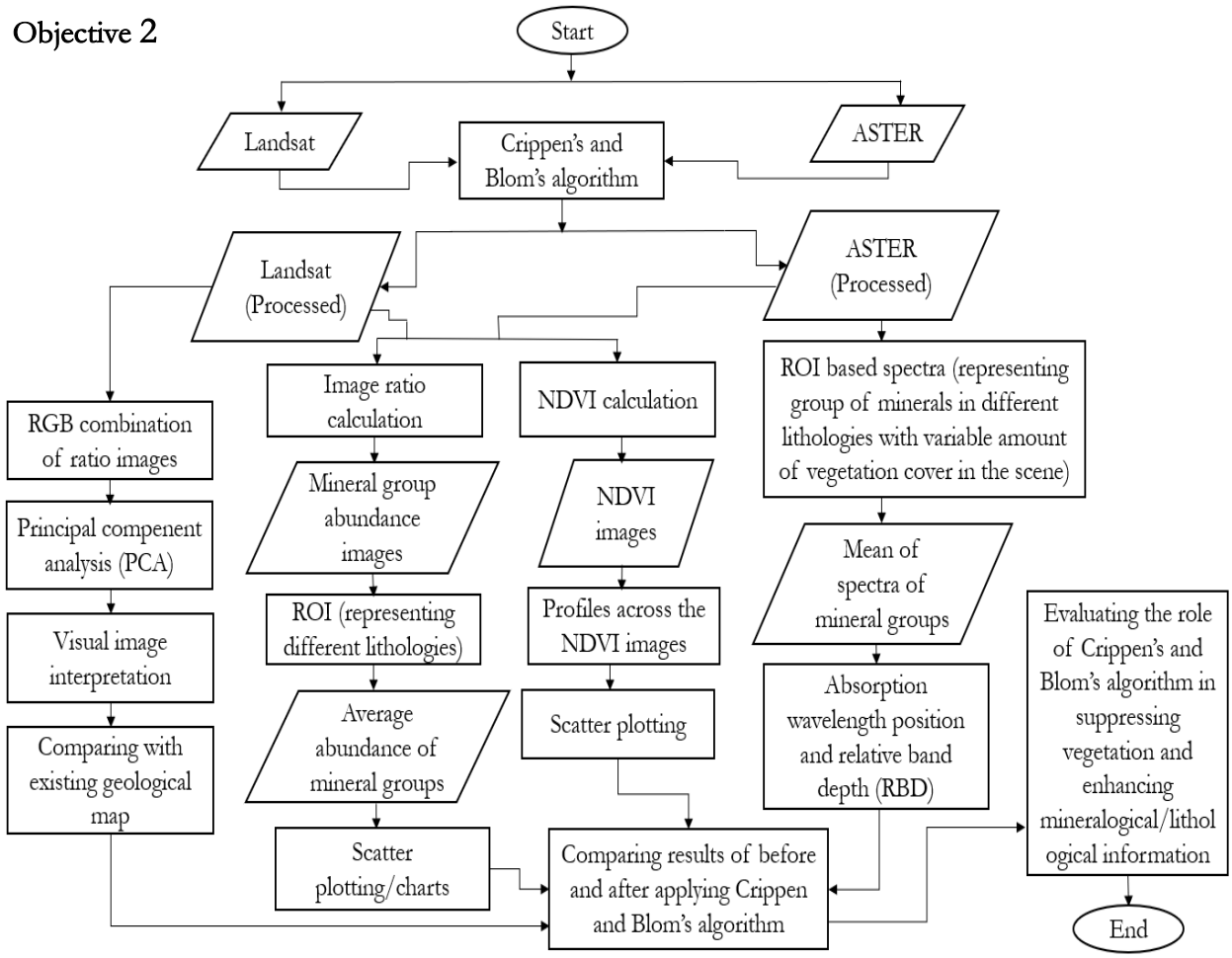

Figure 11: Flow chart showing the summary of the procedures of the evaluation of the role of the Crippen's and Blom's vegetation suppressing algorithm to enhance the spectral response of bare area (mineral/rock) across vegetated terrains.

4. RESULTS

This chapter contains results of the bare-vegetation simulation model to evaluate the effect of vegetation on the spectral responses of a bare ground (mineral, rock) as well as ratio images, NDVI images, ROI based spectral signatures, RGB combinations of ratio images and PCA applied on RGB combinations of ratio images to evaluate the role of Crippen's and Blom's vegetation suppressing algorithm in suppressing vegetation and enhancing the bare. 'Bare', in this research is assumed to represent mineral/rock and/or weathered products minerals/rocks in a non-vegetated terrain and the term vegetation is referring to a green vegetation. Due to limitations in spectral resolution of the datasets used, specific minerals (i.e. kaolinite, alunite) were difficult to be determined from the image data sets, hence a general term 'bare' ground (i.e. mineral/rock of ant type, based on published NDVI ranges, section 3.1) was used in the subsequent processing and interpretation.

4.1. Simulation model: Evaluation of effect of the vegetation on the spectral response of a bare ground

A total of nine bare-vegetation spectral simulation models, when vegetation cover is 5%, 10%, 20%, 40%, 50%, 60%, 80%, 90% and 95% were generated for both the Landsat and ASTER data sets. Spectra of the Landsat and ASTER images showing the spectral signature of a bare ground and the mixed spectra when vegetation cover is 5%, 10%, 20% and 80% plotted with the 100% bare (observed spectra) are shown in the following figures (Figures 12 and 13, A, B, C and D respectively). The remaining results when vegetation cover is 40%, 50%, 60%, 80%, 90% and 95% are given in the appendices (appendix II).

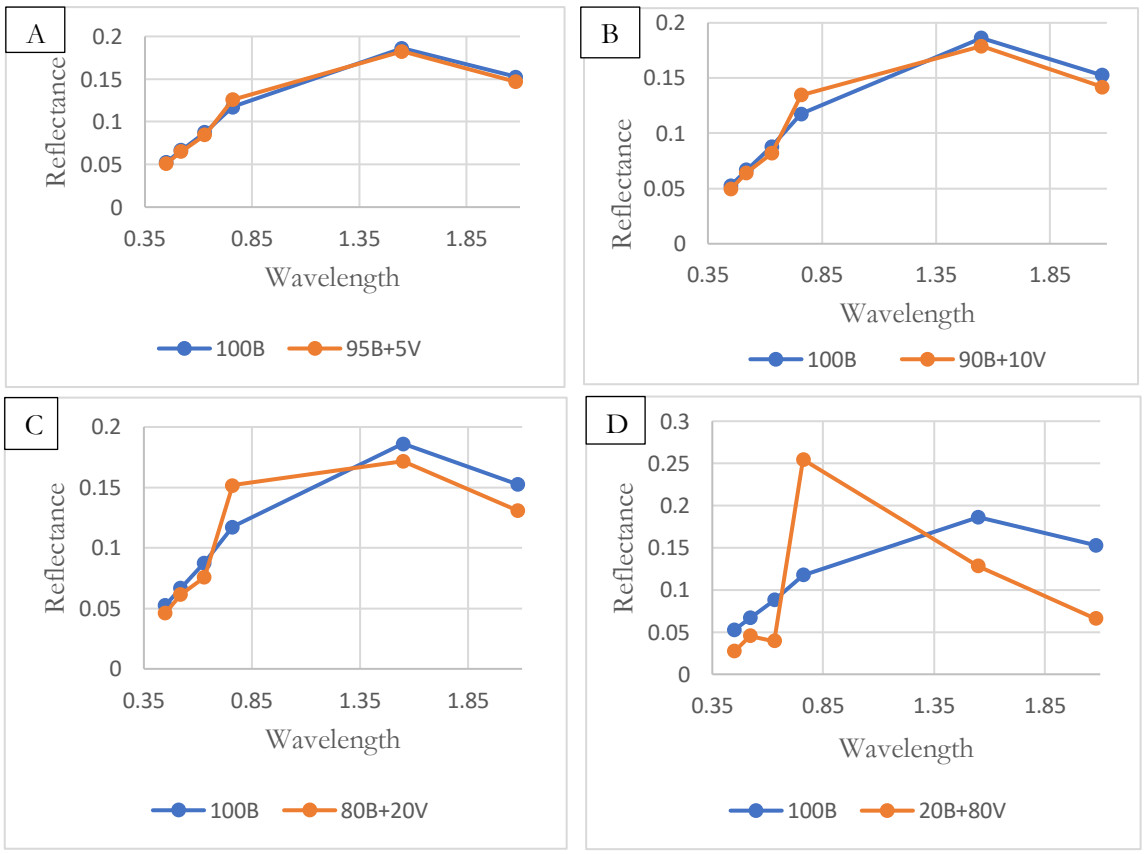

Figure 12: Bare spectra versus mixed spectra of variable amount of vegetation (Landsat)

From figure 12 above, the variations between the mixed spectra and the bare spectrum increases with increase in the % of simulated vegetation cover. This trend of variation is similar for both Landsat and ASTER as can be seen in figure 13 below.

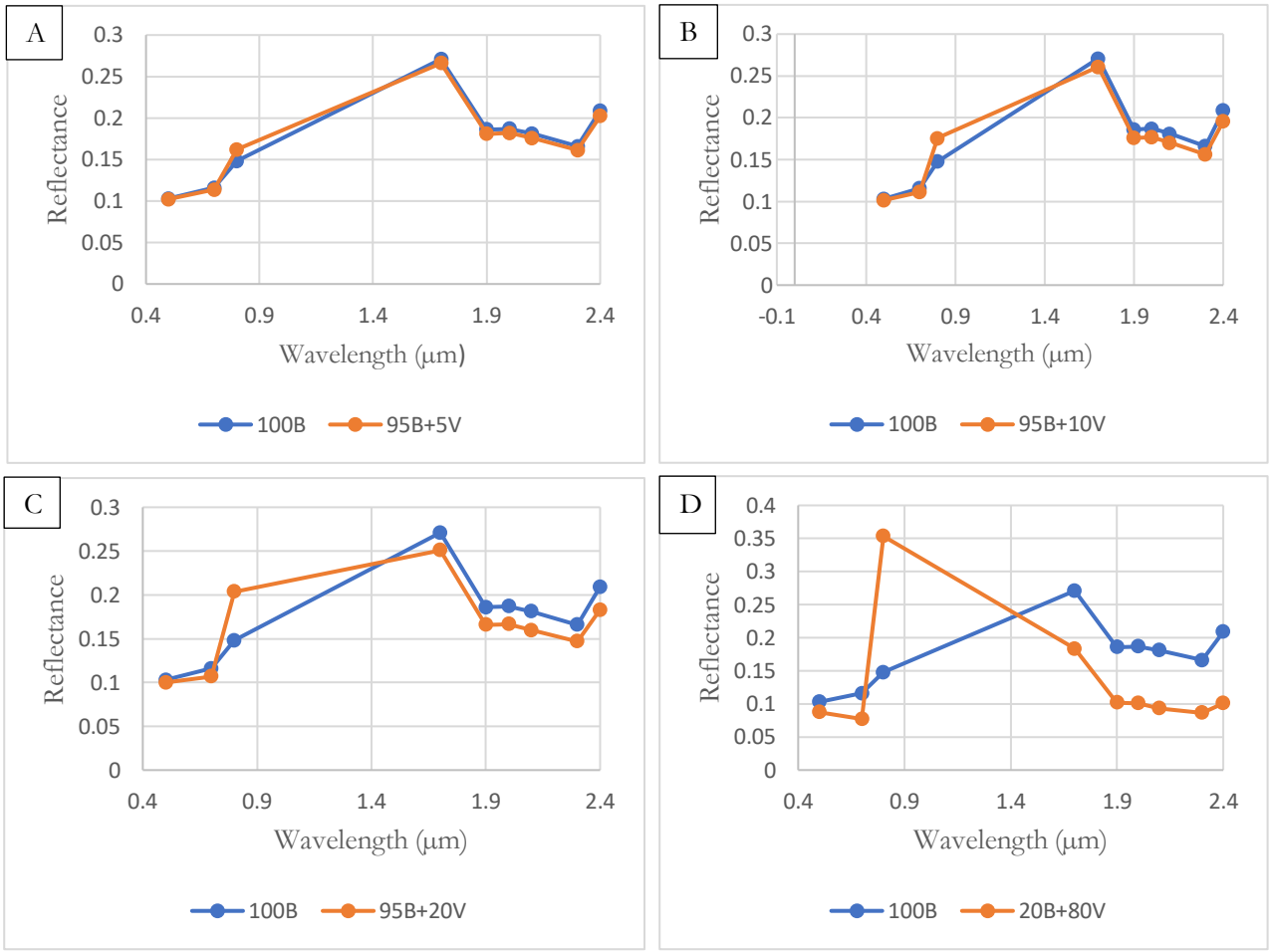

Figure 13: Bare spectra versus mixed spectra of variable amount of vegetation (ASTER)

The effect of vegetation on the spectra of bare described in Figures 12 and 13 above, was further analysed using spectral ratio and line fitting.

4.1.1. Spectral ratios

Generally, the results from spectral ratio analysis reveal that increase in the percentage of vegetation increases the variation in ratio value away from 1. In the case of Landsat image (Figure 14, A below), the first three bands were relatively less affected by vegetation cover of 5%, 10% and 20%, compared to the other bands. Similarly, for the ASTER image (Figure 14, B), a relatively lesser impact is recorded when vegetation cover is 5%, 10% and 20%, and the influence also increases with increasing the amount of vegetation (i.e. 80%). Graphs showing the influence of the remaining vegetation covers (40%, 50%, 60%, 90% and 95%) are given in the appendices (Appendix III; A, B).

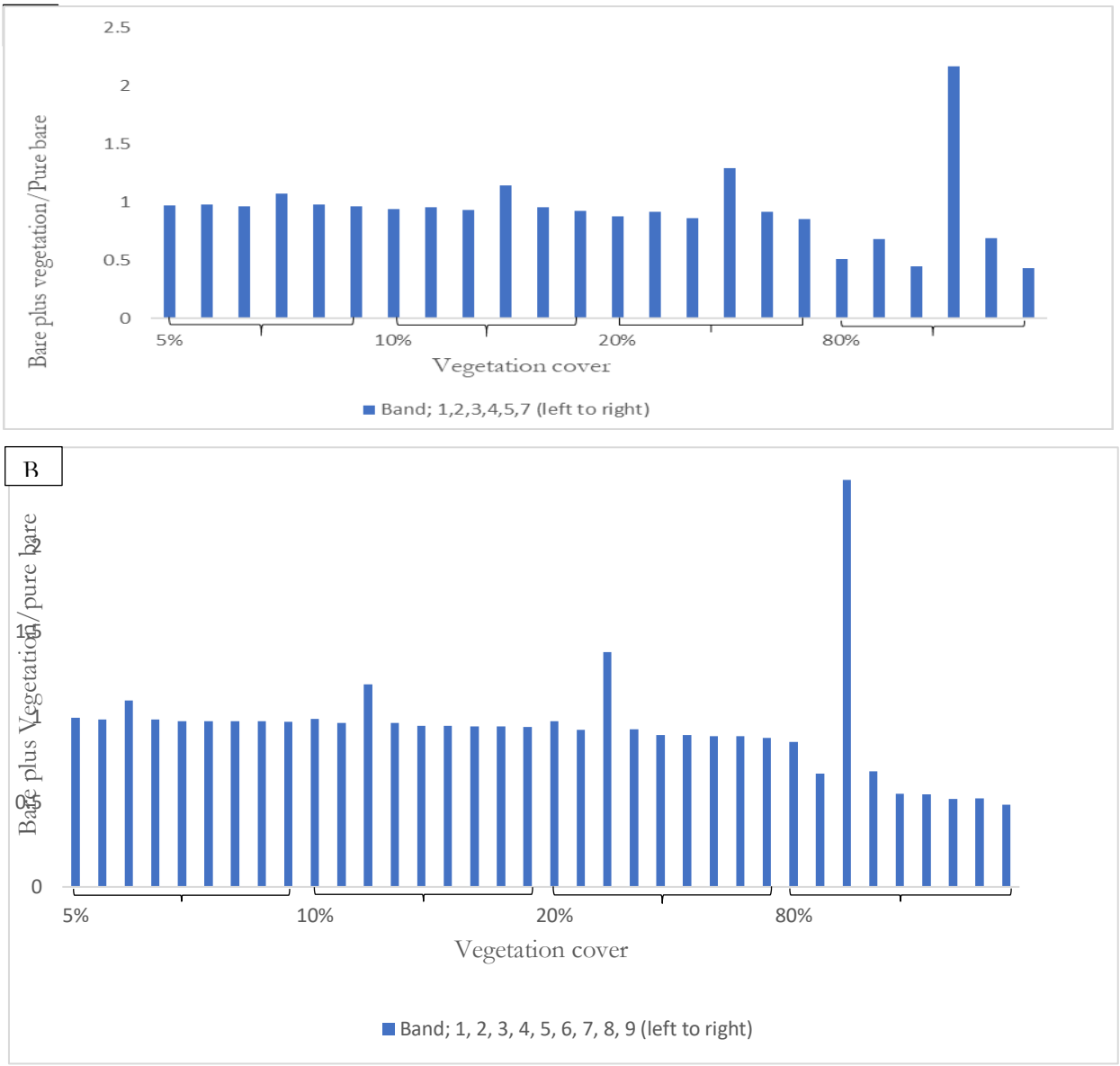

Figure 14: Column charts showing the effect of variable amount of vegetation on spectra of the bare in the Landsat (A) and the ASTER (B) imageries.

4.1.2. Slope of linear equation:

Analysing the slopes of the line of best fit, this study reveal that increase in the percentage of vegetation cover increase the differences in slope. The graphs are shown in (Figures 15 and 16; A, B, C, and D) where vegetation cover is 5%, 10%, 20%, and 80% respectively). The remaining simulation model results for the maximal vegetation effects (when vegetation cover is 40%, 50%, 60%, 90% and 95%) are given in appendix IV.

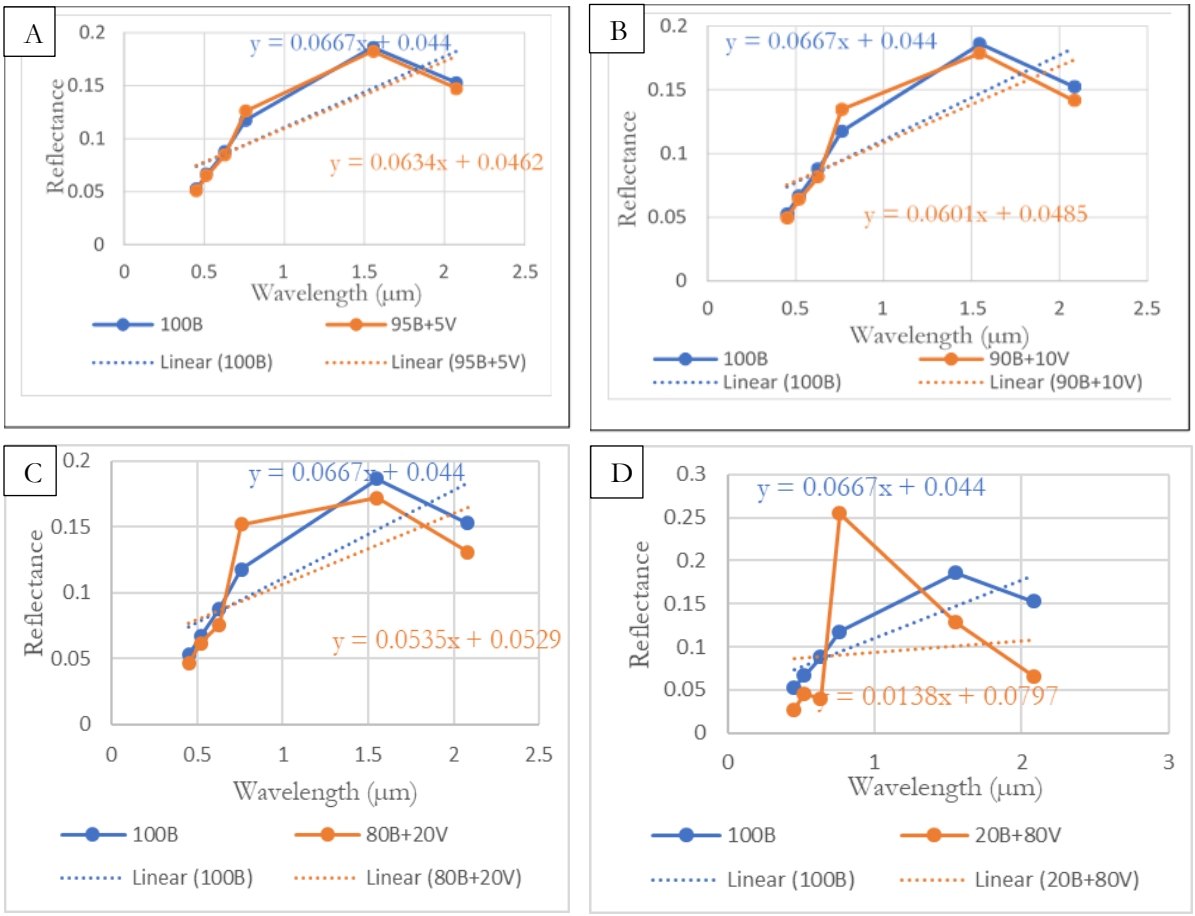

Figure 15: Spectral signature variations of bare area with variable mixture of green vegetation (A-D) of the Landsat scene. The influence of vegetation in the spectra of the bare is less when vegetation cover is 5% (nearly similar slopes of the trend lines (A)) and increases with increasing vegetation cover (the difference in the slope of the trend line gets increased (B, C, D)).

The above results show that for a vegetation cover of 20% or lower, the slope value of the trend lines of the observed spectra and the mixed spectra are almost similar. In this context, this means, the effect of the vegetation is insignificant and thus the higher chance of acquiring maximum information of the mineral/rock of interest. Conversely, when there is very high effect of vegetation on the spectra of the bare (Figure 16, D), the difference in the slopes of the trend lines is higher. That means all the required information that would be acquired from the bare (i.e. mineral/rock) is imperceptible.

The following figure (Figure 16) shows the spectral relationships between the mixed and bare spectra of the ASTER scene when vegetation cover is 5%, 10%, 20%, and 80% (A, B, C, and D respectively).

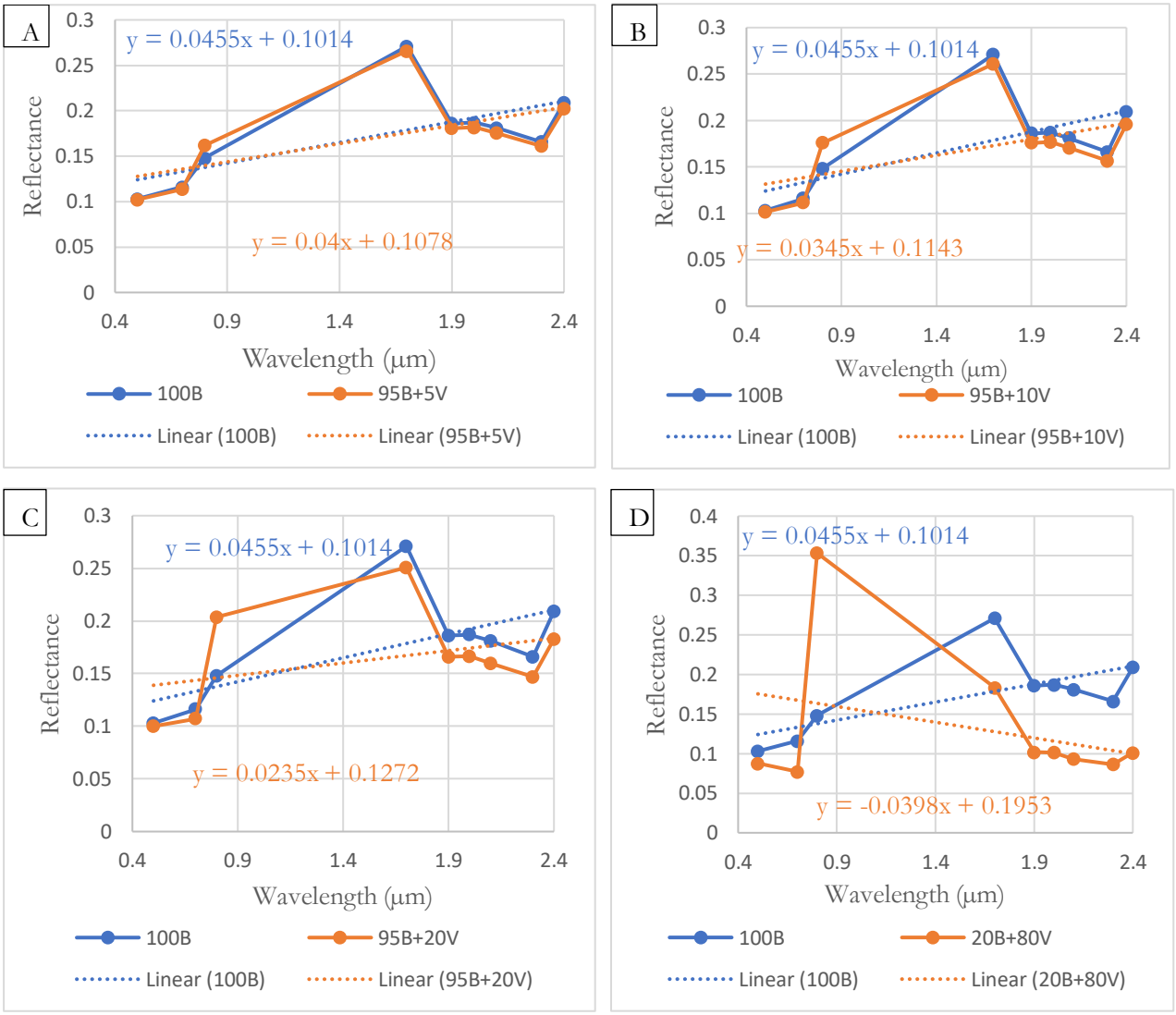

Figure 16: Spectral signature variations of bare area with variable mixture of green vegetation (A-D) of the ASTER scene. The influence of vegetation in the spectra of the bare is less when vegetation cover is 5% (nearly similar slopes of the trend lines (A)) and gets sever with increasing vegetation cover (the difference in the slope of the trend line gets increased (B, C, D)).

The above results in general show that in the presence of less than or equal 20% vegetation cover, the slope value of the trend lines of the observed spectra and the mixed spectra do not show great differences.

4.2. Evaluation of the role of the vegetation suppressing Crippen's and Blom's algorithm

Results, testing the potential of the Crippen and Blom's algorithm in supressing vegetation and enhancing mineralogical/mineralogical information was done using ratio images, NDVI images, ROI based spectral signatures characterization, RGB combinations of ratio images and PCA applied on RGB combinations of ratio images are demonstrated in the following sections.

4.2.1. Ratio images

The results of ratio images show the abundances of given mineral indices contained in the different types of lithologies both before and after applying the Crippen and Blom's algorithm. The basic statistics of the abundances are tabulated below, and the differences in the abundances of the before and after applying the algorithm are shown in scatter plots and column charts of the mean abundances of the mineral indices across each lithology. The abundances of the ratio images were generated from ROI's representing each lithology in the study area. The ROI's were generated from the different lithologies to assesses the differences in the abundances of the mineral groups across the different lithologies before and applying the Crippen and Blom's algorithm.

4.2.1.1. Ratio images (ASTER): AlOH group content [B5+B7)/B6] ((Cudahy, 2012))

According to (Cudahy, 2012), the ASTER band combination of [(B5+B7)/B6] can target absorption features at ASTER band 6 for AlOH group of clay minerals such as muscovite, illite, phengite, kaolinite and Al-smectite. Ratio images of the above index were produced from the ASTER image both before and after applying the Crippen and Blom's algorithm to check whether the algorithm has played a role to enhance the mineral content. A linear type stretching with 2.00 and 2.25 (based on (Cudahy, 2012)) of lower and upper limits respectively were used where the blue and red colours of the rainbow colour in the ratio images represent low and high values respectively (Figure 17; A, B). The geological map representing the study area showing the different lithologies is given side to side of the ratio images (Figure 17; C)

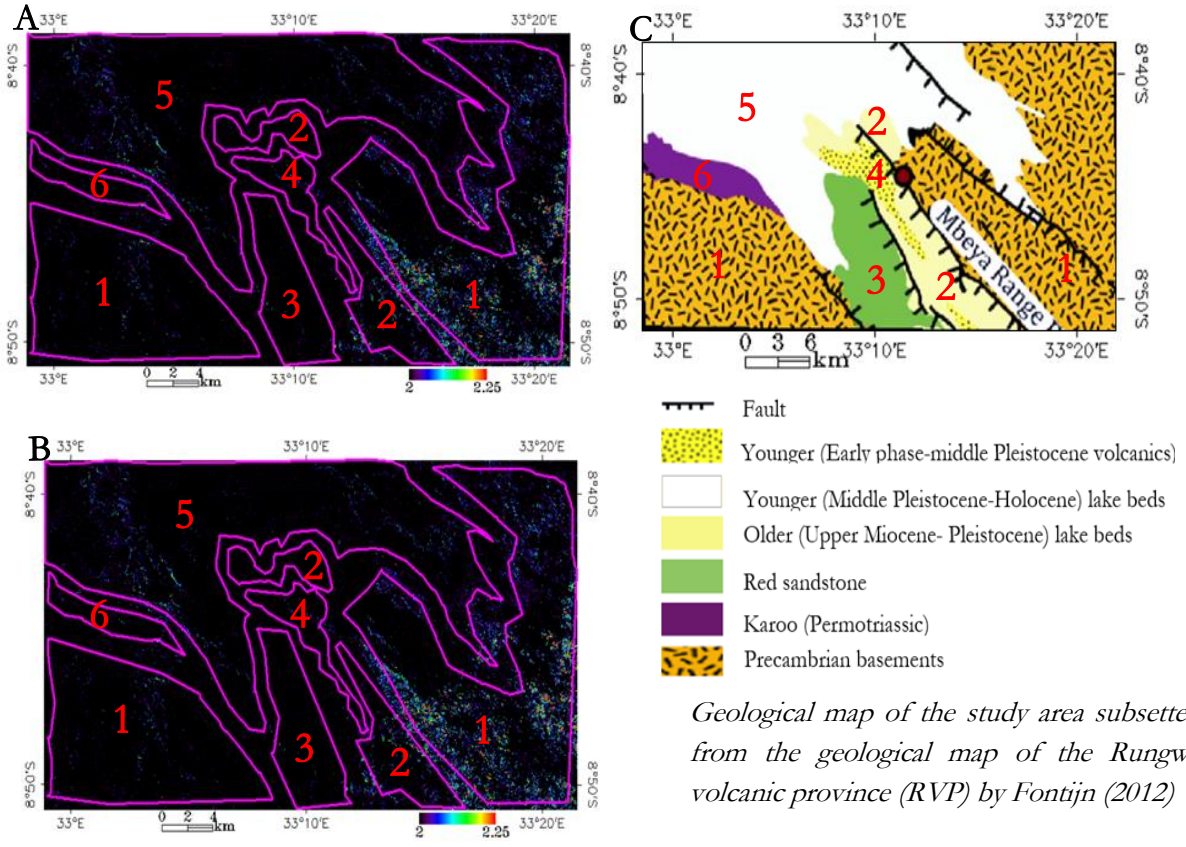

Geological map of the study area subsetted from the geological map of the Rungwe volcanic province (RVP) by Fontijn (2012)

Figure 17: Ratio images of AlOH group content before (A) and after (B) applying the Crippen's and Blom's algorithm in the ASTER. The polygons in magenta represent the different lithologies in the study area where number 1, 2, 3, 4, 5, 6, belongs to Precambrian basement, Older sediments (Lake beds), Red sandstone, Younger volcanics, Younger sediments (Lake beds) and Karoo respectively (C)). The image is divided in to parts based on the lithologic boundaries to assess the abundance of the mineral groups in each lithology both before and after applying the Crippen and Blom's algorithm.

In the figure given above (Figure 17), even though there are AlOH group content abundance values between 2.00 and 2.25 in the different lithologies (as can be seen from the basic statistics of the ratio images in table 3), the mean statistics (average abundance statistics) shows there are no abundance values within the threshold value stated according to (Cudahy, 2012).

Table 3: Basic statistics of the abundance of AlOH across the different types of the lithologies (applying the Crippen and Blom's algorithm (ASTER).

Basic statistics; ASTER: (float (B5) +float(B7)) / float(B6)

Lithology		Min	Max	Mean	Stdev
Precambrian basement (1)	Before	1.524194	2.731707	1.914645	0.080202
	After	1.524194	2.731707	1.914820	0.081254
Older sediments (Lake beds) (2)	Before	1.620690	2.557894	1.907525	0.061657
	After	1.556122	2.574074	1.907080	0.062893
Red sandstone (3)	Before	1.704348	2.196970	1.893407	0.048062
	After	1.704348	2.196970	1.893407	0.048062
Younger volcanics (4)	Before	1.741117	2.247312	1.895192	0.049451
	After	1.741117	2.247312	1.895192	0.049451
Younger sediments (Lake beds) (5)	Before	1.590361	2.560747	1.918835	0.051038
	After	1.590361	2.560748	1.918885	0.051072
Karoo (6)	Before	1.645161	2.210084	1.888574	0.054059
	After	1.645161	2.210084	1.888574	0.054059

To evaluate whether the Crippen and Blom's algorithm has made changes to the abundance images, a scatter plot and a column chart showing the relationship between the abundances of the minerals as well as mean ratio of the abundance images across the different lithologies, produced before and after applying the Crippen and Blom's algorithm are given below (Figure 18).

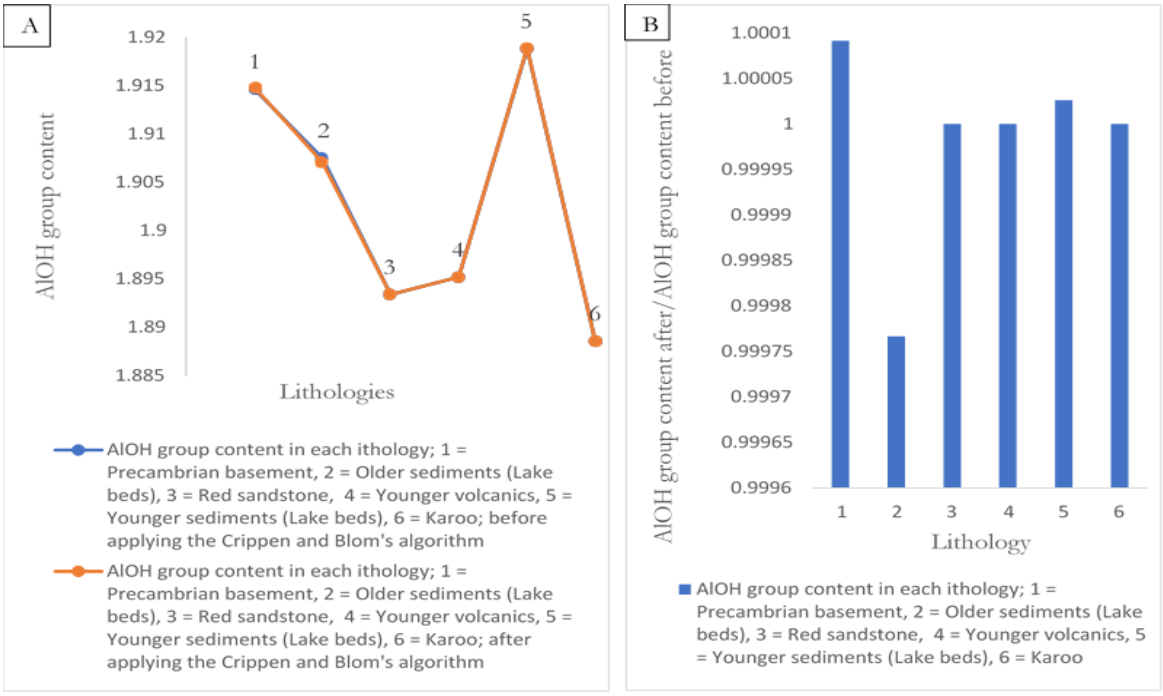

Figure 18: Scatter plot (A) and column chart (B) showing the abundances of the AlOH group content in each lithology (ASTER). The scatter plot (A) is showing the abundance of the AlOH group content before (blue) and after (orange) applying the Crippen and Blom's algorithm. The column chart shows the ratio of the AlOH group content after applying the algorithm to the ratio of the AlOH group content before applying the algorithm.

The above figures (Figure 18; A & B), show that the role of the Crippen and Blom's algorithm is very small to insignificant in the overall ratio images (A, scatter plots are overlapping; meaning there is no change because of the applied algorithm; otherwise the orange colour scatter should have to be above blue scatter plot). The assumption is that if the algorithm is successfully operating to enhance the AlOH group content, either the scatter plot or the column chart should show variations between the ratio images obtained after and before applying the Crippen and Blom's algorithm. Nonetheless, very small differences in the abundance of the AlOH group content in each lithology are observed in the column chart (B). For example, AlOH group content in the Precambrian lithology and the younger lake beds is enhanced to a very small percent (0.009% and 0.004% respectively), which is insignificant, however. The abundance of AlOH group content in the red sandstone is decreased after applying the algorithm. This could be due the effect of the algorithm itself during its process or because of the absence of detectable amount of AlOH in that lithology and the previous anomaly was probably due to vegetation only. The abundance of the AlOH group content in the remaining lithologies show no change (B). In summary, in this case, the Crippen and Blom's algorithm has not a significant role in enhancing the AlOH group content imaged by ASTER for this study area.

4.2.1. 2. Ratio images (Landsat): AlOH group content [B5/B7]

A Similar way to the AlOH group content presented using the ASTER image (section 4.2.1.1.), an AlOH group index (B5/B7) of the Landsat was used to evaluate the role of Crippen and Blom's algorithm in suppressing vegetation and enhancing the mineral (Figure 19). This band ratio is selected with the assumption that it approximately covers similar wavelength region with the ASTER. Thus, comparing the significance of the algorithm to enhance AlOH group content between the ASTER and the Landsat helps to understand in which of these sensors is the algorithm better applicable. The threshold values used are 2.00-2.25 with a linear type of stretch.

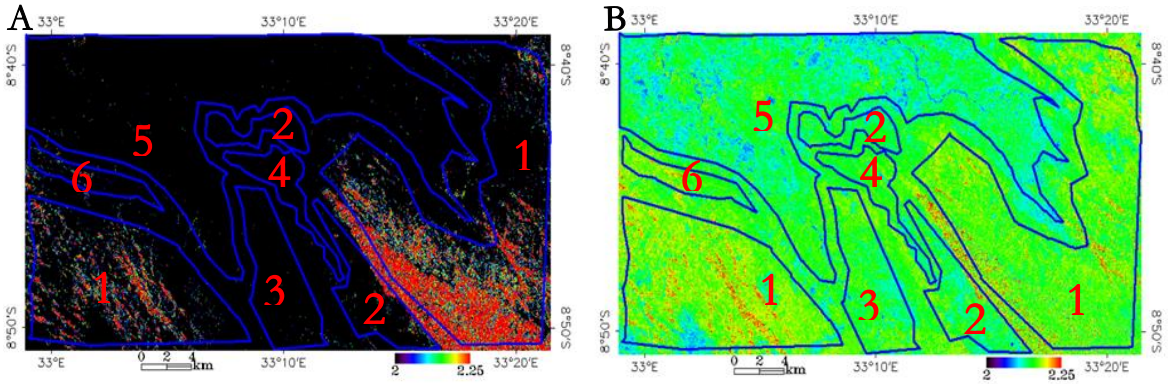

Figure 19: Ratio images of AlOH group content before (A) and after (B) applying the Crippen's and Blom's algorithm on the Landsat scene. The polygons in magenta represent the different lithologies in the study area where number 1, 2, 3, 4, 5, 6, belongs to the Precambrian basement, Older sediments (Lake beds), Red sandstone, Younger volcanics, Younger sediments (Lake beds) and Karoo respectively (C, Figure 18). The image is divided in to parts based on the lithologic boundaries to assess the presence of the mineral groups in each lithology both before and after applying the Crippen and Blom's algorithm.

In the above figure (Figure 19), the image in the left (A) seems to show higher content in the mountainous areas of the Precambrian basement (1). This all high anomaly might not be necessarily the AlOH group content. This is because these areas are the highly vegetated areas in the area so that water content from the leaves of the vegetation might also contribute causing the overall response to increase. In the second image (B), areas which previously were darker seems to be replaced by certain amount of AlOH group content. This could be probably due to the applied algorithm that enables detection of certain amount of AlOH group content. However, as can be seen from the scatter plot (Figure 20) and the basic statistics (table 4), there is no improvement in the abundance of the AlOH after applying the algorithm, all anomalies across the image rather become reduced

which probably could be because of false anomalies related with vegetation so that the previous anomaly was a vegetation and hence suppressed.

Table 4: Basic statistics of the abundance of AlOH across the different types of the lithologies before and after applying the Crippen and Blom's algorithm in the Landsat

Basic statistics; Landsat: B5/B7

Lithology		Min	Max	Mean	Stdev
Precambrian basement (1)	Before	0.632856	8.352942	1.894676	0.269957
	After	0.603782	10.352713	1.622183	0.149057
Older sediments (Lake beds) (2)	Before	1.056270	4.763158	1.622927	0.202385
	After	0.970472	4.119703	1.499393	0.123220
Red sandstone (3)	Before	0.931683	2.415254	1.609864	0.138014
	After	0.929509	2.335177	1.528439	0.114915
Younger volcanics (4)	Before	1.037867	2.220183	1.580528	0.115693
	After	1.048578	2.222788	1.535064	0.100407
Younger sediments (Lake beds) (5)	Before	0.572072	2.864043	1.499241	0.162115
	After	0.610678	2.848939	1.442205	0.124505
Karoo (6)	Before	1.097878	2.749367	1.744450	0.159031
	After	1.106760	2.518373	1.610605	0.111264

The following figures (Figure 20; A, B), show the variations in the abundance of the AlOH group content in the Landsat scene across the different lithologies. Both figures (A and B) show the AlOH group across all lithologies has reduced after applying the Crippen and Blom's algorithm. However, in a common sense the AlOH group abundance values both before and after applying the Crippen and Blom's algorithm are below the standard threshold values of AlOH used in this research (2.00-2.25, (Cudahy, 2012). Thus, the reduction in the detected anomaly could be probably because of the original anomaly was due to vegetation and hence the vegetation gets suppressed by the applied algorithm. Such kind of situation might happen in areas where there is no enough amount of detectable mineral/rock of interest but vegetated.

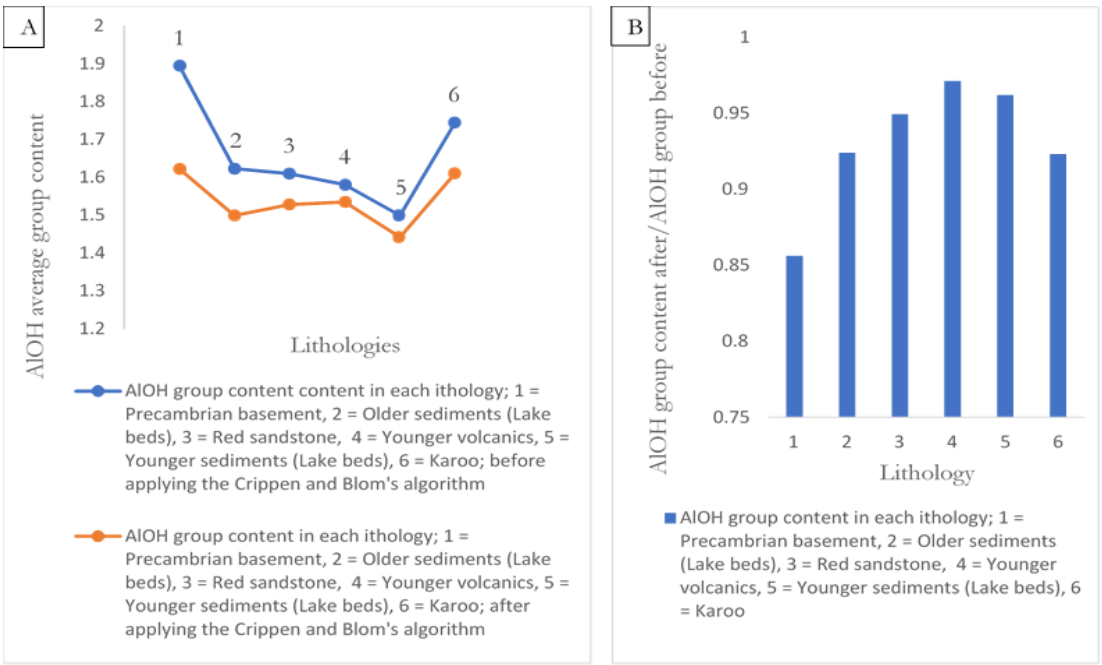

Figure 20: Scatter plot (A) and column chart (B) showing the abundances of the AlOH group content in each lithology (Landsat). The scatter plot (A) is showing the abundance of the AlOH group content before (blue) and after (orange) applying the Crippen and Blom's algorithm. The column chart shows the ratio of the AlOH group content after applying the algorithm to the ratio of the AlOH group content before applying the algorithm.

4.2.1.3. Ratio images: ASTER; Ferrous iron index [(B5/B3) +(B1/B2)], (Rowan et al., 2005)

According to (Rowan et al., 2005)), (B5/B3) and (B1/B2) of the ASTER, can highlight ferrous iron. Thus, in this research, abundance images using combination of these ratio indices, (B5/B3) + (B1/B2) are produced both before and after applying the Crippen and Blom's algorithm (Figure 21; A, B). The threshold values used are 0.5-2.5 with a linear type of stretch.

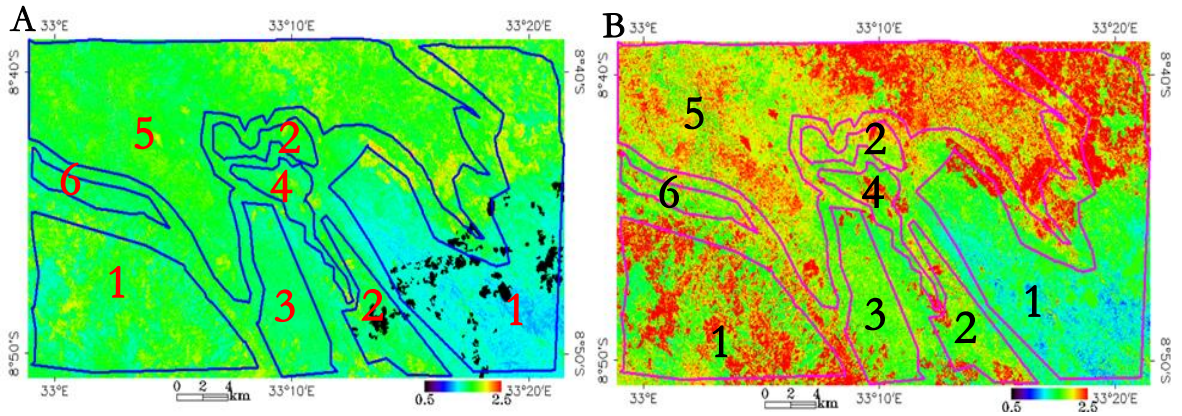

Figure 21: Ratio images of ferrous iron before (A) and after (B) applying the Crippen's and Blom's algorithm on the ASTER scene; the red shades are high values while the blue/dark shades are low values. The polygons correspond to the different lithologies.

As can be seen from the Colour shades of the images (Figure 21 above) and the basic statistics (table 5), there seems to be there is an improvement in the abundances.

Table 5: Basic statistics of the abundance of ferrous iron across the different types of the lithologies before and after applying the Crippen and Blom's algorithm on the ASTER scene.

Basic statistics; ASTER: (B5/B3) +(B1/B2)

Lithology		Min	Max	Mean	Stdev
Precambrian basement (1)	Before	0.000000	2.720507	1.554884	0.361820
	After	0.144444	5.428969	1.951743	0.496534
Older sediments (2)	Before	0.000000	2.420993	1.557443	0.390584
	After	1.017062	5.267783	1.961827	0.312827
Red sandstone (3)	Before	1.259278	2.256300	1.605195	0.107309
	After	1.171521	4.149274	1.889023	0.258090
Younger volcanics (4)	Before	1.345123	2.291598	1.640239	0.137355
	After	1.401414	4.170512	1.973430	0.346180
Younger sediments (5)	Before	0.000000	2.701715	1.749963	0.145681
	After	1.099289	6.207958	2.164272	0.290908
Karoo (6)	Before	1.352067	2.214630	1.626874	0.103443
	After	1.247051	3.776297	1.936452	0.245365

To check how much change is made to the abundances of the ferrous iron in each lithology because of the Crippen and Blom's algorithm, a scatter plot and column chart of the mean abundances are given in Figure 22 below. As can be seen in figure 22 below, there is an overall enhancement in the abundance of the ferrous iron in the ASTER image after applying the Crippen and Blom algorithm (Orange colour, A). For example, the ferrous iron in the older lake beds seems to show 26% increment (B, 2). The assumption in (B) is that if there is no enhancement, the ratio value should be 1. However, the result shows the abundance of ferrous iron is enhanced (all values are above 1). Thus, the Crippen and Blom's algorithm is possibly applicable for the ASTER in cases of mapping ferrous iron in areas like the study area of this research.

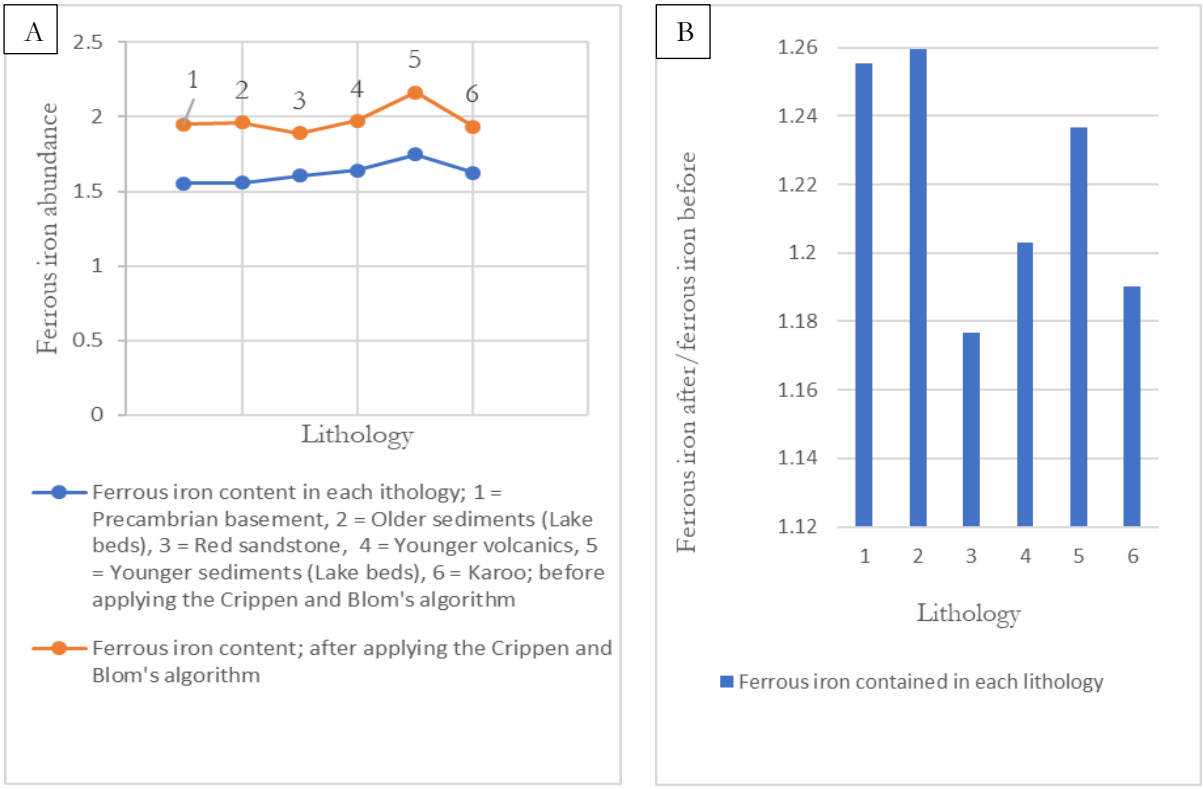

Figure 22: Scatter plot of the before and after applying the Crippen and Blom's algorithm (A) and column chart showing the ratio of the abundance of the ferrous iron after applying the algorithm to the ratio of the ferrous iron before applying the algorithm to show the degree of enhancement (B)).

4.2.1.4. Ratio images: Landsat; Ferrous iron index [(B7/B4) +(B2/B3)] (based on (Rowan et al., 2005) ASTER equivalent bands)

Another ferrous iron abundance images (Figure 23) were produced from the Landsat image using ratio index [(B7/B4) +(B2/B3)], approximately within similar wavelength ranges as in the ASTER. This ratio image is done in order to compare the utility of the Crippen and Blom's algorithm in ASTER with its utility in Landsat to detect ferrous iron. The stretch type used is linear with 0.5-2.5 threshold values.

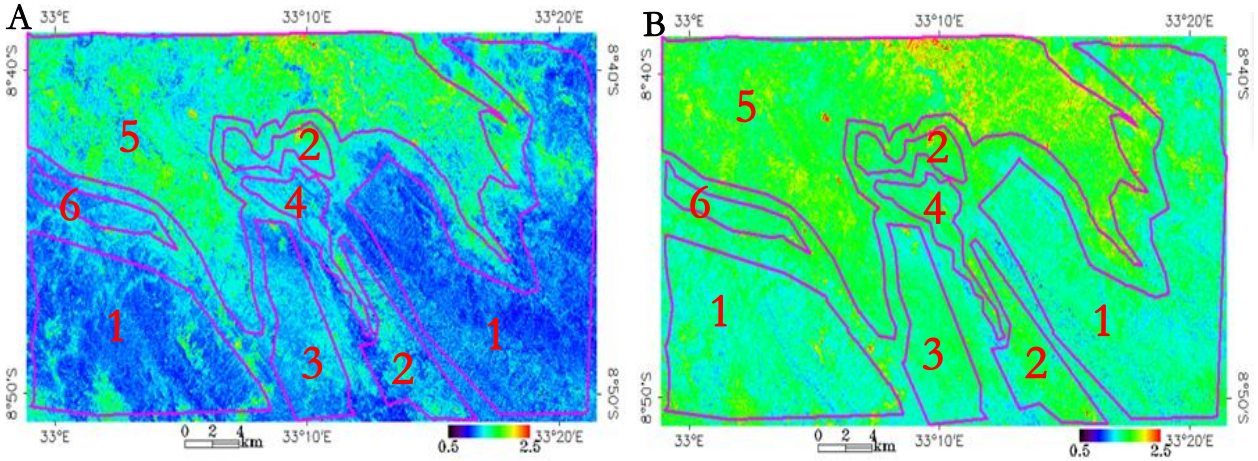

Figure 23: Ratio images of ferrous iron before (A) and after (B) applying the Crippen's and Blom's vegetation suppressing algorithm (Landsat scene); the red shades represent high values while the blue/dark shades represent low values. The polygons correspond to the different lithologies.

As can be seen from the Colour shades of the images above (Figure 23), and the basic statistics (table 6 below), there seems to be an improvement in the abundances of the ferrous iron after applying the algorithm.

Table 6: Basic statistics of the abundance of ferrous iron across the different lithologies before and after applying the Crippen and Blom's algorithm on the Landsat scene.

Basic statistics; Landsat: (B7/B4) +(B2/B3)

Lithology		Min	Max	Mean	Stdev
Precambrian basement (1)	Before	0.873361	2.791256	1.412230	0.127862
	After	0.447506	3.150754	1.512908	0.148776
Older sediments (2)	Before	1.040376	2.665069	1.519103	0.150874
	After	1.012496	3.194058	1.610304	0.158725
Red sandstone (3)	Before	1.130453	2.379714	1.466943	0.102726
	After	1.136206	2.576717	1.530603	0.116052
Younger volcanics (4)	Before	1.089006	2.187847	1.513671	0.108700
	After	1.100438	2.323812	1.558683	0.121282
Younger sediments (5)	Before	1.088941	2.799391	1.666426	0.175946
	After	0.986037	3.388405	1.742849	0.179457
Karoo (6)	Before	1.151476	2.245305	1.472732	0.100385
	After	1.106111	2.542372	1.563655	0.114794

However, to check how much change is made to the abundances of the ferrous iron in each lithology because of the Crippen and Blom's algorithm, a scatter plot and column chart of the mean abundances are given below (Figure 24)

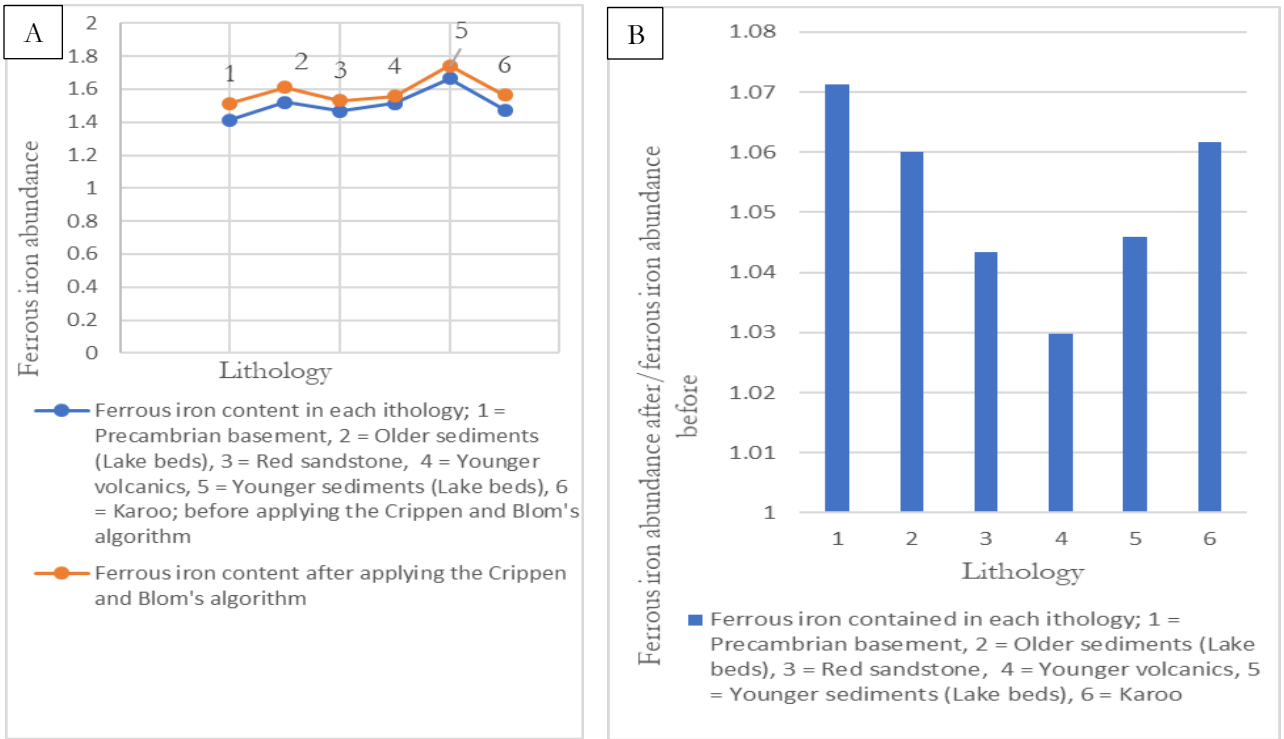

Figure 24: The abundance of the ferrous iron contained in each lithology (scatter plot of the before and after Crippen and Blom's algorithm of (A) and the ratio of the abundance of the ferrous iron after applying the algorithm to the ratio of the ferrous iron before applying the algorithm to show the degree of enhancement (B).

The above figures (Figure 24; A & B) show scatter plot of the abundance of the ferrous iron before and after applying the Crippen and Blom's algorithm across the different lithologies (A) and a column chart showing the ratio of the mean abundances after applying the Crippen and Blom's algorithm to the abundances before applying the Crippen and Blom algorithm to check the degree of change (enhancement) (B). There seems an overall enhancement in the abundance of the ferrous iron in the Landsat image after applying the Crippen and Blom's algorithm (Orange colour, A). For example, the ferrous iron in the older lake beds show 7% increment (B, 1). The assumption in (B) is that if there is no enhancement, the ratio value should be 1. However, the result shows the abundance of ferrous iron is enhanced (all values are above 1). Thus, the Crippen and Blom's algorithm is possibly applicable for the Landsat in cases of mapping ferrous iron in areas like the study area of this research but relatively less as compared to ASTER (section 4.2.1.3, Figure 22 above).

4.2.2. NDVI images

NDVI images of both the Landsat and ASTER images were produced (Figure 25; A, A' and B, B') to be used as additional ways of checking the role of Crippen and Blom's algorithm in the green vegetation (if it suppresses vegetation). The assumption is that if the NDVI values across a given area of the images is reduced after applying the Crippen and the Blom's algorithm as compared to the original images, the algorithm makes a change in the NDVI values of the images. Thus, this helps to understand at least weather the algorithm is applicable to suppress vegetation or not for both the Landsat and ASTER images. But, in order to check how much does the algorithm play a role to enhance spectral response of mineral/rock of interest following the suppression of the vegetation, an example of ROI based spectral signatures generated from the ASTER image are evaluated in section 4.2.3. or we can look back at section 4.2.1 above.

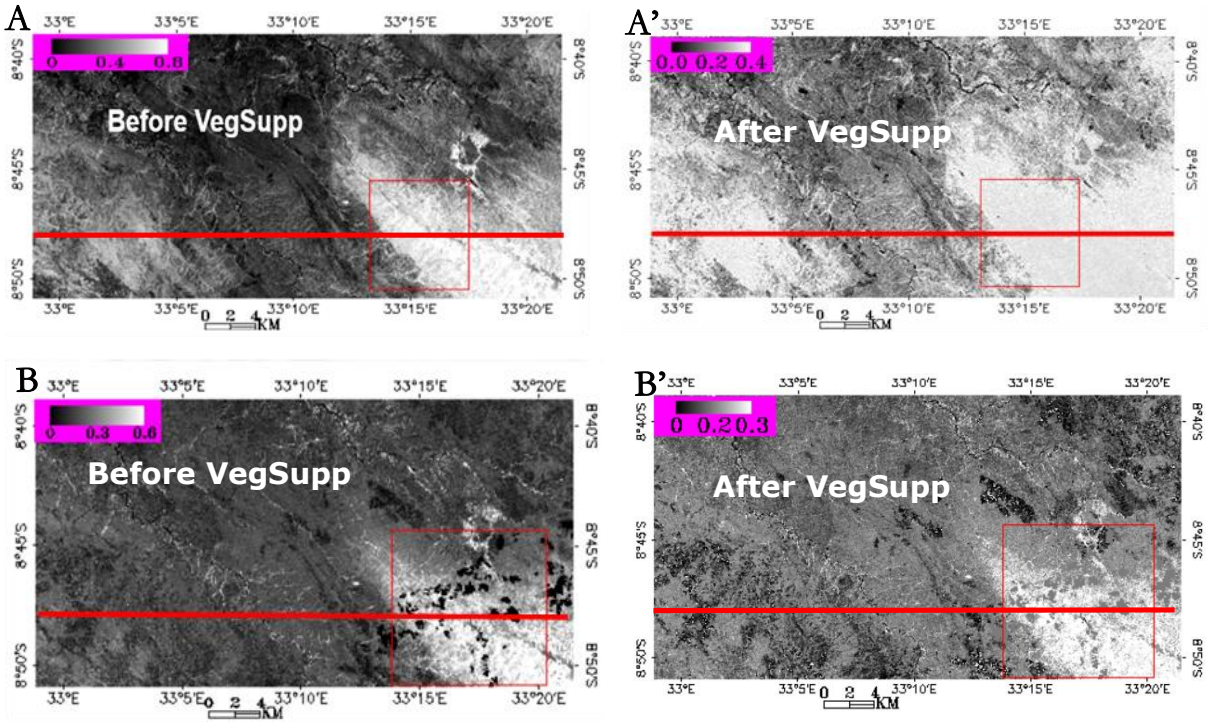

Figure 25: NDVI images generated from both the Landsat (A & A', before and after applying the Crippen and Blom's algorithm respectively) and the ASTER (B & B', before and after applying the Crippen and Blom's algorithm respectively). The red lines are horizontal lines across both the Landsat and ASTER NDVI images which were used as a horizontal profile to check the variations in NDVI values across the images. VegSupp (white text on the images denotes for vegetations suppression).

The following figures (Figure 26; A & B) show the vigour of the green vegetation across the horizontal profiles of both the Landsat and ASTER images.

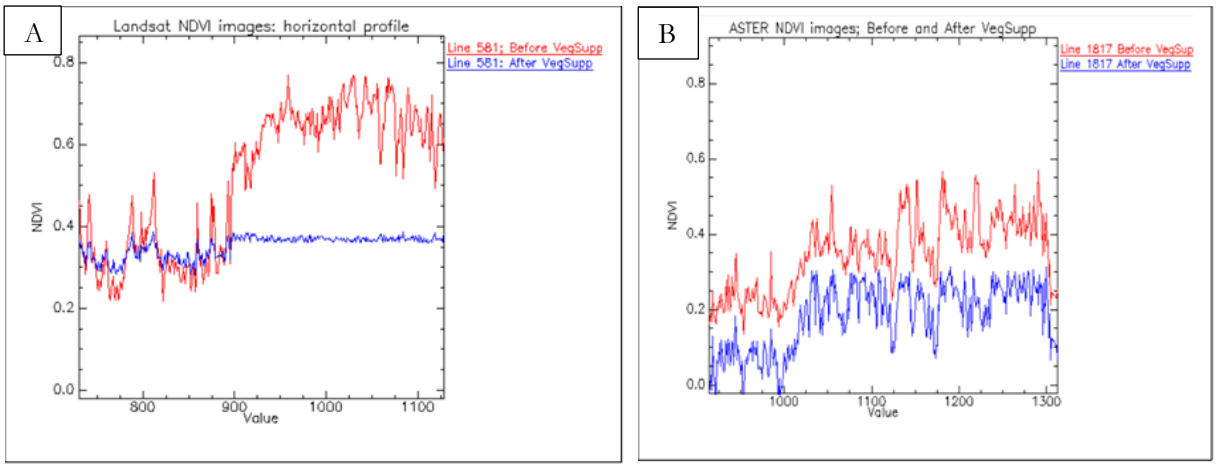

Figure 26: Scatter plots of horizontal profiles along the NDVI images of the Landsat (A) and the ASTER (B) images showing the variations of the NDVI values both before (red colour) and after (blue colour) applying the Crippen's and Blom's algorithm.

From figure 26 above, the NDVI profile across the Landsat scene (A) which is taken from the same spatial position before and after applying the algorithm, shows a general reduction of the NDVI values from near 0.8 (before applying the algorithm) to 0.3-0.4 (after applying the algorithm). Analogous situation is observed in the ASTER where the NDVI values get reduced from around 0.6 to near 0 (B). Both figures show the applied algorithm is suppressing vegetation in general, but to check its geological importance (whether it enhances minerals/rocks) see sections 4.2.3, 4.2.4, and 4.2.5.

4.2.3. ROI based spectral signatures

Spectral signatures generated from the average statistics spectra of three ROI's selected from the ASTER image with variable amount of vegetation cover (with relatively low, (ROI 1), medium (ROI 2) and higher (ROI 3) (Figure 27, A) across the same type of lithology (Figure 27, D) are shown below (Figure 27). The importance of these ROI based spectra is to assess the role of Crippen and Blom's algorithm on the spectral features of the selected ROI spectra across the relatively low, medium and high amount of vegetation. The spectral signatures of the ROI's shown in (Figure 27) both before (B) and after (C) applying the algorithm show variations in the spectral signatures after applying the algorithm in that strength of the red edge is minimized and clear features within the SWIR region are shown.

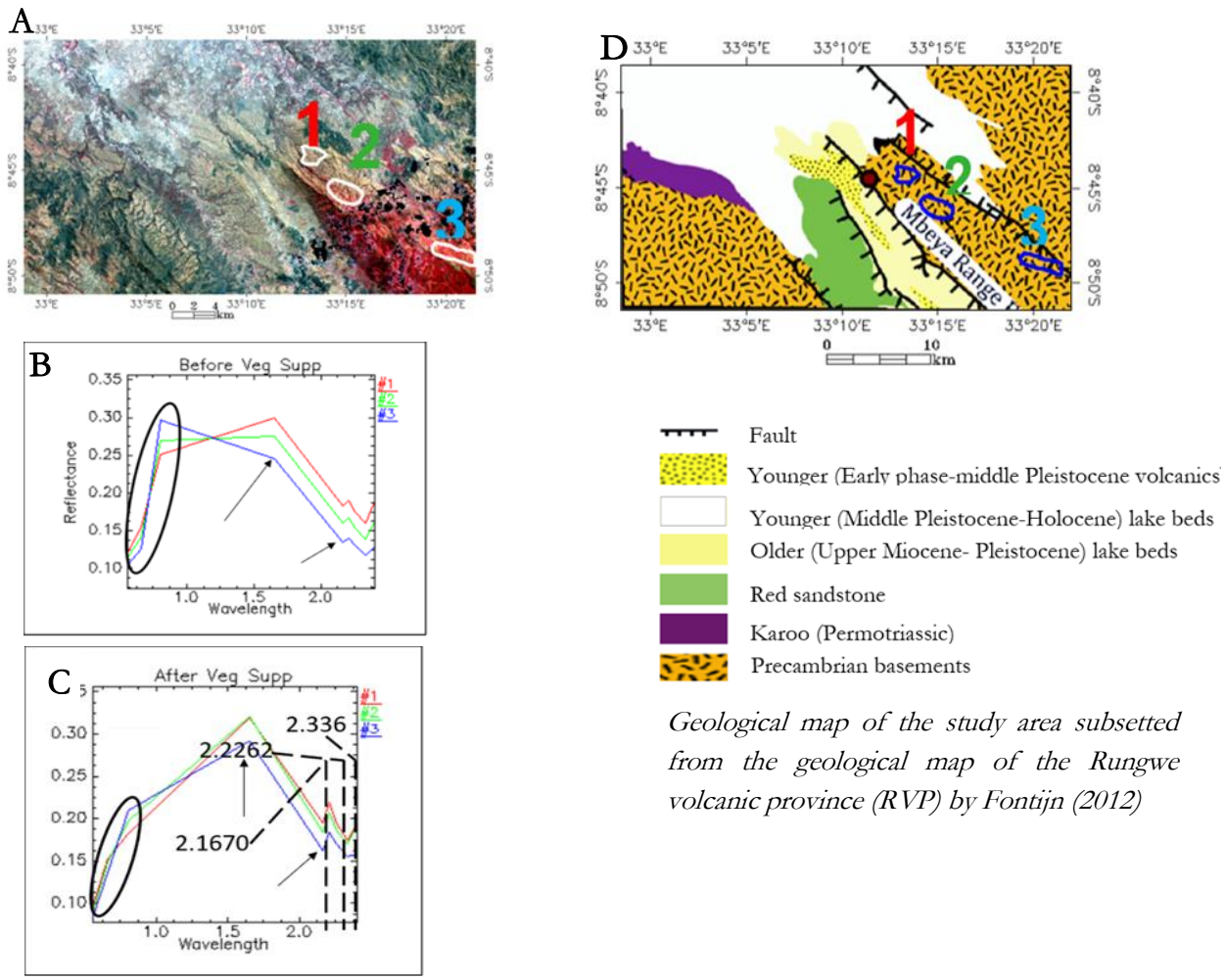

Geological map of the study area subsetted from the geological map of the Rungwe volcanic province (RVP) by Fontijn (2012)

Figure 27: ROI based spectral signatures selected from ASTER image (A) from the same lithology (B) to assess the spectral variations of the three mineral groups before (B) and after (C) applying the Crippen's and Blom's algorithm. The oval shape shows spectral variations of vegetation in the red edge and the arrows show the variations in the general shape of the absorption/reflection features.

Note that the aim of this test is not targeting to identify the target minerals, it is to assess the role of the applied algorithm that might have on the enhancement of mineral features. This is because of the limited resolution of the dataset used, there are no clear diagnostic features that can be used to identify specific minerals (i.e. kaolinite, alunite,). Consequently, some relatively interesting features within the ASTER SWIR which in general are referring to the absorption features of group of clay minerals (i.e. reflectance minimum for AlOH (2.167 μm) and MgOH (2.336 μm)) (Figure 28 below) were used as examples of spectral features to assess whether the Crippen and Blom's algorithm makes a change to these features.

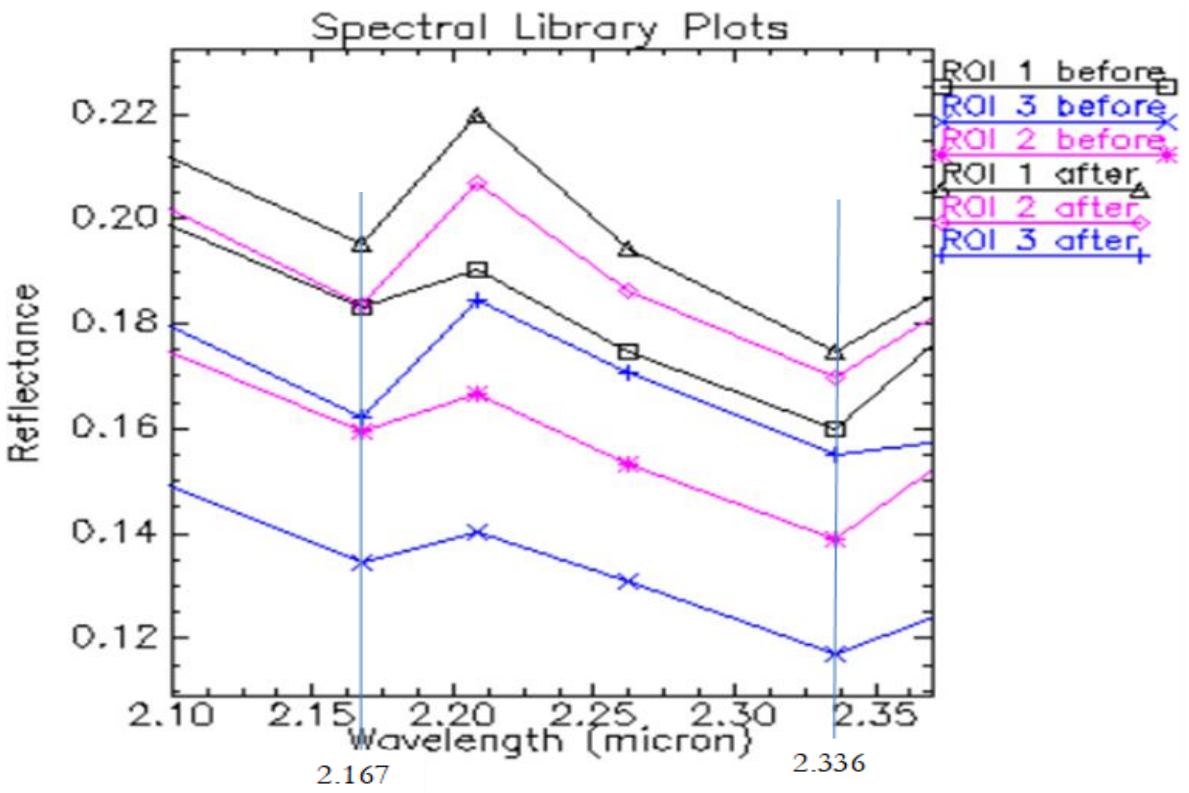

Figure 28: Mean spectra of three ROI's generated from ASTER scene both before and after applying the Crippen and Blom's algorithm.

To check if the variations in the spectral features show an enhancement of spectra of those group of minerals, spectral signatures generated from the mean statistics of the ROI's of both the original and processed (after applying Crippen and Blom's algorithm) were interpreted in terms of wavelength absorption position and relative band depth (RBD) (see sections 4.2.3.1 & 4.2.3.2 below).

Obviously, the reduction of the NDVI values in each ROI after applying the algorithm (table, 7 below) can suggest the suppression of the vegetation is made, but for checking any possible change in the spectral features of the mineral groups (AlOH, MgOH), following the vegetation suppression, their absorption wavelength position and Relative band depth are discussed below (sections 4.2.3.1 and 4.2.3.2)

Table 7: Basic statistics of the NDVI of the three ROI's before and after applying the Crippen and Blom's algorithm.

ROI	Crippen and Blom's algorithm implementation	Min	Max	Mean	Stdv
1	Before	0.18	0.33	0.24	0.02
	After	0	0.22	0.09	0.02
2	Before	0.18	0.68	0.31	0.05
	After	0.02	0.31	0.15	0.05
3	Before	0.17	0.62	0.4	0.07
	After	0.01	0.31	0.22	0.05

4.2.3.1. Maximum absorption wavelength position

The absorption wavelength position is one of the essential parameters in spectroscopy at which a specific type of material can be determined (Kopăcková & Koucká, 2017). In this research, this parameter was used to assess the role of the Crippen and Blom's algorithm that might cause any changes in the wavelength position of the spectra after its implementation. As can be seen from the above figure (Figure 28), the maximum absorption wavelength position of the AlOH and MgOH group minerals are laying in the same position both before and after applying the Crippen and Blom's algorithm. Thus, the Crippen and Blom's algorithm has not made any change with respect to the absorption position. This implies that there are no new minerals/mineral groups shown as the result of applying the Crippen and Blom's algorithm.

4.2.3.2. Relative Band Depth (RBD)

Absorption band-depth is a method of analysis designated to distinguish mineral absorption features, while reducing differences in reflectance related to topographic slope and albedo variations (Crowley, Brickey, & Rowan, 1989). It can be created by dividing the sum of bands located at the shoulders of the absorption feature by the sum of one or more bands located at the reflectance minimum of the absorption features (Crowley et al., 1989; Murphy, 1995). Here, in this research, it is executed to compare the absorption depth of the AlOH and MgOH mineral groups across the three ROI's (see Figure 28, above) before and after applying the Crippen and Blom's algorithm on to the ASTER image. Thus, the RBD of AlOH and MgOH across the ROI's were calculated by summing reflectance at shoulders and dividing by the reflectance at minimum (table 8).

Table 8: The RBD of the AlOH and MgOH mineral groups across three ROI's.

ROI	Crippen and Blom's algorithm implementation	Reflectance at shoulders (Bands: 4, 6, 9 and) and reflectance minimum (Bands: 5, 7, and 8)						AlOH (Band 4 + Band 6)/Band 5	MgOH (Band 6 + Band 9)/ (Band 7 + Band 8)
		Band 4	Band 5	Band 6	Band 7	Band 8	Band 9		
ROI 1	Before	0.3	0.18	0.19	0.17	0.17	0.16	2.72	1.03
	After	0.32	0.2	0.22	0.19	0.19	0.17	2.7	1.03
ROI 2	Before	0.28	0.16	0.17	0.15	0.15	0.14	2.81	1.03
	After	0.32	0.18	0.2	0.18	0.19	0.17	2.89	1
ROI 3	Before	0.25	0.13	0.14	0.13	0.13	0.18	3	1.23
	After	0.29	0.16	0.18	0.17	0.16	0.16	2.94	1.03

As can be seen from the following figure (Figure 29), the RBD before (blue colour) and after (orange colour) applying the Crippen and Blom's algorithm show very little to no differences. Thus, the Crippen and Blom's algorithm does not make significant changes.

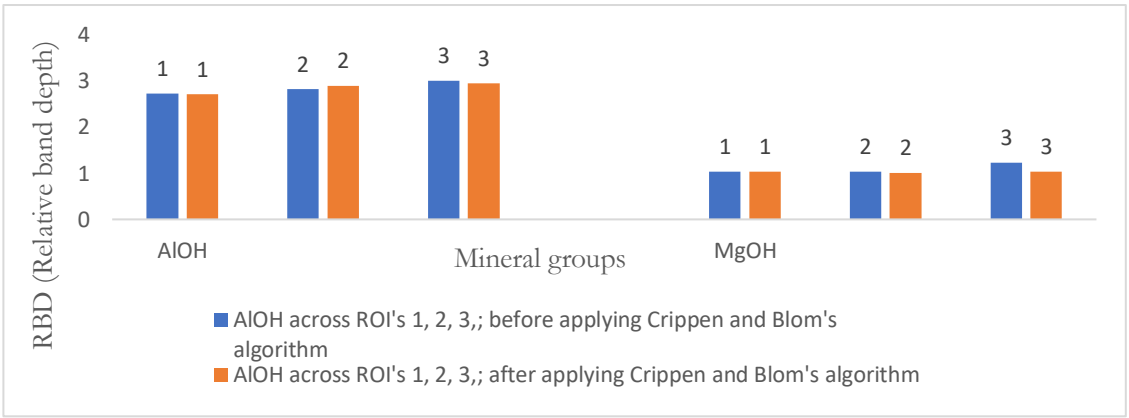

Figure 29: Variations in the relative band depth (RBD) of the AlOH and MgOH mineral groups before and after applying the Crippen and Blom's algorithm

In addition to the above three ROI's, more spectral signatures were collected from the ASTER scene in order to observe any possible differences in the spectral responses representing different areas with a variable amount of vegetation cover. Thus, fourteen ROI's were selected from the ASTER image (Figure 30, A) across various parts of the image assumed to represent the different types of the lithologies (Figure 30; geological map, B) with variable amount of vegetation cover. Vectors representing the ROI's selected from the ASTER scene are shown below (Figure 30, A).

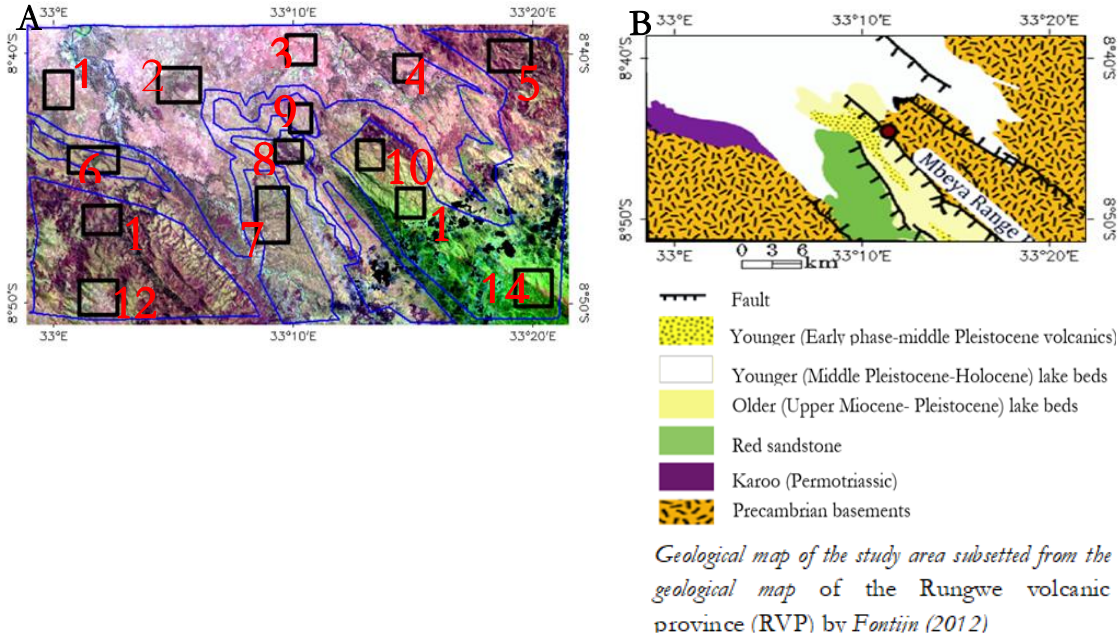

Geological map of the study area subsetted from the geological map of the Rungwe volcanic province (RVP) by *Fontijn (2012)*

Figure 30: Fourteen region of interests (ROI's) (dark box, on the ASTER scene (A)) across areas where all the lithologies are crossing in the ground. The blue polygons in the image (A) belong to the boundaries of different lithologies (B).

The mean spectral signatures of the fourteen ROI's (Figure 30, A above) were generated both before and after applying the Crippen and Blom's algorithm and the four ROI's are shown in the following figure (Figure 31 below).

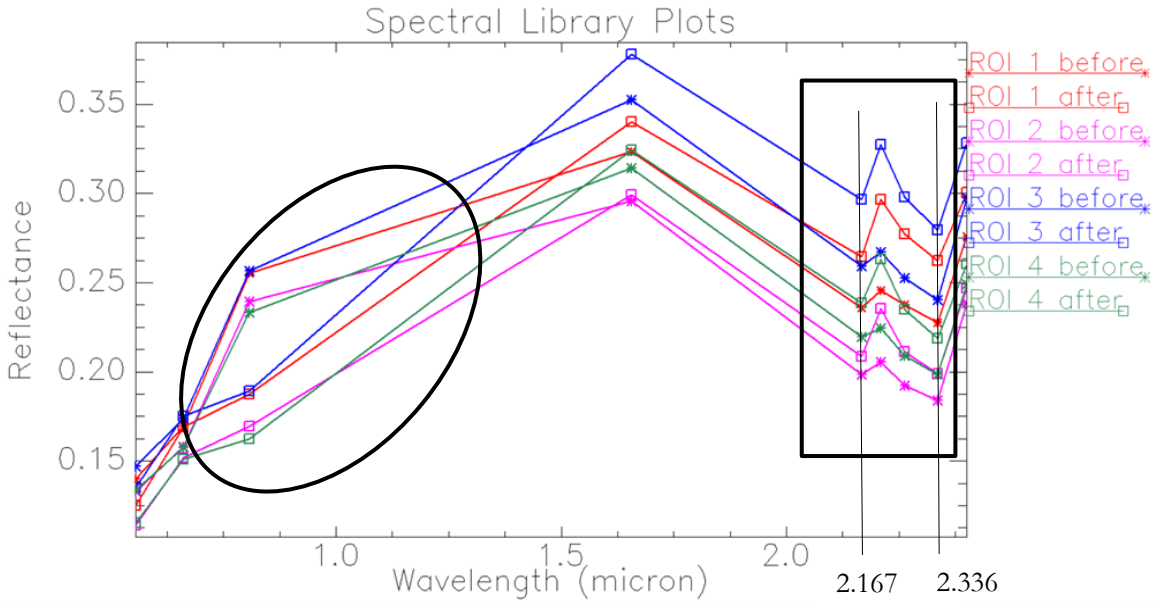

Figure 31: Mean spectra of four ROI's of the ASTER scene both before and after applying the Crippen and Blom's algorithm. The oval shapes show the variations in the red edge because of the applied algorithm while the rectangular box shows the absorption features of the AlOH and MgOH mineral groups.

As can be seen from the spectral signatures (Figure 31 above), the spectral features of the ROI's are the same as the previously described three ROI's (Figure 29; sections 4.4.1, 4.4.2 above) where there is no variation in terms of the absorption wavelength position because of the applied algorithm. Thus, the remaining ten ROI's, because of no differences with four ROI's shown above (Figures 28 & 31), it is not necessary to repeat them here and they are shown in the appendices including the mean of the NDVI values of each ROI's (appendix V).

The spectral signatures show that the red edge (in the VNIR range) is reduced in all the ROI's, implying the suppression of the vegetation due to the applied algorithm. The spectral features in the SWIR range show there is a difference in the signal (reflectance values) between the spectra collected before applying the Crippen and Blom's algorithm and the spectra collected after applying the algorithm. Thus, this seems to imply that there is a little enhancement of the mineral groups which previously might be obscured by the vegetation. However, like section 4.2.3 of the three ROI's, there are no differences observed in terms of absorption wavelength position and relative band depth (RBD). Thus, the results in general suggest the Crippen and Blom's algorithm has not made significant changes in the spectral information content of the mineral groups.

The average NDVI values of the four ROI'S are given below (table 9).

Table 9: NDVI values of the above four ROI's before and after applying the Crippen and Blom's algorithm.

NDVI_Basic statistics

ROI	Crippen and Blom's implementation	Mean
1	Before	0.2
	After	0.05
2	Before	0.21
	After	0.06
3	Before	0.19
	After	0.04
4	Before	0.19
	After	0.04

In summary the results on the spectra of the ROI's show the signal of the vegetation seems to be diminished (see the red edge, Figure 31 above). However, in terms of spectral information content on the mineral groups, there is no significant changes on the spectra obtained from the processed images (after applying the algorithm) compared to the spectra obtained from the original images.

4.2.4. RGB combinations of ratio images

RGB combinations of the ratio images of the Landsat scene including 4/3, 5/2, 3/1; and 4/2, 5/3, 4/3 were produced both before and after applying the Crippen and Blom's algorithm (Figure 32 A, A'; B, B';). The selection of the combination of these ratio images is based on (Simon et al., 2016), where he has used them to discriminate lithologies using Landsat. This was done to check for any improvement on the lithologies/lithologic boundaries of the study area after applying the Crippen and Blom's algorithm. The results on the images were compared to existing geological map of the study area (Figures, 32 and 33, C).

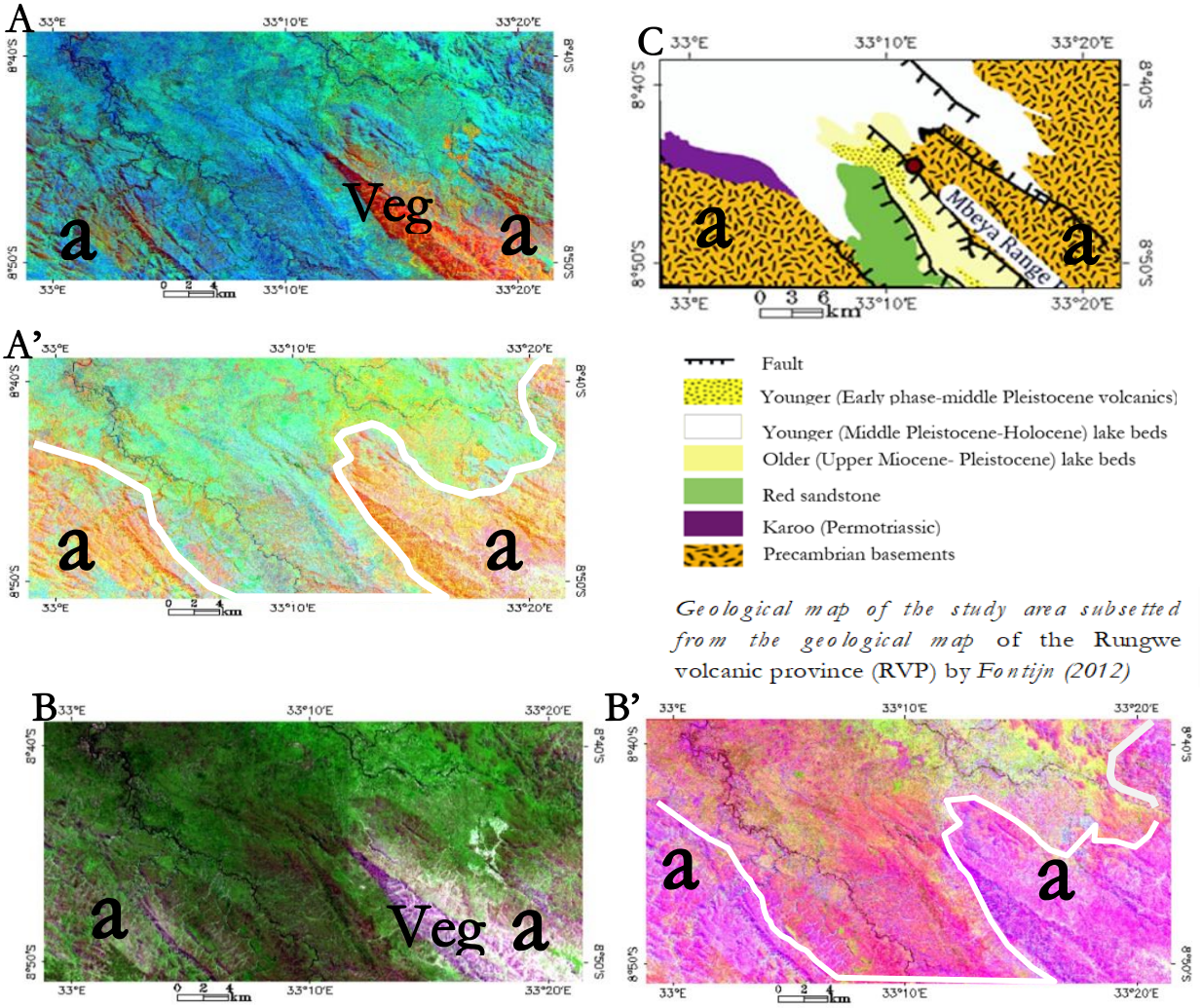

Figure 32: RGB combinations of ratio images (4/3, 5/2, 3/1; A, A and 4/2, 5/3, 4/3; B, B' of the Landsat image showing the different lithological units in different colours. A, B and and A', B' are representing the ratio images before and after applying the Crippen and Blom's algorithm respectively. 'Veg' on the images represent for vegetation (i.e. reddish colour in A) and 'a' is representing the Precambrian rock. The 'white' polygons are indicating for lithological boundaries.

As can be seen from the above images, the RGB composites after applying the algorithm (A', B') seems to show clear features on the lithologic boundaries which probably were obscured by vegetation. This can be observed especially in the Precambrian rock (greyish yellow and greyish pink colours in A' and B' respectively). Thus, the algorithm seems to make the RGB composites clearer where some lithologies appear brighter and distinguishable.

4.2.5. PCA applied on RGB combinations of ratio images

However, here in this research, we applied PCA transformation up on the above RGB composite images and we got relatively better results where the Precambrian rock show more clearer boundaries (Figure 33, below). This clearly observed especially in the RGB combinations of the ratio images: 4/3, 5/2, 3/1 (Figure 33, A'). These images are displayed as RGB combinations of PCA1, PCA2 and PCA3 respectively.

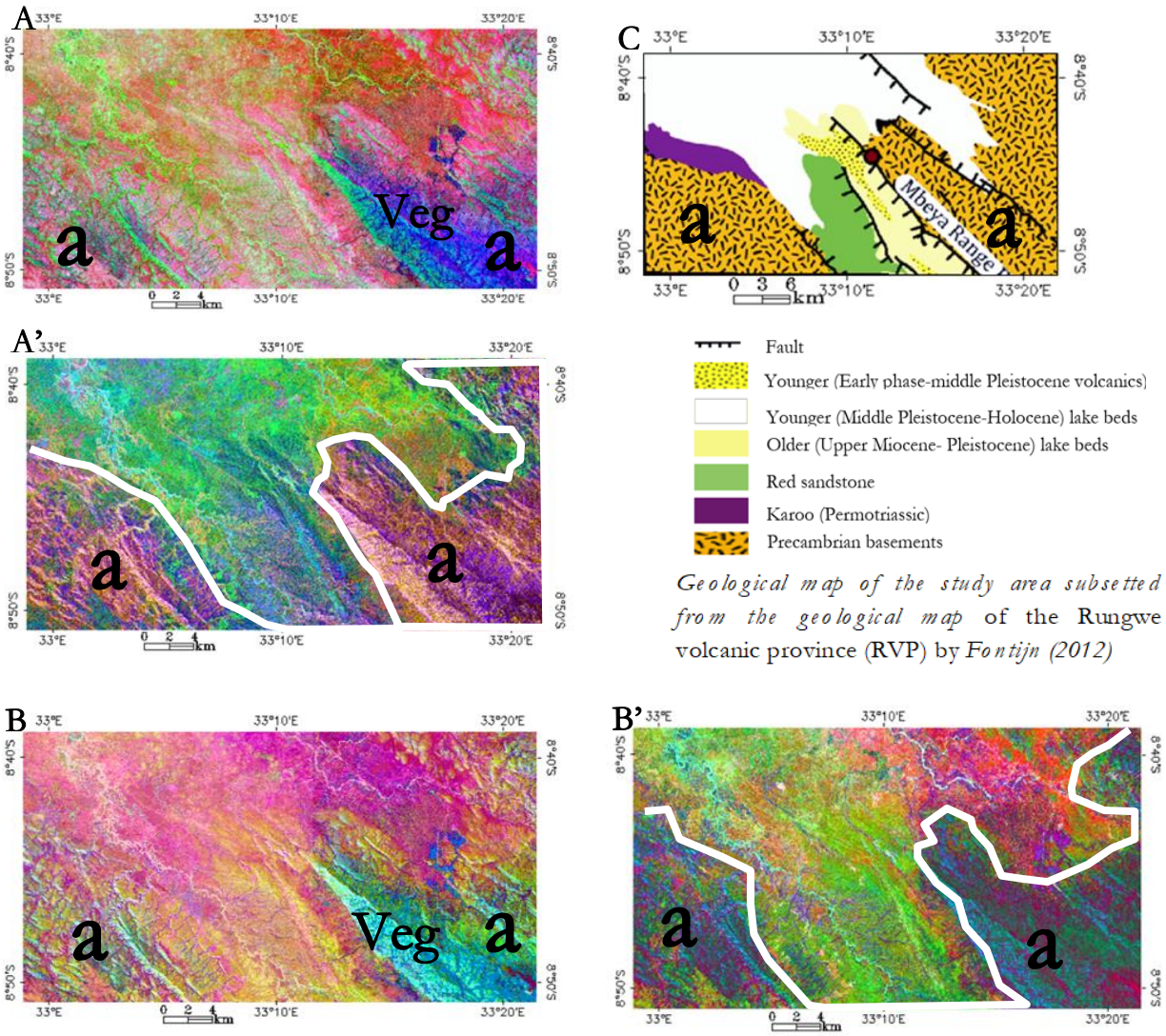

Figure 33: PCA applied RGB combinations of ratio images (4/3, 5/2, 3/1; A, A and 4/2, 5/3, 4/3; B, B' of the Landsat image showing the different lithological units in different colours. A, B and and A', B' are representing the ratio images before and after applying the Crippen and Blom's algorithm respectively. 'Veg' on the images represent for vegetation (i.e. Blue colour in A) and 'a' is representing the Precambrian rock. The 'white' polygons are indicating for lithological boundaries.

So, the above results (Figure 33) suggest that there appears to be a better qualitative enhancement because of the PCA, on top of the qualitative Crippen & Bloom technique.

5. DISCUSSION

5.1. Evaluating the effect of vegetation on the spectral response of a bare ground (mineral/rock).

The results of the bare-vegetation simulation model in this research, suggest that the effect of vegetation on the spectral responses of bare ground varies with the amount of vegetation cover and the spectral characteristics of the datasets used. Variable amount of vegetation causes spectral mixing and shifting problems for the different VNIR-SWIR bands of the Landsat and ASTER to a variable degree of influence.

From the spectral ratio analysis, with a 5% vegetation cover on the ground simulated by Landsat in this model (Figure 14, A; in chapter four) the spectral information acquired from band 4 is above the expected (falsely enhanced response) and this effect increases with increasing vegetation cover. This is probably because, band 4 in Landsat is highly sensitive to vegetation. Also, in the first three bands of Landsat, and all but band 3 of the ASTER (Figure 14, B; in chapter four), the vegetation shows a relatively lesser impact when it is 5%, and the influence increases with increasing amount of the vegetation. The results of the simulation model show that the vegetation affects the spectral response of bare ground both by obscuring (hiding) and overestimating the spectral information of the bare ground. Obscuring and overestimating in this context mean, lowering and falsely increasing the signal of the bare ground below or above expectation according to the bare-vegetation simulation model. Additionally, the results from the slope values of the trend lines reveal that the smaller the difference in the slope values, the lower the influence of vegetation and vice versa (see Figures 15 & 16; section 4.1.2).

According to the results of this research, a green vegetation cover of 20% or above seems to cause relatively stronger mixing and shifting problems on the spectral responses of the bare ground within the SWIR range of the Landsat image, including band 4 in the VNIR. Note that in this context the threshold of these percentages is depending our bare-vegetation simulation model where we start with 100% pure vegetation and 100% pure bare of the two end members. Thus, we used 5%, 10%, 20%, 40%, 50%, 60%, 80%, 90% and 95% vegetation cover as threshold values to assess the influence of the variable amount of vegetation cover on the spectra of the bare ground. A vegetation cover of >=20 % shows significant effect on almost all bands of the ASTER (VNIR-SWIR bands). In relation to geological interpretations both images would be better interpretable across area of less than 20% vegetation cover. However, in cases of higher vegetation cover, it is recommendable either to look for techniques that successfully can suppress the vegetation and enhance the geological information or use another high spectral and spatial resolution data set (i.e. air borne data) that might relatively be able to acquire more information with minimal mixing effects. In addition, note that our results are based on the particular area and environment where we derived the original bare ground and vegetation endmembers. Thus, it could be suggested that, further studies in other areas could be important to observe the varying effects of vegetation versus bare ground spectral signatures since spectral responses of the vegetation and the bare ground might vary in areas of different vegetation types and bare ground.

The results in general, can be related to some previous works, (Carranza & Hale, 2002; Crippen & Blom, 2001; Fraser & Green, 1987; Grebby, 2011; Grebby et al., 2014; Murphy, 1995; Murphy & Wadge, 1994; Yu et al., 2011) who have shown that the vegetation could affect the geologic image interpretation either by obscuring the spectra of underlying minerals and lithologies or by completely dominating the overall spectrum (Siegal & Goetz, 1977). Most of the previous works were based on airborne datasets and or MSS, except (Crippen & Blom, 2001; Yu et al., 2011); who have used Landsat. The added value of this research is the quantitative simulated demonstration of the influence of variable amount of vegetation (amount of vegetation in percentages using bare-vegetation simulation model) on the spectra of bare ground in Tanzania imaged by the Landsat and ASTER including all bands within the VNIR-SWIR ranges (six Landsat and nine ASTER bands) which previously were given a little focus.

5.2. Evaluation of the role of the vegetation suppressing Crippen's and Blom's algorithm

The results of the ratio images, the ROI based spectral signatures and the RGB combinations of the ratio images in general suggest that the algorithm has little or no role in enhancing mineral/lithological information in both the Landsat and ASTER images. The results on the ratio images of the mineral groups (chapter-4, section 4.2.1) shows a little to no difference in the abundances (mineral content) of the images produced before and after applying the Crippen and Blom's algorithm.

For example, the AlOH group content on the ASTER image shows no change between the images before and after applying the Crippen and Blom's algorithm. Moreover, the same type of mineral group (AlOH) on the Landsat image showed a decline in the original content (Figure 20; chapter four) which seems not related with AlOH. The reduction in the detected anomaly could be probably because the original anomaly was mostly due to vegetation and hence once the vegetation was suppressed by the applied algorithm, and the response reduced. Possibly, it could be related to the relative band depth values of the ASTER AlOH product that they were low and below the 2.0 threshold as used by (Cudahy, 2012). Also, such results might be observed in areas where there is no enough amount of detectable mineral/rock of interest but vegetated. Consequently, a given mineral is supposed to be enhanced only if a given area is characterized by the presence of that mineral, an argument that agrees with Crippen & Blom (2001).

The results on the ratio images of the ferrous iron show a little difference between the images produced before and after applying the Crippen and Blom's algorithm in that the abundances of the mineral groups relatively increased to a little extent in both the Landsat and ASTER images, with relatively better results in the ASTER image. This might be an indication that the Crippen and Blom's algorithm has a better impact on the VNIR ranges than the SWIR. The NDVI images show that the Crippen and Blom's algorithm is suppressing the vegetation. However, with respect to improving the geologic information from within the diagnostic SWIR wavelength region, it has a little to insignificant changes.

For the ROI based spectra, there were a very little to no differences in the wavelength absorption position as well as on the relative band depth (RBD) (sections 4.2.3.1; 4.2.3.2, chapter four). The general trends of all the spectra of the ROI's show that the red edge seems to be declining and the general spectral trend before and after applying the algorithm show relative differences in the actual reflectance positions. But these actual reflectance values could be affected by topographic slope and albedo variations. Hence, we calculated the RBD that can distinguish absorption features, while reducing differences in reflectance related to topographic slope and albedo variations (Crowley et al., 1989). We have used bands 4, 5, and 6 and 6, 7, 8, 9 RBD calculations to approximately represent for AlOH and MgOH mineral groups respectively (see section 4.2.3.2; chapter four) to check any possible variations in the diagnostic absorption or spectral features before and after applying the Crippen and Blom's algorithm. However, there are not significant differences on the results of the RBD's of both mineral groups (Figure 29, section 4.2.3.2).

The results of the RGB combinations of the ratio images on the Landsat scene show that there seems to be qualitative improvements on the visual interpretation of some lithologic boundaries (especially on the Precambrian rocks, section 4.2.4, A').

Previous researches (Çorumluoğlu et al., 2013), have shown that principal component analysis (PCA) and ratio images can be used for visual rock identification from images. In this research we found that RGB combinations of ratio images obtained before and after applying the Crippen and Blom's algorithm are better interpretable for qualitative rock discriminations, given that the RGB combination of the ratio products are subject to PCA. In this research we applied a PCA transformation up on the qualitative RGB composite images of the Crippen and Blom's algorithm. Each of the 3 ratio band products were used as input to PCA processing and then displayed as RGB images of the produced PC1, PC2 and PC3 (see Figure 33, section 4.2.5). Our results show that the RGB

combinations of the PCA's are better interpretable for the discrimination of the lithologic boundaries. For example, especially the Precambrian rock (Figure 33, A') show more clearer features and boundaries than the one with only Crippen and Blom's applied RGB result (Figure 32, A').

In general, the results on the ratio images and the ROI based spectra signatures show little to no quantitative changes to the spectrally interpretable content of the mineral groups while the RGB combinations of ratio images show changes in the relative contrast in the images qualitatively.

In summary, the overall results imply that the Crippen and Blom's algorithm has made some changes in terms of image contrast (made increased the contrasting of the images), but in terms of spectral information content it does not make significant changes/improvements. Thus, the algorithm seems to be useful for discrimination of possible spectrally related geological boundaries, but not useful for mineral group identification via diagnostic spectral absorption features.

As described earlier in this study, the another objective was to quantitatively demonstrate the role of the Landsat TM based Crippen & Blom (2001) algorithm in enhancing mineralogical/lithological information imaged by Landsat and to compare its impacts on ASTER, which has not been published previously. This is vital to understand if the algorithm can successfully be adopted to the multiband ASTER (including all bands in the VNIR-SWIR), for the acquisition of mineralogical/lithological information across vegetated terrains.

According to the results in this research, comparatively, the algorithm works for both sensors producing similar results. The algorithm seems to increase the clarity or contrast of the images in both sensors, but it does not significantly enhance the spectrally interpretable content of mineralogical/lithological information on both sensors.

6.CONCLUSIONS AND RECOMMENDATIONS

6.1. Conclusions

Based on this research, the following conclusions are drawn;

Research question 1: How does a green vegetation affect the spectral responses (reflectance) of minerals and/or rocks imaged by Landsat and ASTER?

The bare-vegetation simulation model has successfully modeled the influence of vegetation on the spectral responses of the bare ground, assuming representative endmembers for this particular study area of SW Tanzania. The effect of vegetation on the spectral responses of the bare ground varies with the amount of vegetation cover and the spectral characteristics of the datasets used. Vegetation causes mixing within the 30-meter image pixels of the spectral response of bare ground both by obscuring (hiding) the spectral information of the bare and overestimating the spectral responses of the bare-ground.

Research question 2: What amount of green vegetation cover can have a significant effect on the spectral responses (reflectance) of minerals and/or rocks imaged by Landsat and ASTER?

The density of vegetation cover causes spectral mixing and shifting problems for the different VNIR-SWIR bands of the Landsat and ASTER to a different degree of influence. The first three bands of Landsat are relatively less affected and the influence increases relatively with increase in vegetation thickness (> 20%). Also, for the ASTER image, the first two bands of the ASTER are relatively less affected and the influence increases relatively with increase a vegetation thickness of > 20%. This is specifically true for the case of the study area and using the bare-vegetation simulation model of this study.

Research question 3: How comparable is the Crippen's and Blom's algorithm applied to ASTER VNIR-SWIR bands with the previously utilized Landsat to enhance the spectral responses of minerals and rocks?

Despite of differences in terms mineral groups and lithologic discriminations possible between Landsat and ASTER, the Crippen and Blom's algorithm work for both cases in a comparable way. The abundances estimated by ratio parameters of the ferrous iron mineral groups increased to a little extent in both the Landsat and ASTER images with relatively better results for the ASTER suppressed product. For mineral groups, it seems that the algorithm relatively better work with ASTER while for lithological discrimination from an RGB combination image, the algorithm seems to better work with the Landsat.

Research question 4: How good is the Crippen and Blom's algorithm to quantitively enhance spectral responses of the minerals/rocks as applied to both sensors?

The algorithm qualitatively increased the clarity/contrast of the features in images of both sensors. However, the algorithm does not show a significant role to enhance the spectrally interpretable content of mineralogical/lithological information from both sensors. It seems useful for qualitative discrimination of geological boundaries, but not useful for mineral group identification via diagnostic spectral absorption features. Also, for the case of the lithological boundary discriminations, it shows more better qualitative enhancement results given that PCA is applied on top of the qualitative Crippen & Bloom RGB products of the Landsat image.

6.2. Recommendations

The following recommendations are suggested for a further research.

1. In addition to the techniques of NDVI and RGB colour composite, it is recommended to crosscheck or completely acquire field data for endmembers representing a real bare ground exposure (different minerals or rocks of interest) and a real vegetation within in this study area.
2. Apart from quantifying the amount of the green vegetation cover with field observations, further research is recommended to test the effect of vegetation on the spectral responses of mineral and/or rocks as it varies with the type, species, health, season and any other characteristics of the vegetation.

LIST OF REFERENCES

Ager, C. M., & Milton, N. M. (1987). Spectral reflectance of lichens and their effects on the reflectance of rock substrates, *52*(7), 898–906.

Bhandari, A. K., Kumar, A., & Singh, G. K. (2012). Feature Extraction using Normalized Difference Vegetation Index (NDVI): A Case Study of Jabalpur City. *Procedia Technology*, *6*, 612–621. https://doi.org/10.1016/j.protcy.2012.10.074

Biehl, L., & Landgrebe, D. (2002). MultiSpec — a tool for multispectral – hyperspectral image data, *28*, 1153–1159.

Bierwirth, P. N. (1990). Mineral mapping and vegetation removal via data-calibrated pixel unmixing, using multispectral images. *International Journal of Remote Sensing*, *11*(11), 1999–2017. https://doi.org/10.1080/01431169008955157

Carranza, E. J. M., & Hale, M. (2002). Mineral imaging with Landsat Thermatic Mapper data for hydrothermal alteration mapping in heavily vegetated terrane. *International Journal of Remote Sensing*, *23*(22), 4827–4852. https://doi.org/10.1080/01431160110115014

Chabrillat, S., Ceuleneer, G., Pinet, P. C., Mustard, J. F., & Johnson, P. E. (2000). Ronda peridotite massif: Methodology for its geological mapping and lithological discrimination from airborne hyperspectral data. *International Journal of Remote Sensing*, *21*(12), 2363–2388. https://doi.org/10.1080/01431160050030510

Chen, P. Y., Srinivasan, R., Fedosejevs, G., & Kiniry, J. R. (2003). Evaluating different NDVI composite techniques using NOAA-14 AVHRR data. *International Journal of Remote Sensing*, *24*(17), 3403–3412. https://doi.org/10.1080/0143116021000021279

Chouhan, Rajlaxmi; Neeraj, R. (2004). Vegetation Detection in Multispectral Remote Sensing Images : Protective Role-Analysis of Vegetation in 2004 Indian Ocean tsunami. *Gi4DM 2011, GeoInformation For Disaster Management*, 3–7.

Clark, R. N. (1999). Spectroscopy of Rocks and Minerals, and Principles of Spectroscopy - Roger N. Clark.

Çorumluoğlu, Ö., Çorumluoğlu AVural, Ö., & Asri, İ. (2013). PCA of Landsat Band Ratio Images for Capturing Kula Basalts in Turkey GPS Aero-Triangulation View project TÜBİTAK Project: Investigation of Heavy Metal/Trace Element Pollution in Harşit Valley (Gümüşhane) Arising From (Abandoned) Mining Sites in the Regio, (February 2016), 651. https://doi.org/10.13140/RG.2.1.2439.1440

Crippen, R. E., & Blom, R. G. (2001). Unveiling the lithology of vegetated terrains in remotely sensed imagery. *Photogrammetric Engineering and Remote Sensing*, *67*(8), 935–943.

Cŕosta, A. P., De Souza Filho, C. R., Azevedo, F., & Brodie, C. (2003). Targeting key alteration minerals in epithermal deposits in Patagonia, Argentina, using ASTER imagery and principal component analysis. *International Journal of Remote Sensing*, *24*(21), 4233–4240. https://doi.org/10.1080/0143116031000152291

Crowley, J. K., Brickey, D. W., & Rowan, L. C. (1989). Airborne Imaging Spectrometer Data of the Ruby Mountains , Montana : Mineral Discrimination Using Relative Absorption Band-Depth Images, *134*, 121–134.

Cudahy, T. (2012). ASTER VNIR-SWIR Geoscience Products – Version 1.

Dagodzo, D. (2014). HYDROTHERMAL ALTERATION INTERPRETATION OF LANDSAT AND ASTER DATA FOR IRON ORE DETECTION IN THE SHEINI AREA, NORTH EASTERN GHANA, (10440156).

Delvaux, D., Kraml, M., Sierralta, M., Wittenberg, a, Mayalla, J. W., Kabaka, K., & Makene, C. (2010). Surface Exploration of a Viable Geothermal Resource in Mbeya Area , Sw Tanzania . Part I : Geology of the Ngozi - Songwe Geothermal System. *Proceedings World Geothermal Conference*, (April), 25–29.

Dong, P., & Leblon, B. (2004). Rock unit discrimination on Landsat TM, SIR-C and Radarsat images using spectral and textural information. *International Journal of Remote Sensing*, *25*(18), 3745–3768. https://doi.org/10.1080/01431160310001632675

Fontijn, K., Williamson, D., Mbede, E., & Ernst, G. G. J. (2012). The Rungwe Volcanic Province , Tanzania – A volcanological review. *Journal of African Earth Sciences*, *63*, 12–31. https://doi.org/10.1016/j.jafrearsci.2011.11.005

Fraser, S. J., & Green, A. A. (1987). A software defoliant for geological analysis of band ratios. *International Journal of Remote Sensing*, *8*(3), 525–532. https://doi.org/10.1080/01431168708948659

Gad, S., & Kusky, T. (2006). Lithological mapping in the Eastern Desert of Egypt, the Barramiya area, using Landsat thematic mapper (TM). *Journal of African Earth Sciences*, *44*(2), 196–202. https://doi.org/10.1016/j.jafrearsci.2005.10.014

Government, M. regional. (2016). *A brief about mbeya regionand round potato subsector given to the Netherlands potato trade mission on 17th June 2017*.

Grebby, S. (2011). Integrating airborne multispectral imagery and airborne LiDAR data for enhanced lithological mapping in vegetated terrain 10.1016/j.rse.2010.08.019 : Remote Sensing of Environment | ScienceDirect.com, *44*(0). Retrieved from http://www.sciencedirect.com.libproxy.txstate.edu/science/article/pii/S0034425710002592

Grebby, S., Cunningham, D., Tansey, K., & Naden, J. (2014). The impact of vegetation on lithological mapping using airborne multispectral data: A case study for the north Troodos region, Cyprus. *Remote Sensing*, *6*(11), 10860–10887. https://doi.org/10.3390/rs61110860

Gupta, R. P. (2017). *Remote sensing geology: Third edition. Remote Sensing Geology: Third Edition*. https://doi.org/10.1007/978-3-662-55876-8

Haest, M., & Caccetta, T. C. A. R. C. L. E. M. M. (2013). Unmixing the effects of vegetation in airborne hyperspectral mineral maps over the Rocklea Dome iron-rich palaeochannel system (Western Australia). *Remote Sensing of Environment*, *129*, 17–31. https://doi.org/10.1016/j.rse.2012.10.011

Hewson, R., Carlton, A., Gilmore, P., Jones, S., & Robson, D. (2018). Geological mapping within NSW using remotely sensed and proximal spectral data ., (July), 1–5. https://doi.org/10.1190/nsapc2015-038

Hewson, R. D., Cudahy, T. J., & Huntington, J. F. (2001). Geologic and alteration mapping at Mt Fitton, South Australia, using ASTER satellite-borne data. *IGARSS 2001. Scanning the Present and Resolving the Future. Proceedings. IEEE 2001 International Geoscience and Remote Sensing Symposium (Cat. No.01CH37217)*, *2*(June 2014), 724–726. https://doi.org/10.1109/IGARSS.2001.976615

Hewson, R. D., Cudahy, T. J., Mizuhiko, S., Ueda, K., & Mauger, A. J. (2005). Seamless geological map generation using ASTER in the Broken Hill-Curnamona province of Australia. *Remote Sensing of Environment*, *99*(1–2), 159–172. https://doi.org/10.1016/j.rse.2005.04.025

Hewson, R., Robson, D., Carlton, A., & Gilmore, P. (2017). Geological application of ASTER remote sensing within sparsely outcropping terrain, Central New South Wales, Australia. *Cogent Geoscience*, *3*(1), 1–22. https://doi.org/10.1080/23312041.2017.1319259

HUNT, G. R. (1977). SPECTRAL SIGNATURES OF PARTICULATE MINERALS IN THE VISIBLE AND NEAR INFRARED. *Geophysics*, *42*(3), 501–513.

Kopăcková, V., & Koucká, L. (2017). Integration of absorption feature information from visible to longwave infrared spectral ranges for mineral mapping. *Remote Sensing*, *9*(10), 8–13. https://doi.org/10.3390/rs9101006

Macheyeki, A. S. (2016). PETROGRAPHIC AND GEOCHEMICAL CHARACTERISTICS OF THE KIEJO , RUNGWE AND NGOZI VOLCANIC ROCKS , SOUTHERN TANZANIA : IMPLICATION FOR TECTONIC ACTIVITIES AND MAGMATIC DIFFERENTIATION.

Morison, M., Cloutis, E., & Mann, P. (2014). Spectral unmixing of multiple lichen species and underlying substrate. *International Journal of Remote Sensing*, *35*(2), 478–492. https://doi.org/10.1080/01431161.2013.871085

Msanya, B. M., Otsuka, H., Araki, S., & Fujitake, N. (2007). Characterization of Volcanic Ash Soils in Southwestern Tanzania: Morphology, Physicochemical Properties, and Classification. *African Study Monographs*, *Supplement*(34), 39–55. Retrieved from http://jambo.africa.kyoto-u.ac.jp/kiroku/asm_suppl/abstracts/pdf/ASM_s34/3.msanya6.edit.pdf

Mshiu, E. E. (2011). Remote Sensing Data as an Alternative Approach for Geological Mapping in Tanzania: A Case Study in the Rungwe Volcanic Province, South-Western Tanzania. *Tanzania Journal of Science*, *37*(1), 26–36. https://doi.org/10.4314/tjs.v37i1.

Murphy, R. J. (1995). The effects of surficial vegetation cover on mineral absorption feature parameters. *International Journal of Remote Sensing*, *16*(12), 2153–2164. https://doi.org/10.1080/01431169508954548

Murphy, R. J., & Wadge, G. (1994). The effects of vegetation on the ability to map soils using imaging spectrometer data. *International Journal of Remote Sensing*, *15*(1), 63–86. https://doi.org/10.1080/01431169408954051

Novak, I. D., & Soulakellis, N. (2000). Identifying geomorphic features using LANDSAT-5/TM data processing techniques on Lesvos, Greece. *Geomorphology*, *34*(1–2), 101–109. https://doi.org/10.1016/S0169-555X(00)00003-9

Pournamdari, M., Hashim, M., & Pour, A. B. (2014). Application of ASTER and Landsat TM data for geological mapping of esfandagheh ophiolite complex, southern Iran. *Resource Geology*, *64*(3), 233–246. https://doi.org/10.1111/rge.12038

Range, E. M. (2016). EIA OF GEOTHERMAL EXPLORATION IN TANZANIA : THE LAWS AND REGULATIONS , EIA PROCESS AND PRELIMINARY EIA OF EXPLORATION DRILLING IN NGOZI AREA , SW-TANZANIA, (35), 751–770.

Rodger, A., & Cudahy, T. (2009). Vegetation corrected continuum depths at 2.20 μm: An approach for hyperspectral sensors. *Remote Sensing of Environment*, *113*(10), 2243–2257. https://doi.org/10.1016/j.rse.2009.06.011

Rogge, D., Rivard, B., Grant, B., & Pardy, J. (2010). Mapping Ni-Cu (PGE) bearing ultramafic rocks with hyperspectral imagery, Nunavik, Canada. In *2nd Workshop on Hyperspectral Image and Signal Processing: Evolution in Remote Sensing, WHISPERS 2010 - Workshop Program* (pp. 1–4). IEEE. https://doi.org/10.1109/WHISPERS.2010.5594870

Rowan, L. C., Mars, J. C., & Simpson, C. J. (2005). Lithologic mapping of the Mordor, NT, Australia ultramafic complex by using the Advanced Spaceborne Thermal Emission and Reflection Radiometer (ASTER). *Remote Sensing of Environment*, *99*(1–2), 105–126. https://doi.org/10.1016/j.rse.2004.11.021

Siegal, B. S., & Goetz, A. F. H. (1977). Effect of vegetation on rock and soil type discrimination. *Photogrammetric Engineering and Remote Sensing*, *43*(2), 191–196.

Simon, N., Ali, C. A., Mohamed, K. R., & Sharir, K. (2016). Best Band Ratio Combinations for the Lithological Discrimination of the Dayang, *45*(5), 659–667. https://doi.org/10.1111/jgs.13475

Sultan, M., Arvidson, R. E., & Sturchio, N. C. (1986). Mapping of serpentinites in the Eastern Desert of Egypt by using Landsat Thematic Mapper data. *Geology*, *14*(12), 995–999. https://doi.org/10.1130/0091-7613(1986)14<995:MOSITE>2.0.CO;2

Tilumanywa, V. T. (Stellenbosch U. (2013). Land Use and Livelihood Changes in The Mount Rungwe Ecosystem, Tanzania. *Dissertation, Doctor of Philosophy*, (December), 232.

URT, U. R. of T. (2017). *Mount Rungwe Nature Forest Reserve Management Plan*.

van der Meer, F. D., van der Werff, H. M. A., van Ruitenbeek, F. J. A., Hecker, C. A., Bakker, W. H., Noomen, M. F., … Woldai, T. (2012). Multi- and hyperspectral geologic remote sensing: A review. *International Journal of Applied Earth Observation and Geoinformation*, *14*(1), 112–128. https://doi.org/10.1016/j.jag.2011.08.002

Yu, L., Porwal, A., Holden, E.-J., & Dentith, M. C. (2011). Suppression of vegetation in multispectral remote sensing images. *International Journal of Remote Sensing*, *32*(22), 7343–7357. https://doi.org/10.1080/01431161.2010.523726

Zhang, J., Rivard, B., & Sánchez-Azofeifa, A. (2005). Spectral unmixing of normalized reflectance data for the deconvolution of lichen and rock mixtures. *Remote Sensing of Environment*, *95*(1), 57–66. https://doi.org/10.1016/j.rse.2004.11.019

APPENDICES

Appendix I: A

Calculated reflectance values of each end members (A, B) and the mixed values of the endmembers (C) of the Nine models in each bands of the Landsat (for the evaluation of the effect of vegetation). The symbols B and V refers to the bare and vegetation respectively and the coefficient in each symbol represents the percent coverage of the endmembers.

A

Band	Wavelength	100Bare (Observed)	95B	90B	80B	60B	50B	40B	20B	10B	5B
1	0.45	0.0527	0.050065	0.04743	0.04216	0.03162	0.02635	0.02108	0.01054	0.00527	0.002635
2	0.52	0.0668	0.06346	0.06012	0.05344	0.04008	0.0334	0.02672	0.01336	0.00668	0.00334
3	0.63	0.0879	0.083505	0.07911	0.07032	0.05274	0.04395	0.03516	0.01758	0.00879	0.004395
4	0.76	0.1175	0.111625	0.10575	0.094	0.0705	0.05875	0.047	0.0235	0.01175	0.005875
5	1.55	0.1862	0.17689	0.16758	0.14896	0.11172	0.0931	0.07448	0.03724	0.01862	0.00931
7	2.08	0.1526	0.14497	0.13734	0.12208	0.09156	0.0763	0.06104	0.03052	0.01526	0.00763

B

Band	Wavelength	100Vegetation (Observed)	95V	90V	80V	60V	50V	40V	20V	10V	5V
1	0.45	0.0207	0.019665	0.01863	0.01656	0.01242	0.01035	0.00828	0.00414	0.00207	0.001035
2	0.52	0.0403	0.038285	0.03627	0.03224	0.02418	0.02015	0.01612	0.00806	0.00403	0.002015
3	0.63	0.0273	0.025935	0.02457	0.02184	0.01638	0.01365	0.01092	0.00546	0.00273	0.001365
4	0.76	0.2889	0.274455	0.26001	0.23112	0.17334	0.14445	0.11556	0.05778	0.02889	0.014445
5	1.55	0.1136	0.10792	0.10224	0.09088	0.06816	0.0568	0.04544	0.02272	0.01136	0.00568
7	2.08	0.0444	0.04218	0.03996	0.03552	0.02664	0.0222	0.01776	0.00888	0.00444	0.00222

C

Band	Wavelength	100B	95B+5V	90B+10V	80B+20V	60B+40V	50B+50V	40B+60V	20B+80V	10B+90V	5B+95V	100V
1	0.45	0.0527	0.0511	0.0495	0.0463	0.0399	0.0367	0.0335	0.0271	0.0239	0.0223	0.0207
2	0.52	0.0668	0.065475	0.06415	0.0615	0.0562	0.05355	0.0509	0.0456	0.04295	0.041625	0.0403
3	0.63	0.0879	0.08487	0.08184	0.07578	0.06366	0.0576	0.05154	0.03942	0.03336	0.03033	0.0273
4	0.76	0.1175	0.12607	0.13464	0.15178	0.18606	0.2032	0.22034	0.25462	0.27176	0.28033	0.2889
5	1.55	0.1862	0.18257	0.17894	0.17168	0.15716	0.1499	0.14264	0.12812	0.12086	0.11723	0.1136
7	2.08	0.1526	0.14719	0.14178	0.13096	0.10932	0.0985	0.08768	0.06604	0.05522	0.04981	0.0444

Appendix I: B

Calculated reflectance values of each end members (A, B) and the mixed values of the endmembers (C) of the Nine models in each bands of the ASTER (for the evaluation of the effect of vegetation). The symbols B and V refers to the bare and vegetation respectively and the coefficient in each symbol represents the percent coverage of the endmembers.

A

Band	Wavelength	Bare (Observed)	95B	90B	80B	60B	50B	40B	20B	10B	5B
1	0.556	0.103	0.09785	0.0927	0.0824	0.0618	0.0515	0.0412	0.0206	0.0103	0.00515
2	0.661	0.116	0.1102	0.1044	0.0928	0.0696	0.058	0.0464	0.0232	0.0116	0.0058
3	0.807	0.148	0.1406	0.1332	0.1184	0.0888	0.074	0.0592	0.0296	0.0148	0.0074
4	1.656	0.271	0.25745	0.2439	0.2168	0.1626	0.1355	0.1084	0.0542	0.0271	0.01355
5	2.167	0.186	0.1767	0.1674	0.1488	0.1116	0.093	0.0744	0.0372	0.0186	0.0093
6	2.209	0.187	0.17765	0.1683	0.1496	0.1122	0.0935	0.0748	0.0374	0.0187	0.00935
7	2.262	0.181	0.17195	0.1629	0.1448	0.1086	0.0905	0.0724	0.0362	0.0181	0.00905
8	2.336	0.166	0.1577	0.1494	0.1328	0.0996	0.083	0.0664	0.0332	0.0166	0.0083
9	2.4	0.209	0.19855	0.1881	0.1672	0.1254	0.1045	0.0836	0.0418	0.0209	0.01045

B

Band	Wavelength	Vegetation (Observed)	95V	90V	80V	60V	50V	40V	20V	10V	5V
1	0.556	0.088	0.0836	0.0792	0.06688	0.0528	0.044	0.0352	0.0176	0.0088	0.0044
2	0.661	0.071	0.06745	0.0639	0.05396	0.0426	0.0355	0.0284	0.0142	0.0071	0.00355
3	0.807	0.426	0.4047	0.3834	0.32376	0.2556	0.213	0.1704	0.0852	0.0426	0.0213
4	1.656	0.17	0.1615	0.153	0.1292	0.102	0.085	0.068	0.034	0.017	0.0085
5	2.167	0.085	0.08075	0.0765	0.0646	0.051	0.0425	0.034	0.017	0.0085	0.00425
6	2.209	0.084	0.0798	0.0756	0.06384	0.0504	0.042	0.0336	0.0168	0.0084	0.0042
7	2.262	0.075	0.07125	0.0675	0.057	0.045	0.0375	0.03	0.015	0.0075	0.00375
8	2.336	0.07	0.0665	0.063	0.0532	0.042	0.035	0.028	0.014	0.007	0.0035
9	2.4	0.078	0.0741	0.0702	0.05928	0.0468	0.039	0.0312	0.0156	0.0078	0.0039

C

Band	Wavelength	100B	95B+5V	90B+10V	80B+20V	60B+40V	50B+50V	40B+60V	20B+80V	10B+90V	5B+95V	100V
1	0.556	0.103	0.10225	0.1015	0.1	0.097	0.0955	0.094	0.08748	0.0895	0.08875	0.088
2	0.661	0.116	0.11375	0.1115	0.107	0.098	0.0935	0.089	0.07716	0.0755	0.07325	0.071
3	0.807	0.148	0.1619	0.1758	0.2036	0.2592	0.287	0.3148	0.35336	0.3982	0.4121	0.426
4	1.656	0.271	0.26595	0.2609	0.2508	0.2306	0.2205	0.2104	0.1834	0.1801	0.17505	0.17
5	2.167	0.186	0.18095	0.1759	0.1658	0.1456	0.1355	0.1254	0.1018	0.0951	0.09005	0.085
6	2.209	0.187	0.18185	0.1767	0.1664	0.1458	0.1355	0.1252	0.10124	0.0943	0.08915	0.084
7	2.262	0.181	0.1757	0.1704	0.1598	0.1386	0.128	0.1174	0.0932	0.0856	0.0803	0.075
8	2.336	0.166	0.1612	0.1564	0.1468	0.1276	0.118	0.1084	0.0864	0.0796	0.0748	0.07
9	2.4	0.209	0.20245	0.1959	0.1828	0.1566	0.1435	0.1304	0.10108	0.0911	0.08455	0.078

Appendix: II, A

Bare-vegetation simulation model results from the Landsat image when vegetation cover is 40%, 50%, 60%, 90% and 95% (A, B, C, D, E respectively).

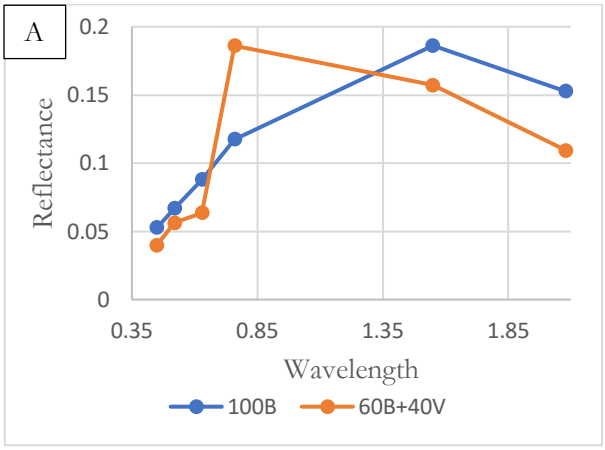

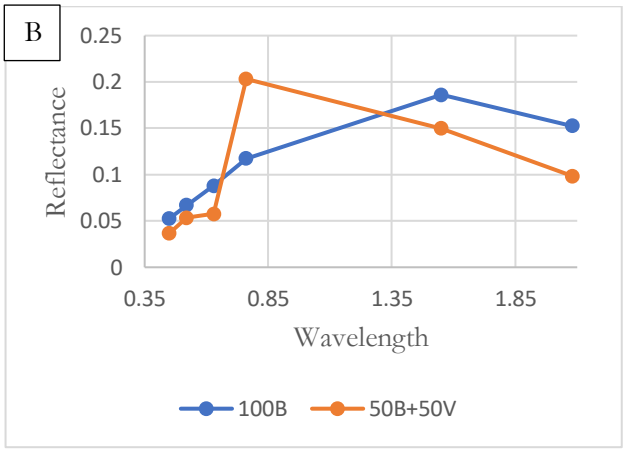

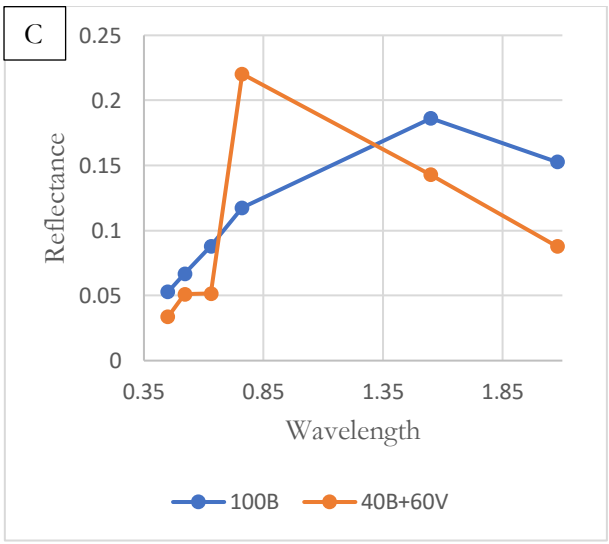

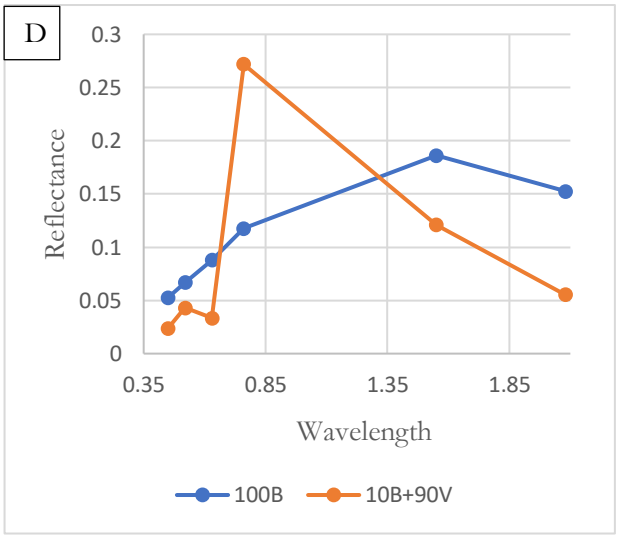

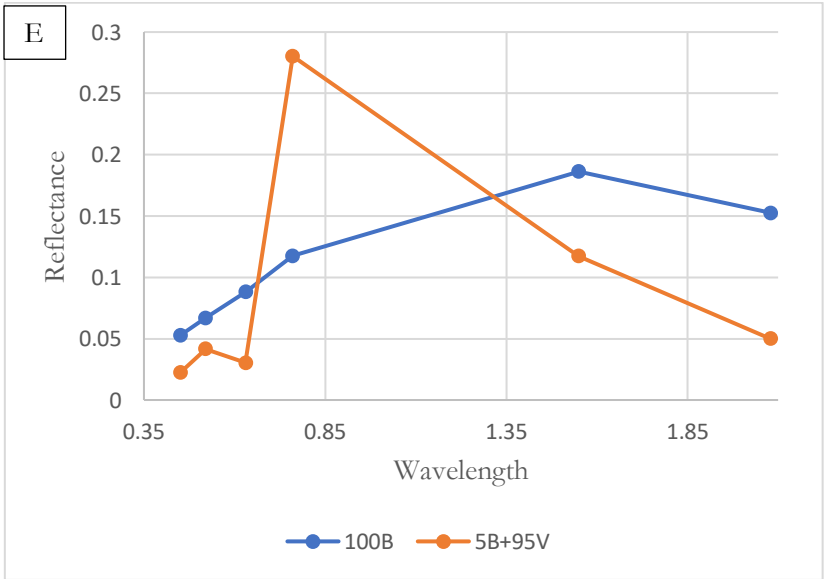

Appendix: II, B

Bare-vegetation simulation model results from the ASTER image when vegetation cover is 40%, 50%, 60%, 90% and 95% (A, B, C, D, E respectively).

A

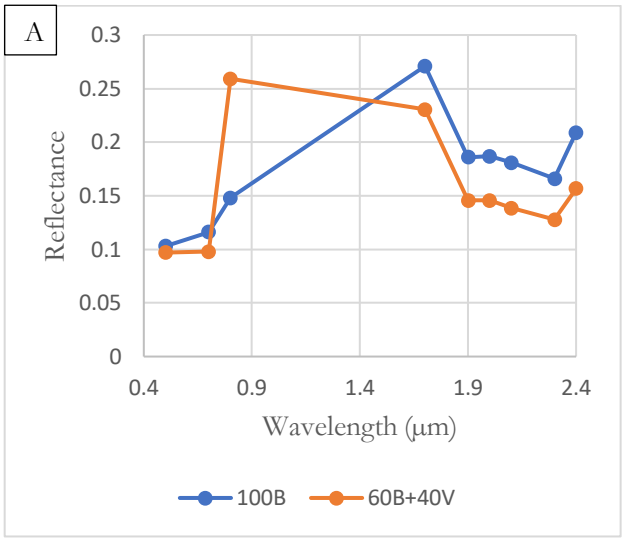

B

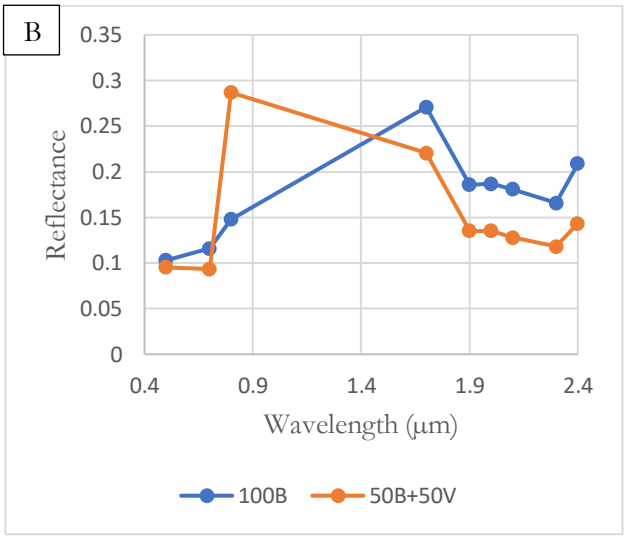

C

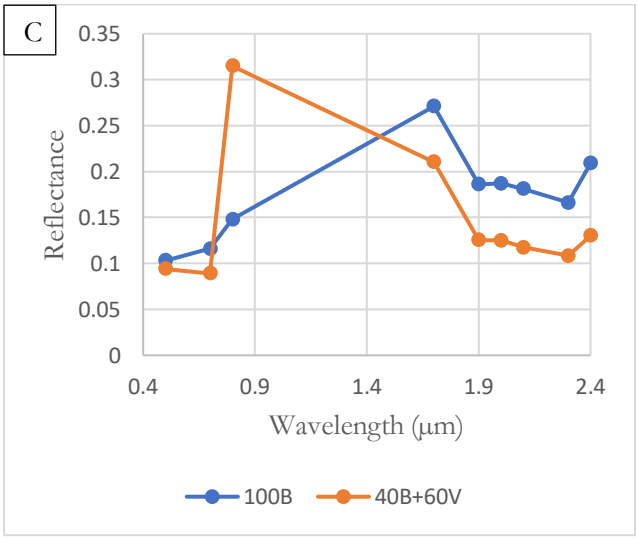

D

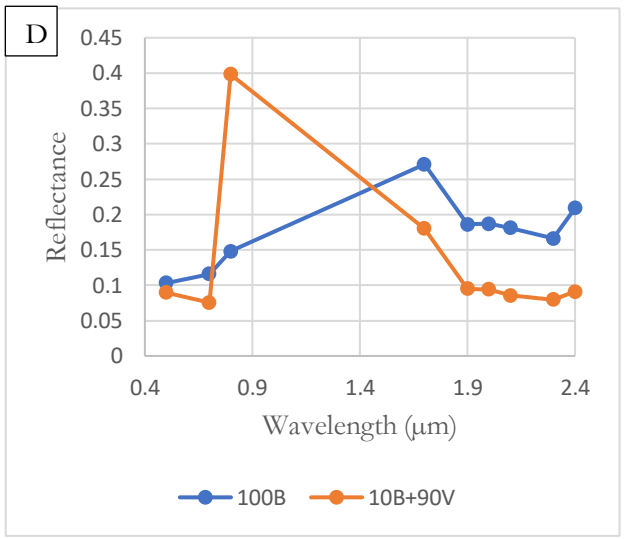

E

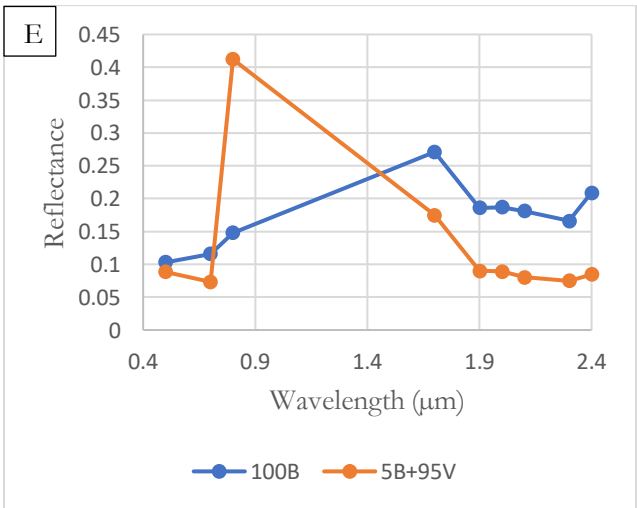

Appendix III:

Column charts showing the effect of variable amount of vegetation (when vegetation cover is 40%, 50%, 60%, 90% and 95%) on the spectra of the bare ground in the Landsat (A) and ASTER (B) scenes.

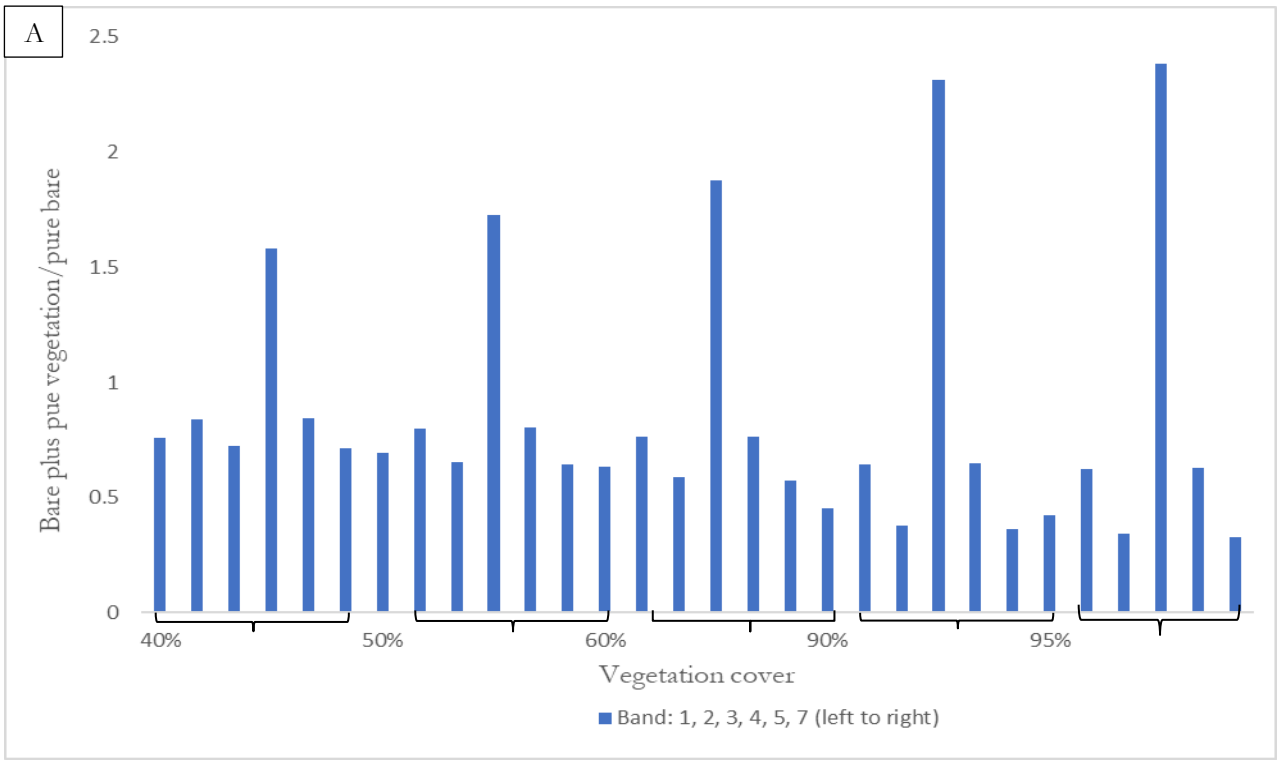

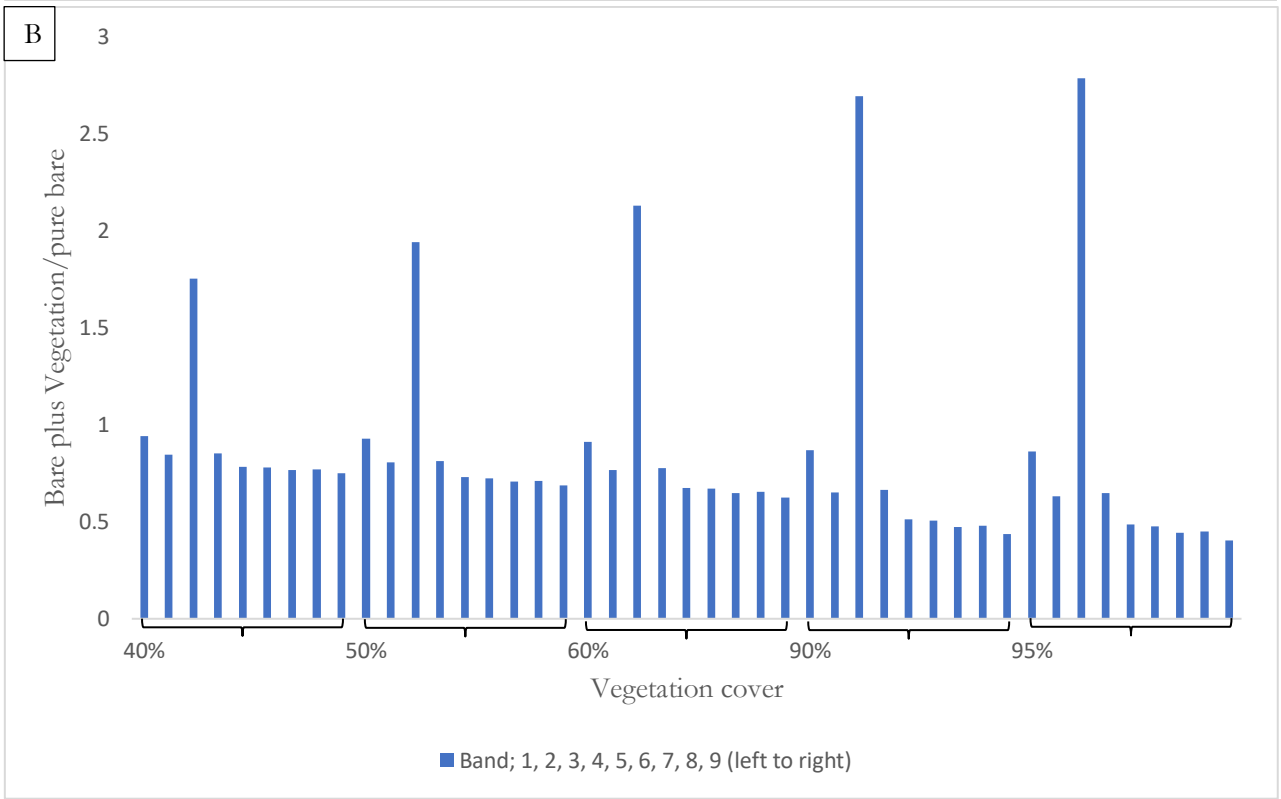

Appendix IV: A

Bare-vegetation simulation results when vegetation cover is 40%, 50%, 60%, 90% and 95% (A-E respectively) (Landsat); with trend lines showing the relationship between the bare and the mixed spectra.

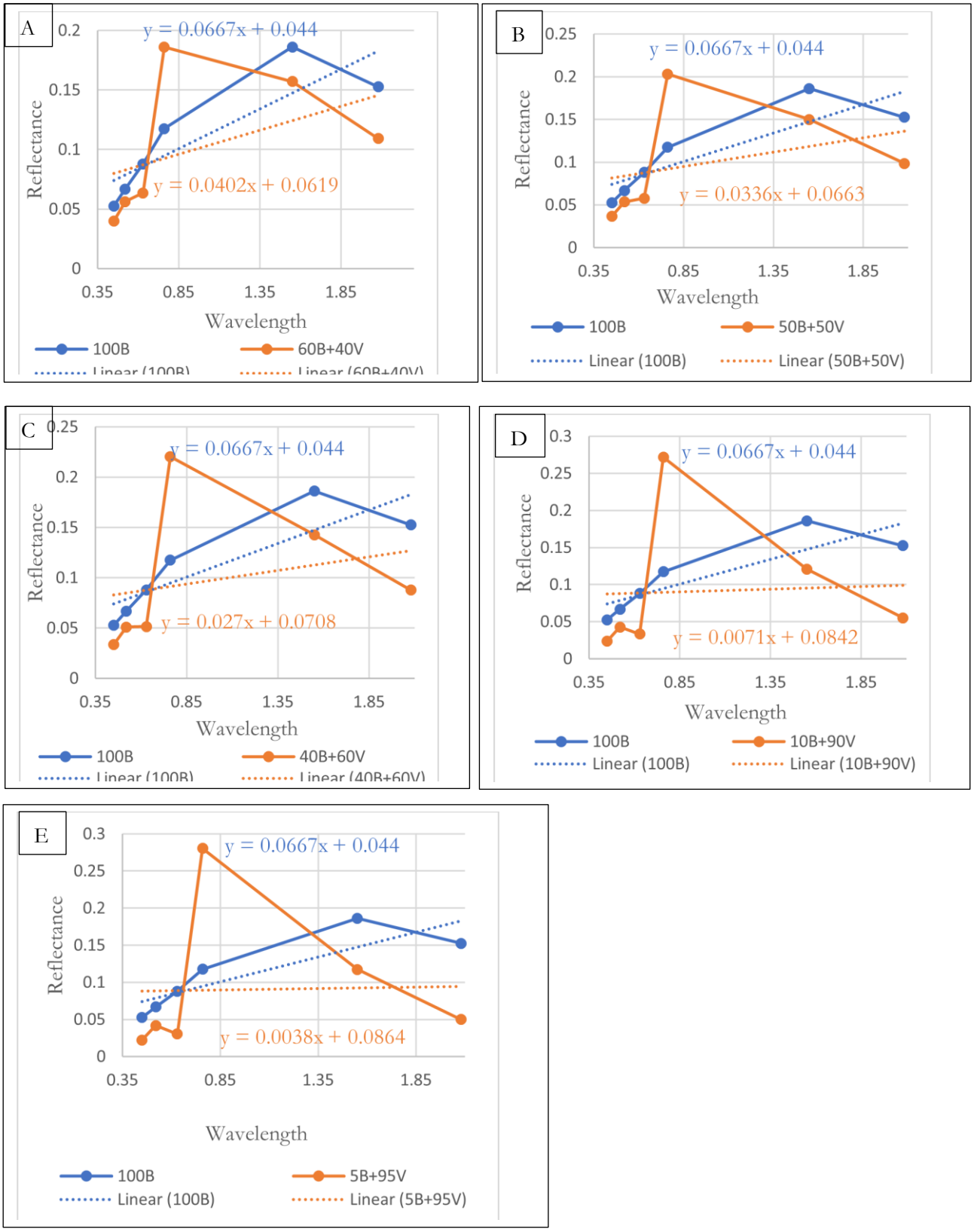

Appendix IV: B

Bare-vegetation simulation results when vegetation cover is 40%, 50%, 60%, 90% and 95% (A-E respectively) (ASTER); with trend lines showing the relationship between the bare and the mixed spectra.

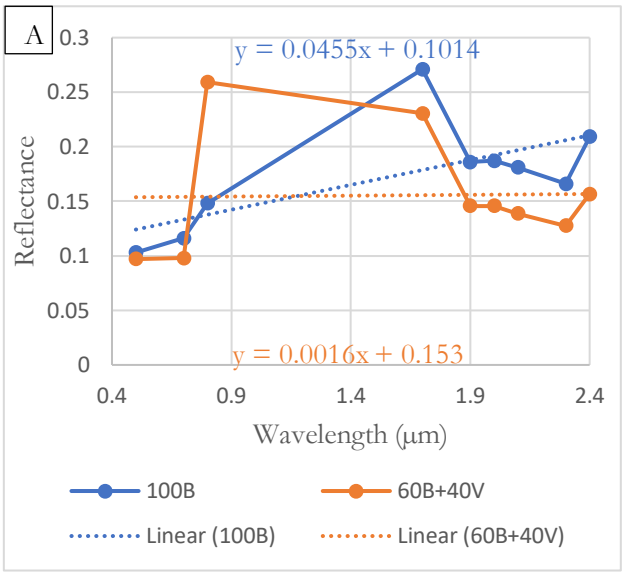

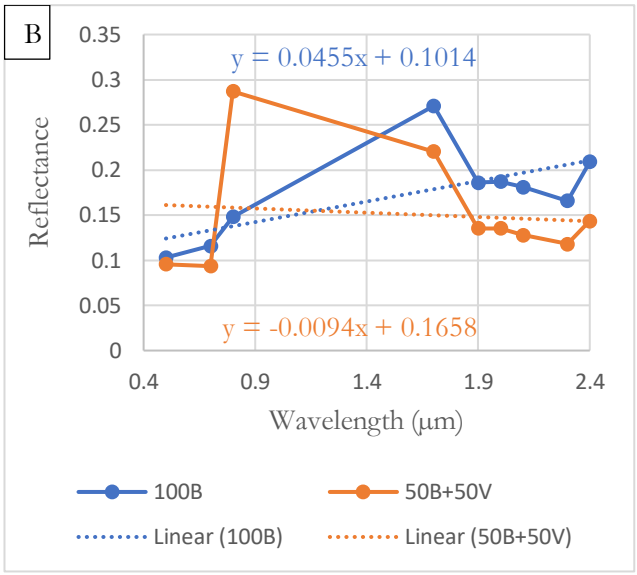

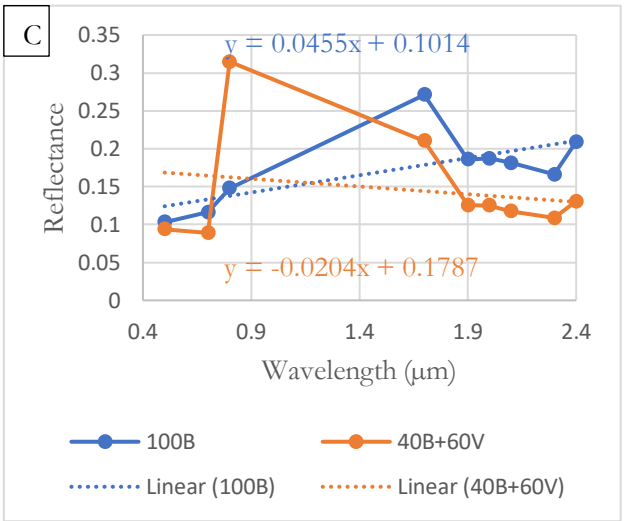

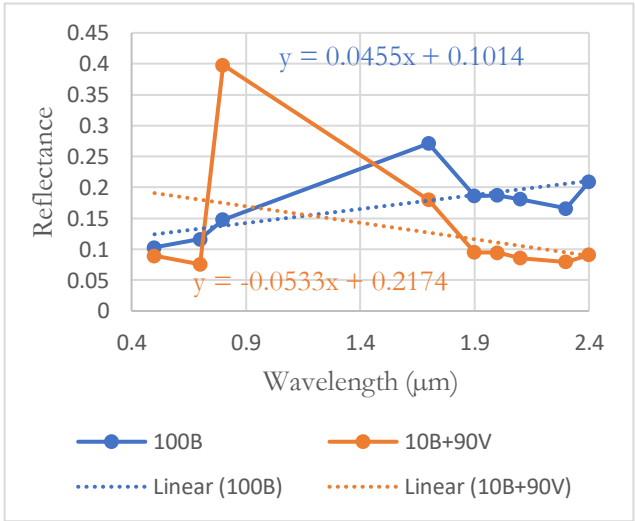

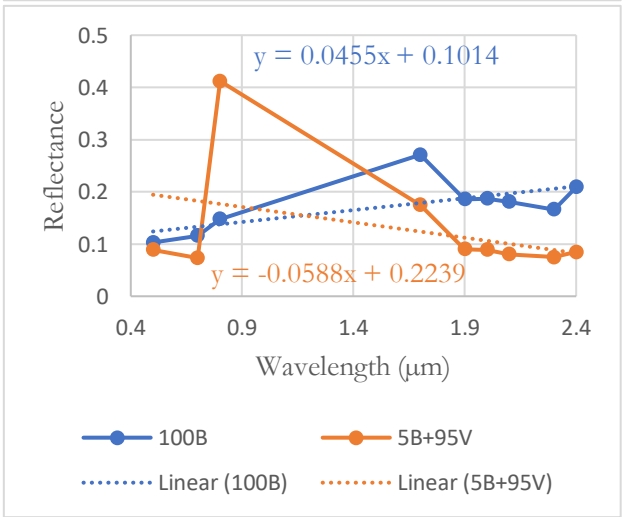

Appendix V:

Mean spectra of ten ROI's of the ASTER scene both before and after applying the Crippen and Blom's algorithm (A, B, C).

A

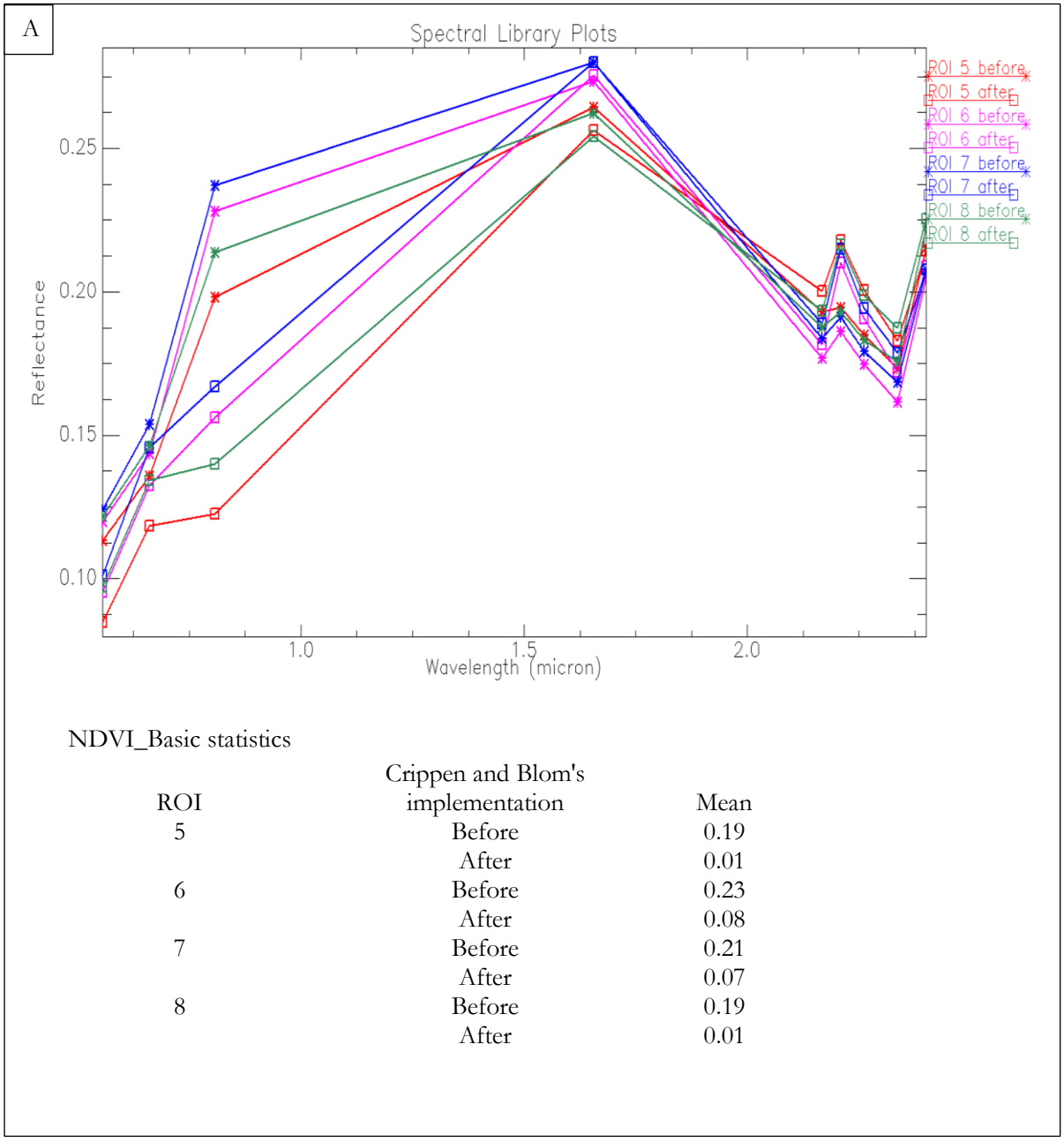

NDVI_Basic statistics

ROI	Crippen and Blom's implementation	Mean
5	Before	0.19
	After	0.01
6	Before	0.23
	After	0.08
7	Before	0.21
	After	0.07
8	Before	0.19
	After	0.01

B

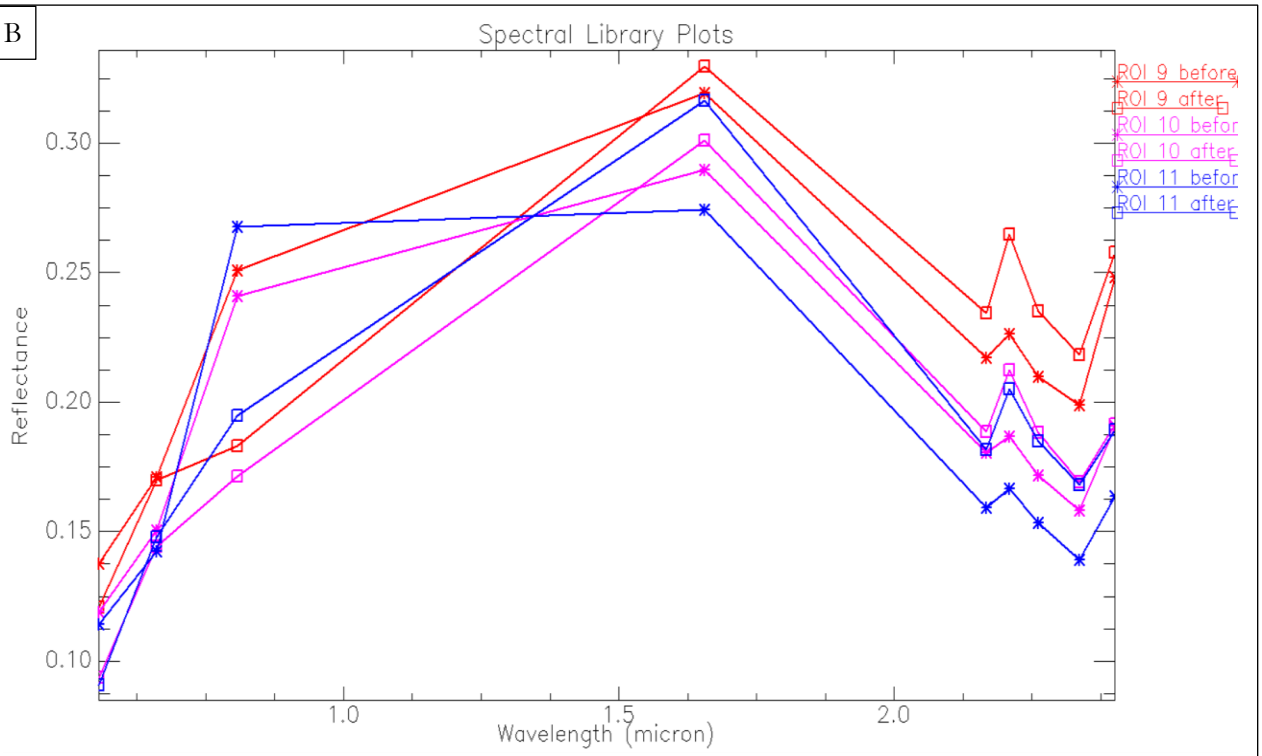

NDVI_Basic statistics

ROI	Crippen and Blom's implementation	Mean
9	Before	0.19
	After	0.04
10	Before	0.23
	After	0.08
11	Before	0.31
	After	0.14

C

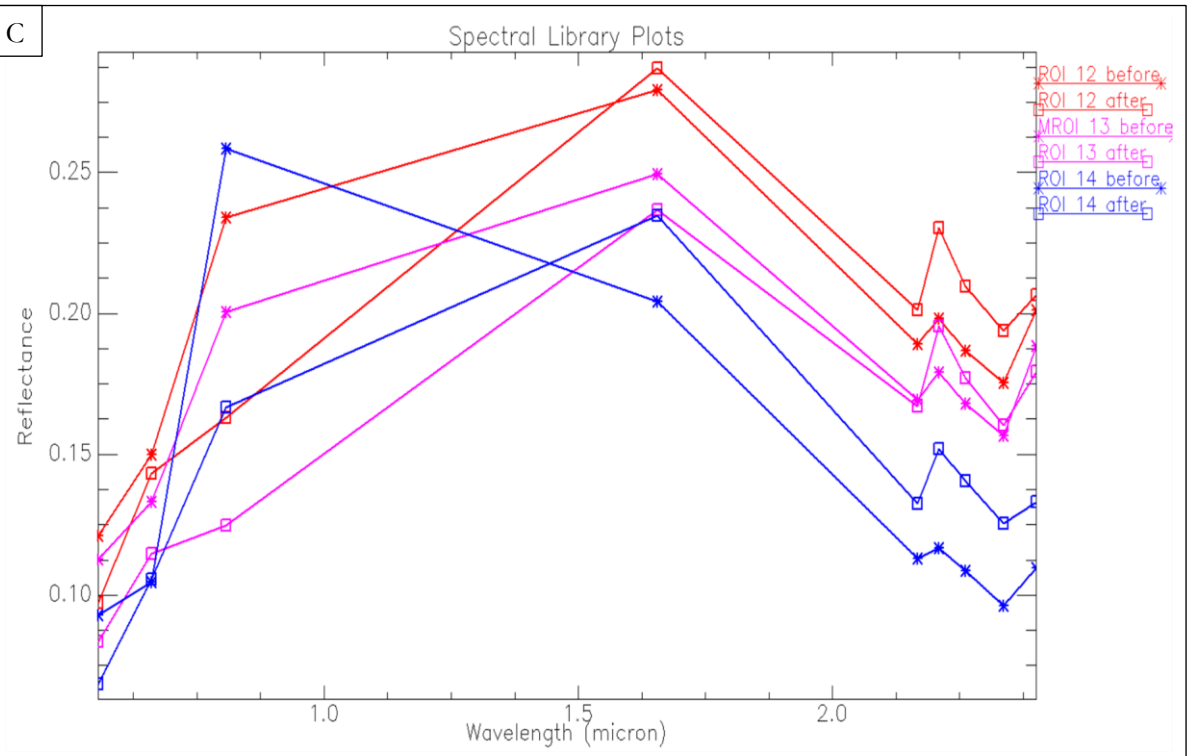

NDVI_Basic statistics

ROI	Crippen and Blom's implementation	Mean
12	Before	0.22
	After	0.06
13	Before	0.2
	After	0.03
14	Before	0.43
	After	0.23